Strangeness nuclear physics: a critical review on selected topics

Elena Botta, Tullio Bressani and Gianni Garbarino

Review

Strangeness nuclear physics: a critical review on selected topics

Elena Botta[a], Tullio Bressani, and Gianni Garbarino

INFN, Sezione di Torino and Dipartimento di Fisica, Università di Torino, Torino, Italy

Abstract. Selected topics in strangeness nuclear physics are critically reviewed. This includes production, structure and weak decay of Λ-Hypernuclei, the $\bar{K}$ nuclear interaction and the possible existence of $\bar{K}$ bound states in nuclei. Perspectives for future studies on these issues are also outlined.

Contents

1 Introduction

The interaction between hadrons is one of the most interesting topics among the basic subjects since the very beginning of the discoveries of hadrons. Due to its relatively easy access, the nucleon-nucleon (NN) interaction played historically the key role. The theoretical works at low energies constructed either purely phenomenological interaction potentials or potentials based on the meson-exchange picture initiated by Yukawa [1]. A good description of the NN interaction is of paramount importance since it is the basic ingredient for the understanding of the nuclear world. There has been a recent theoretical progress to derive the nuclear force potential from quantum chromodynamics (QCD) using Lattice QCD techniques. It successfully reproduced long-range attraction and short-range repulsion at the same time.

Effective field theories (EFTs) provide a crucial test for analyzing the properties and interactions of hadrons and nuclei. The theories that describe low-energy hadron physics embody the symmetries of the underlying theory,

^{a} e-mail: `botta@to.infn.it`

QCD, in effective Lagragians for the relevant degrees of freedom, such as pions, photons and nucleons: they lead to systematic expansions of observables in ratios of low-energy to high-energy scales, making it possible to estimate the uncertainties in their predictions and to systematically improve the accuracy of the pertinent calculations.

Chiral perturbation theory (ChPT) is the most important of these for low-energy hadronic and nuclear physics. It embodies the approximate $SU(2)_R \times SU(2)_L$ symmetry of QCD, which is a consequence of the very small current masses of the u and d quarks. Pions are, to a good approximation, the Goldstone bosons that arise from the spontaneous breaking of this symmetry by the condensation of quark-antiquark pairs in the QCD vacuum. The small mass of the pions and the weakness of their interactions at low energy are all consequences of this symmetry and are embodied in the effective Lagrangian of ChPT. Extensions of the theory can describe heavy particles, such as nucleons or D or B mesons interacting with pions. Enlarging the symmetry to $SU(3)_R \times SU(3)_L$ leads to EFTs that include strange particles.

EFTs can be used to connect different experimental observables within the symmetries of QCD. Increasingly, they are also being used to relate experimental observables to quantities that can be calculated using the methods of Lattice QCD.

Considerable progress has been made in the derivation of nuclear forces from chiral EFT. Although there is still an on-going debate about the renormalisation of these forces and the resulting expansion scheme, in practice very successful potentials have been constructed using Weinberg's original scheme at order Q4 or N3LO. They provide an accurate representation of two-body scattering data and are currently being used as input to *ab initio* nuclear structure calculations, using, for example, the no-core shell model or the coupled cluster method. In addition, EFT provides a consistent framework for the construction of three- and four-body interactions and also effective electroweak current operators. Calculations of light nuclei show that these three-body forces are essential for an accurate description of their binding energies.

These techniques are now being extended to hyperon-nucleon (YN) and hyperon-hyperon (YY) forces. The longest-range parts of these interactions arise from pion-exchange and so they can be calculated using the same chiral EFT. Here the smaller scattering lengths and weaker pion-hyperon coupling mean that the Weinberg's expansion scheme is appropriate.

A relevant agreement from theoreticians is the strong request of more experimental data on the YN and YY interactions. At present, the experimental data on the ΛN and ΣN interactions consist of not more than 850 spin-averaged scattering events, in the momentum region from 200 to 1500 MeV/c, while no data is available for the YY scattering. The low-energy data, in particular, fail to adequately define even the sizes of the dominant s-wave spin-triplet and spin-singlet scattering lengths and effective ranges.

Due to the inherent difficulty in obtaining precise direct experimental data with beams of low momentum (200–400 MeV/c) hyperons due to their short life, the only way to obtain such data is that of performing experiments on nuclear systems which bind one or more hyperons, *i.e.* Hypernuclei. The possibility of exploiting in different ways the Pauli principle for complex systems composed by many nucleons and one or more hyperons is the key issue for obtaining reliable and precise data.

In the last decade, spectroscopy of Λ-Hypernuclei showed an impressive step forward in determining the energy levels of nearly all p-shell Hypernuclei both by γ-ray spectroscopy from the decay of low-lying excited states and by missing-mass measurements with magnetic spectrometers at KEK (SKS), JLab (Hall A and Hall C) and LNF-INFN (FINUDA). A ΛN effective interaction which is expressed by five strength parameters was introduced and determined for the first time from a fit of γ-ray data on p-shell Hypernuclei: of particular relevance, we mention the extraction of the spin-spin term in the ΛN interaction. In the spectroscopy of Λ-Hypernuclei the Pauli principle plays the crucial role that all the possible states of the Λ in the many-body system are allowed, contrarily to nucleons. For this reason, the calculation of the quantum numbers of Hypernuclei is fully reliable.

In addition to information on the strong YN interaction, Hypernuclei may give access to experimental information, not otherwise accessible, on the weak YN interaction by their decays, in particular the non-mesonic decay. A free Λ decays almost at 100% into a pion and a nucleon, with a release of kinetic energy of about 5 MeV to the nucleon, corresponding to a final momentum of about 100 MeV/c. The situation changes dramatically when the Λ is embedded in a nucleus, since the nucleon of the mesonic decay is emitted with a momentum which is much smaller than the nucleon Fermi momentum $k_F \sim 280$ MeV/c. The Pauli principle acts now in the opposite way and the pionic decay modes are strongly hindered in all but the lightest Hypernuclei. However, new non-mesonic weak decay (NMWD) modes are switched on and are due to the weak interaction of the Λ with one nucleon of the medium ($\Lambda n \to nn$, $\Lambda p \to np$). The above weak decay reactions are possible only in Hypernuclei, thanks to the stability of the Λ against the mesonic weak decay due to the Pauli blocking and to the impossibility of strong interaction processes involving the hyperon due to strangeness conservation.

The study of the NMWD is of fundamental importance, since it provides primary means of exploring the four-baryon, strangeness changing, weak interactions. The non-mesonic process resembles the weak $\Delta S = 0$ $NN \to NN$ interaction, which was studied experimentally in parity-violating NN scattering. However, the $\Lambda N \to nN$ two-body interaction mode offers more information, since it can explore both the parity-conserving and the parity-violating sectors of the $\Delta S = 1$ weak four-baryon interaction. In the NN system, the strong force masks the signal of the weak parity-conserving part of the interaction.

In addition, the large momentum transfer in NMWD processes implies that they probe short distances and might therefore explore the role of explicit quark/gluon substructures of the baryons. It is also possible to envisage

in a nuclear medium a weak interaction of a Λ with two correlated nucleons, $\Lambda NN \to nNN$. It appears then that an exhaustive study of the weak interaction in Hypernuclei needs a big amount of correlated information from a very systematic and coordinated series of measurements. After several decades during which the experimental information was scarce, due to the hardness of the measurements, in the last years some very interesting new measurements were carried out. For NMWD, coincidence measurements of nucleon pairs emitted in quasi–back-to-back kinematics performed at KEK provided values of the observables in agreement with the most updated theoretical calculations.

The spectroscopic study of the proton distributions from NMWD of all the p-shell Hypernuclei carried out at DAΦNE-LNF allowed to ascertain experimentally the existence of the $\Lambda NN \to NNN$ weak interaction, whose contribution to the total NMWD width turned out to be non-negligible. The NMWD of Hypernuclei may be considered, literally, as the first and more spectacular example of nuclear medium modifications of the properties of an hadron. However with this definition or more concisely with nuclear medium modifications we intend today the changes of the mass and width of a strong interacting particle when produced inside a nucleus.

Theory predicts strong modifications of the kaon and antikaon properties in a dense hadronic environment. While a repulsive kaon-nucleus potential of a few tens of MeV is predicted for the K^+, the potential could be attractive up to $100\,\mathrm{MeV}$ or more for the K^-, depending on the model. A broadening is also predicted for the antikaon. Note that in the case of the strange mesons, no clean decay channel can be used to access directly their in-medium mass and width. The data taken so far, mostly based on the study of the yield under different kinematics and geometrical conditions (flow pattern) are well explained by transport models who consistently lead to a repulsive K^+N potential, as predicted by QCD based calculations. The case of the K^- meson is especially difficult because strangeness exchange reactions considerably disturb the already weak signals. More theoretical work, taking into account off-shell dynamics, is severely needed here.

Recently, a quite unexpected observation related to the production of Hypernuclei by K^- at rest on nuclei at LNF-DAΦNE was reported. The mesonless absorption of K^- at rest by 2, 3, 4 nucleons in light nuclei occurs with similar and quite high rates (10^{-3}/stopped K^-). Rates of a similar order of magnitude were found only for the production of some Hypernuclear states ($^{12}_{\Lambda}$C). This fact suggests that the absorption of K^- at rest should lead to the formation of some intermediate state(s), decaying at rest into back-to-back correlated pairs, Λp, Λd and Λt for 2, 3 and 4 nucleon absorption, respectively. These states could be the so-called AntiKaon Nuclear Clusters (AKNC), *i.e.*, states in which a $\overline{K}$ (K^-) is strongly bound to few nucleons. A phenomenological approach to this problem predicted for these systems a large binding energy (more than $100\,\mathrm{MeV}$) with narrow width (20–30 MeV) and a density that should be several times larger than the normal nuclear density. The determination of the invariant mass of the Λp back-

to-back correlated events seems to confirm the existence of the AKNCs, but this conclusion must be strengthened by other experiments with better statistics.

The study of nuclear and hadronic systems with strangeness —including hyperonic atoms, Hypernuclei, kaonic atoms and nuclei, exotic hadronic states such as strangelets, H-dibaryons and pentaquark baryons, compact stars and the phenomenon of strangeness production in heavy-ion collisions— has attracted great interest and experienced major advances in the last years [2,3]. Nowadays, one can safely say that strangeness nuclear physics plays a major role in modern nuclear and hadronic physics and involves important connections with astrophysical processes and observables as well as with QCD.

In the present paper we critically review some selected topics in strangeness nuclear physics, including production, structure and weak decays of Λ-Hypernuclei and the controversial issue of kaonic nuclear states. We discuss the present status of these issues from both the experimental and theoretical viewpoints. We shall point out the most recent achievements but also some flaws in the present understanding. The key experimental aspects and the calculations that must be considered in the near future will be discussed.

The paper is organized as follows. In sect. 2 we summarize the most important issues concerning general properties of Hypernuclei: the production reactions and the evolution of the experimental facilities for Λ-Hypernuclei are described in details. In sect. 3 we discuss the recent results on Hypernuclear spectroscopy and their relevance on the study of the baryon-baryon strong interaction. In sect. 4 we discuss the recent results on Hypernuclear weak decays and their relevance on the study of the baryon-baryon weak interaction. In sect. 5 we describe recent experimental results on an unexpected high rate of mesonless multinucleon absorption of stopped K^-, with hints on the possible existence of exotic antikaon nuclear aggregates. Finally, in sect. 6, we conclude with a critical summary of the last achievements of strangeness nuclear physics, with hints on the key measurements and calculations that must be carried out in order to achieve the final results so far anticipated.

2 Basic issues of Hypernuclear physics

In the present section we discuss general properties of strangeness -1 and -2 Hypernuclei with emphasis on the production reactions and the development of the facilities in the experimental study of Λ-Hypernuclei.

2.1 General properties of Hypernuclei and relevance for other fields

Hypernuclei are bound nuclear systems of non-strange and strange baryons. On the one hand, studies on the production mechanism and the structure of Hypernuclei [4,5] are of interest since they provide indications on the Y-N and Y-Y strong interactions which cannot be

determined from the difficult scattering experiments. Hypernuclear (strangeness-violating) weak decay is, on the other hand, the only available tool to acquire knowledge on strangeness-changing weak baryon interactions [6]. The mentioned strong and weak interactions, whose determination requires the solution of complex many-body problems, have a direct connection with astrophysics: they are important inputs when investigating the composition and macroscopic properties (masses and radii) of compact stars, their thermal evolution and stability [7]. Moreover, interactions involving hyperons are also relevant in the physics of heavy-ion collisions, whose main purpose is the study of the nuclear equation of state, the possible phase transition from hadronic matter to a quark-gluon plasma and the modification of hadron properties in dense strong interacting matter.

Among Hypernuclei, the most known and long studied are Λ-Hypernuclei, in which a Λ hyperon replaces a nucleon of the nucleus; they are indicated by the suffix Λ preceding the usual notation of nuclei: $^A_\Lambda Z$. Λ-Hypernuclei are stable at the nuclear time scale (10^{-23} s) since the Λ particle, the lightest of the hyperons, maintains its identity even if embedded in a system of other nucleons, the only strong interaction which conserves strangeness and is allowed being, in fact, ΛN scattering. Similarly, two Λ's may stick to a nuclear core, forming the so-called double Λ-Hypernuclei, indicated by the symbol $^A_{\Lambda\Lambda} Z$. Σ-Hypernuclei do not exist, at least as nuclear systems surviving for times longer than 10^{-23} s. The reason is that the strong $\Sigma N \to \Lambda N$ conversion reaction occurring in nuclei prevents the observation of narrow Σ nuclear states as for Λ-Hypernuclei. A similar situation occurs for Ξ^--Hypernuclei, whose importance lies in the fact that the strong conversion reaction $\Xi^- p \to \Lambda\Lambda$ in nuclei may be used as a breeder for the formation of $\Lambda\Lambda$-Hypernuclei. We may also think of Ω^--Hypernuclei, possibly breeders of 3Λ-Hypernuclei through a sequence of the two strong conversion reactions: $\Omega^- n \to \Lambda\Xi^-$, $\Xi^- p \to \Lambda\Lambda$ occurring in the same nucleus.

A series of experiments (BNL, KEK, JLab, FINUDA) and calculations clearly showed the hyperon single-particle structure of light to heavy Λ-Hypernuclei (from $^5_\Lambda$He to $^{208}_\Lambda$Pb) and a substantial part of the energy level structure (spin-doublets, spin-orbit separations, etc.) of s- and p-shell Λ-Hypernuclei [8]. This enabled us to obtain important information on the Λ-nucleus mean potential and on the spin-dependence of the ΛN interaction. The next generation of high-precision spectroscopy experiments of Λ-Hypernuclei is under preparation at J-PARC and JLab.

Analyses [9–11] of Σ formation spectra in the $(K^-, \pi^\pm)$ [12] and (π^+, K^+) reactions [13,14] showed that the Σ-nucleus potential has a substantial isospin-dependence and, with the exception of very light systems, is repulsive: $\mathrm{Re}\, V_\Sigma(\rho_0) \sim +(10\text{–}50)\,\mathrm{MeV}$, $\rho_0 = 0.17\,\mathrm{fm}^{-3}$ being the normal density of nuclear matter. The $\Sigma N \to \Lambda N$ conversion width is theoretically evaluated to be of about 30 MeV for a Σ in nuclear matter at normal density (see, for instance, the ΣN G-matrix calculation of ref. [15]). We note that repulsive values for the Σ-nucleus potential can be obtained theoretically [15] only in calculations with the

most recent Nijmegen YN potentials, ESC08, [16] or with quark-cluster models [17], thanks to the particular modeling of the short-range part of the ΛN interaction provided by these approaches. We note that the construction of the repulsive core part of the ESC08 potentials was guided by quark-cluster model studies. The only quasibound state of a Σ in a nucleus has been observed in $^4_\Sigma$He. By using an isospin decomposition of the hyperon-nucleus potential, one has $V_\Sigma = V^0_\Sigma + V^1_\Sigma \boldsymbol{T}_A \cdot \boldsymbol{t}_\Sigma/A$, V^0_Σ and V^1_Σ being the isoscalar and isovector potentials, respectively. Phenomenologically, one has positive values for both $\mathrm{Re}\, V^0_\Sigma$ and $\mathrm{Re}\, V^1_\Sigma$, which produces the above-mentioned repulsion. However, for a nuclear core with $N < Z$ and small A, the isovector term produces a significant attraction and can bind the Σ in $^4_\Sigma$He.

Despite their implications on the possible existence of dibaryon states and multi-strangeness Hypernuclei and on the study of compact stars, much less is known for strangeness -2 Hypernuclei [2, 3]. We have very little phenomenological information on the Ξ-nucleus potential V_Ξ: fits performed on an inclusive (K^-, K^+) production experiment [18, 19] provided a shallow potential, $\mathrm{Re}\, V_\Xi(\rho_0) \sim -14\,\mathrm{MeV}$. This experiment is interpreted as the formation of a Ξ^- bound state in $^{12}_{\Xi^-}$Be. Coulomb-assisted Ξ^- bound states are expected for medium and heavy Hypernuclei. In calculations based on ΞN NSC89 and NSC97 Nijmegen potentials, the Ξ-nucleus potential turns out to be repulsive; only the recent ESC04 and ESC08 models were constructed to provide an attractive Ξ-nucleus potential [16]. The existence of the strong $\Xi^- p \to \Lambda\Lambda$ reaction makes Ξ-Hypernuclei unstable with respect to the strong interaction. According to ΞN G-matrix calculations in nuclear matter at normal density [15], the width of the $\Xi^- p \to \Lambda\Lambda$ conversion reaction is of about 3–8 MeV for the NSC08 interaction model but can be as large as 15 MeV for the NSC04 model, thus making the experimental investigation of the level structure of Ξ-Hypernuclei in the latter case difficult. Recently, an experiment to study the spectroscopy of $^{12}_{\Xi^-}$Be via the (K^-, K^+) reaction on ^{12}C target has been approved at J-PARC [20] as a first priority. Valuable information on the $S = -2$ baryon-baryon interaction will be obtained with a high-resolution magnetic spectrometer; the first experimental results will also stimulate further theoretical work.

Only a few $\Lambda\Lambda$-Hypernuclei events have been studied experimentally up to date. In recent KEK experiments, $^4_{\Lambda\Lambda}$H, $^6_{\Lambda\Lambda}$He and $^{10}_{\Lambda\Lambda}$Be have been identified, while less unambiguous events were recorded for $^6_{\Lambda\Lambda}$He and $^{10}_{\Lambda\Lambda}$Be in the '60s and for $^{13}_{\Lambda\Lambda}$B in the early' 90s [21]. The recent observations imply a weak and attractive $\Lambda\Lambda$ interaction, *i.e.*, a bond energy $\Delta B_{\Lambda\Lambda}(^6_{\Lambda\Lambda}\mathrm{He}) \equiv B_{\Lambda\Lambda}(^6_{\Lambda\Lambda}\mathrm{He}) - 2B_\Lambda(^5_\Lambda\mathrm{He}) = (0.67 \pm 0.16)\,\mathrm{MeV}$ for the so-called NAGARA event [22]. However, this indication may not be conclusive, as it has not yet been possible to interpret with certainty all the old events consistently with the NAGARA event. Theoretical approaches to the structure of strangeness -2 nuclear systems have been proposed using various models. Small and attractive $\Lambda\Lambda$ bond energies can be obtained by the NSC89, NSC97 and ESC04 and ESC08 Nijmegen

YY models in three-body 2Λ + core calculations based on a $\Lambda\Lambda$ and ΛN G-matrix interaction [15,16]. However, the microscopic calculation of ref. [23], based on realistic NSC97 ΛN and $\Lambda\Lambda$ interactions, provided values of the bond energy which are smaller than the experimental value for the NAGARA event. Future experiments on strangeness -2 Hypernuclei will be carried out at J-PARC and FAIR (PANDA Collaboration).

We note that information derived from Hypernuclear structure have important implication in the study of compact astrophysical objects. The composition and equation of state of supernovae and neutron star cores sensitively depend on the hyperon content and are poorly known at present: these properties are mainly controlled by the depths of the hyperon-nucleus mean field potentials $V_Y(\rho)$ at high densities ρ. Various scenarios can be envisaged which correspond to different hyperon compositions and influence observable properties such as the mass-radius relation, the maximum mass and the temperature of neutron stars. Hyperons and hyperon interactions are also important in the study of failed supernovae. These stars evolve by first collapsing into proto-neutrons stars, which have very high density and temperature. The appearance of hyperons in failed supernovae makes the equation of state of the proto-neutron star softer and triggers a second collapse which finally ends with the formation of a black hole [24]. The black hole formation can be studied by detecting neutrino bursts on Earth originated in the failed supernova collapse. The duration of neutrino bursts becomes shorter in the presence of hyperons: this could allow one to probe the hyperon content in failed supernovae.

Concerning the weak decay, for Λ-Hypernuclei one has the mesonic mode, $\Lambda \to \pi N$, which resembles what happens to the Λ in the free space, and the so-called non-mesonic mode, with channels $\Lambda N \to nN$, $\Lambda NN \to nNN$, etc., which can only occur in nuclear systems. Nowadays, a good agreement has been reached between the theoretical description and the experimental data on the mesonic decay of Λ-Hypernuclei. Because of the Pauli blocking on the final nucleon, the mesonic decay is disfavored for medium and (especially) heavy Hypernuclei (say from $^{12}_\Lambda$C). Innovative experiments (KEK, FINUDA) on non-mesonic decay of Λ-Hypernuclei, which dominates for medium and heavy Hypernuclei, have been performed in recent times [25–29]. These advances were accompanied by the advent of elaborated theoretical models (a variety of both finite nucleus and nuclear matter approaches) and allowed us to reach a reasonable agreement between data and predictions for the non-mesonic rate $\Gamma_{\rm NM}$, the ratio $\Gamma_n/\Gamma_p \equiv \Gamma(\Lambda n \to nn)/\Gamma(\Lambda p \to np)$ between the neutron and the proton-induced decay rates and the intrinsic asymmetry parameter a_Λ for the decay of polarized Hypernuclei. However, discrepancies between theory and experiment (and in some case even between different experiments) are still present for the emission spectra involving protons [30,31]. This could signal an imperfect implementation of final state interaction effects in the theoretical and/or experimental analyses. Furthermore, it is still unclear the role played in the non-mesonic decay by

the Δ-baryon resonance and by possible violations of the $\Delta I = 1/2$ rule on the isospin change. New experiments on non-mesonic decay will be carried out at J-PARC, GSI and FAIR (HypHI Collaboration), while new analyses are expected also from FINUDA.

No data is available on the Λ-induced Λ decays which are possible in $\Lambda\Lambda$-Hypernuclei: $\Lambda\Lambda \to \Lambda n$, $\Lambda\Lambda \to \Sigma^- p$, $\Lambda\Lambda \to \Sigma^0 n$ ($\Delta S = 1$) and $\Lambda\Lambda \to nn$ ($\Delta S = 2$), apart from the claim for the observation of a single event [32] at KEK. Only a couple of predictions (in disagreement with each other) are available for such interesting strangeness-changing processes [33,34]. Realistic calculation of these decays could also provide important hints on the possible existence of the H-dibaryon. Moreover, a reliable calculation will be important in the design of future experiments at J-PARC and FAIR (PANDA Collaboration), where the corresponding processes could be observed for the first time.

Finally, we note that also Hypernuclear non-mesonic weak decay has a relevant impact on the physics of dense stars. The equilibrium between $NN \to \Lambda N$ and $\Lambda N \to NN$ non-mesonic weak processes is expected to be extremely important for explaining the stability of rotating neutron stars with respect to the emission of gravitational waves [7]. The fundamental property which controls the stability of a neutron star is the viscosity, which dominantly depends on non-mesonic weak processes involving hyperons. Other related hyperon-induced weak interactions (the so-called Urca processes) provide a relevant contribution to the cooling mechanism of neutron stars. The occurrence of hyperon superfluidity is indispensable for this hyperon cooling scenario to be consistent with the observations of cold neutron stars. In particular, the weakly attractive $\Lambda\Lambda$ interaction derived from the mentioned NAGARA event turned out to affect very much the hyperon cooling scenario [35].

2.2 Production of Hypernuclei and experimental facilities

2.2.1 The most used reactions for production of Hypernuclei

The first observation of a Hypernucleus (or more precisely a Hyperfragment) is due to Danysz and Pniewski in 1953 [36], by analyzing the events recorded by a stack of photographic emulsions exposed to the cosmic radiation at about 26 km from the Earth surface with a balloon. Up to the early '70s visualizing techniques (photographic emulsions, but also bubble chambers filled with ^{4}He or heavy liquids) were the experimental tool used to study the properties of Hypernuclei. Cosmic rays and afterward K^- beams were employed for producing Hypernuclei. Notwithstanding the inherent difficulty of this technique (low statistics), the basic features of Hypernuclear physics and more generally of strangeness nuclear physics (production, decay modes, inclusive spectra of charged particles) were assessed. Twenty Hypernuclear species were unambiguously identified by the kinematic
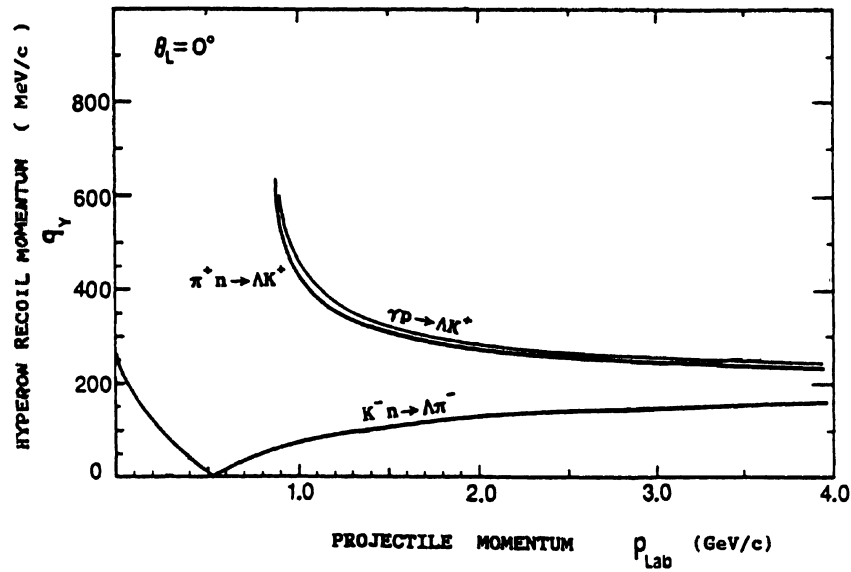
Fig. 1. Kinematics of reactions (2), (3) and photoproduction (5) for forward Λ emission ($\theta_L = 0°$). The momentum transferred to the hyperon is plotted as a function of the incoming particle (K^-, π^+ or γ) in the Laboratory system. From ref. [5].

analysis of the disintegration star. In particular measurements were performed of the Λ binding energy, B_Λ, of the $^A_\Lambda Z$ Hypernuclear ground state, defined as

$$B_\Lambda = M_{core} + M_\Lambda - M_{hyp}, \tag{1}$$

where M_{core} is the mass of the $^{(A-1)}Z$ nucleus well known from nuclear physics, M_Λ is the Λ hyperon mass and M_{hyp} is the measured $^A_\Lambda Z$ Hypernuclear mass. It was found that B_Λ varies linearly with A, with a slope of around $1\,\mathrm{MeV}/(\mathrm{unit\ of\ }A)$, saturating at about $27\,\mathrm{MeV}$ for heavy Hypernuclei. This result is the most important from the emulsion era and even today, in spite of the tremendous experimental effort on the magnetic spectrometers that we will discuss later, the B_Λ from the emulsion technique are the most precise and serve as a reference, due to their extraordinary precision.

From 1972 two-body reactions producing Λ on a nuclear target have been studied. The two-body reactions that led to practically all the present bulk of experimental information are the following.

1) The "strangeness exchange" reaction,

$$K^- + \mathcal{N} \to \Lambda + \pi, \tag{2}$$
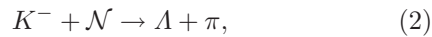
exploited mainly in the $K^- + n \to \Lambda + \pi^-$ charge state, for evident reasons of easiness in spectroscopizing the π final state. The reaction can be seen as a transfer of the s-quark from the incident meson to the struck baryon.
2) The "associated production" reaction,

$$\pi^+ + n \to \Lambda + K^+. \tag{3}$$
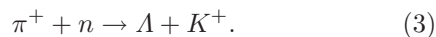
This reaction proceeds by the creation of a $(s\bar{s})$ pair by the incident meson.

3) The electroproduction of strangeness on protons in the very forward direction,

$$e + p \to e' + \Lambda + K^+, \tag{4}$$
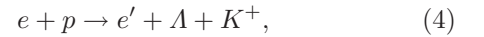
exploited quite recently. The virtual photons associated to the reaction (4) can be regarded as quasi-real and reaction (4) is often rewritten as a two-body photoproduction reaction:

$$\gamma + p \to \Lambda + K^+. \tag{5}$$

It must be noted that whereas with reactions (2) and (3) it is possible to replace a neutron in the target nucleus by a Λ, with reaction (4) a proton is replaced by a Λ, and the neutron-rich mirror Hypernucleus is obtained out from the same nuclear target. Just for example, with reactions (2) and (3) on a ^{12}C target $^{12}_\Lambda$C is obtained, while with reaction (4) $^{12}_\Lambda$B is produced.

Each one of the aforesaid reactions has its own characteristics in the elementary cross-section, internal quantum numbers transfer, momentum transfer, absorption of incoming and outgoing particles in nuclear matter. The most important parameter in determining the selectivity of the different reactions is the momentum transfer. Figure 1 shows the momentum transferred to the Λ hyperon, q_Y, as a function of the momentum of the projectile in the laboratory frame, p_{Lab}, for reactions (2), (3) and (4) at $\theta_{Lab} = 0°$. A striking kinematics difference appears: for (2), which is exoenergetic with a Q value of $\sim 178\,\mathrm{MeV}$, there is a value of p_{Lab} ($505\,\mathrm{MeV}/c$), usually referred to as "magic momentum" [37] for which q_Λ vanishes and recoiless production takes place; for (3), which is endoenergetic with a Q value of $\sim -530\,\mathrm{MeV}$, q_Λ decreases monotonically with p_{Lab}, staying always at values exceeding $200\,\mathrm{MeV}/c$. A further degree of freedom in selecting q_Λ is given by the detection angle of the produced

meson. It is important to notice that q_Λ for (2) with K^- at rest is not very different from that for (3).

In order to get insight on how the features of the elementary reaction affect the production of Hypernuclei in well-defined states the impulse approximation may be used. The two-body reaction t-matrix in the nuclear medium is replaced by the free space t-matrix at the same incident momentum and the differential cross-section for the reaction

$$\left.\begin{array}{c} K^- \\ \pi^+ \end{array}\right\} + {}^A Z \rightarrow {}^A_\Lambda Z + \left\{\begin{array}{c} \pi^- \\ K^+ \end{array}\right. \qquad (6)$$

may be written as

$$\mathrm{d}\sigma(\theta)/\mathrm{d}\Omega_L = \xi\,[\mathrm{d}\sigma(\theta)/\mathrm{d}\Omega_L]_{\mathrm{free}}\,N_{\mathrm{eff}}(i \rightarrow f, \theta). \qquad (7)$$

In (7) $\mathrm{d}\sigma(\theta)/\mathrm{d}\Omega_L$ is the Lab. cross-section for the production of the Hypernucleus ${}^A_\Lambda Z$ in a given final state f, ξ a kinematic factor arising from two-body to many-body frame transformation, $[\mathrm{d}\sigma(\theta)/\mathrm{d}\Omega_L]_{\mathrm{free}}$ the cross-section for the elementary (or free) reactions (2) and (3) and $N_{\mathrm{eff}}(i \rightarrow f, \theta)$ the so-called "effective nucleon number".

Equation (7), simple and easy to understand, was used by Bonazzola *et al.* [38] for the first time to describe the production of Hypernuclei by the (K^-, π^-) reaction at $390\,\mathrm{MeV}/c$. All the complications and difficulties related to the many-body strong interaction system are obviously contained in the term $N_{\mathrm{eff}}(i \rightarrow f, \theta)$ (the nuclear physics "black box"). In the simplest plane wave approximation (PWA) $N_{\mathrm{eff}}(i \rightarrow f, \theta)$ can be written as

$$N_{\mathrm{eff}}(i \rightarrow f, \theta) = (\text{Clebsh-Gordan coefficients}) \times F(q), \qquad (8)$$

in which $F(q)$ is a form factor, related to q by simple relationships, at least in the frame of the independent particle nuclear model.

PWA is only a rough approximation for describing Hypernuclei production reactions and is unable to provide reliable values of the cross-sections. A better insight is given by the Distorted Wave Impulse Approximation (DWIA). The K and π distorted waves are calculated separately by solving the Klein-Gordon equation with the use of appropriate optical potentials, conventionally taken proportional to the nucleon density. DWIA calculations are quite successful in describing the features of the production of Hypernuclei by meson beams. A comprehensive and updated account on this subject can be found in ref. [39].

Similar theoretical considerations may be applied also for describing the electroproduction of Hypernuclei by means of the elementary reaction (4), even though the relevant expressions are somehow complicated by the three-body final-state kinematics and by the dynamics described by the electromagnetic interaction. The relevant relationships can be found, *e.g.*, in ref. [4] and in the recent paper of ref. [40].

From the above considerations and from fig. 1 it appears that, with the (K^-, π^-) in-flight reaction, substitutional states of the Hypernucleus, obtained by converting a neutron of the target nucleus into a Λ hyperon in the same orbit and spin state with no orbital angular momentum transfer, are preferentially populated. On the other hand, the (π^+, K^+) and $(e, e'K^+)$ reactions and also the (K^-, π^-) reaction at rest transfer a significant recoil momentum (200–300 MeV$/c$) to the Hypernucleus, and then several high-spin Hypernuclear states are preferentially populated.

This feature is of paramount importance for Hypernuclear spectroscopy studies (see sect. 3) and also for investigations on the weak decay, which occurs mainly for Hypernuclei in the ground state (see sect. 4). Furthermore, since the spin-flip amplitudes in reactions (2) and (3) are generally small, they populate mainly non–spin-flip states of Hypernuclei. On the contrary, since the amplitude for reaction (4) has a sizable spin-flip component even at zero degrees due to the spin 1 of the photon, both spin-flip and spin–non-flip final Hypernuclear states may be populated in electroproduction. From the above considerations it appears that, in principle, we have at disposal all the tools needed for a complete study of all the Hypernuclei we wish to investigate. In practice the experimenters have to face many other constraints in designing their detectors. These are:

a) the values of the cross-sections for producing Hypernuclei with reactions (2), (3) and (4);
b) the presence of physical backgrounds in which the signals due to Hypernuclei formation could be blurred;
c) the intensity and energy resolution of the beams of projectiles (K^-, π^+, e);
d) the availability of the above beams at the different laboratories, in competition with other experiments in nuclear and particle physics.

A simple answer to question a) is given in fig. 2. It must be noted that the production of Hypernuclei by means of the (K^-, π) reaction with K^- at rest is reported too on a cross-section scale, which is formally wrong, since the production by particles at rest is defined by a capture rate and not by a cross-section [5]. Unfortunately, the intensities and the qualities (point c)) of the beams scale inversely to the values of the production cross-sections. The electron beams were always excellent concerning the intensity and the energy resolution. Unfortunately, in the past years, the duty cycle of the machines was very low, and the smallness of the cross-section joined to the need of measuring the e' and K^+ from (4) in coincidence did not allow to study the production of Hypernuclei. Only the advent of CEBAF, a machine with an excellent duty cycle, allowed the start up of experiments on Hypernuclei. The best projectiles for producing Hypernuclei, and in general strange nuclei, are K^-. Unfortunately the intensity of such secondary beams is quite low, and even worse is the quality (contamination by π^-, energy spread). For these reasons the magnetic spectrometers that were designed were quite complicated and the running times needed to obtain adequate statistics long. The powerful complex of machines J-PARC, that was recently put into operation and for which strange nuclei and atoms physics will be among the top priorities, will allow a real breakthrough in this field. Production of Hypernuclei by pion beams is midway concerning both the cross-sections and the quality of the beams. For these reasons experiments using reaction (3) performed mostly at
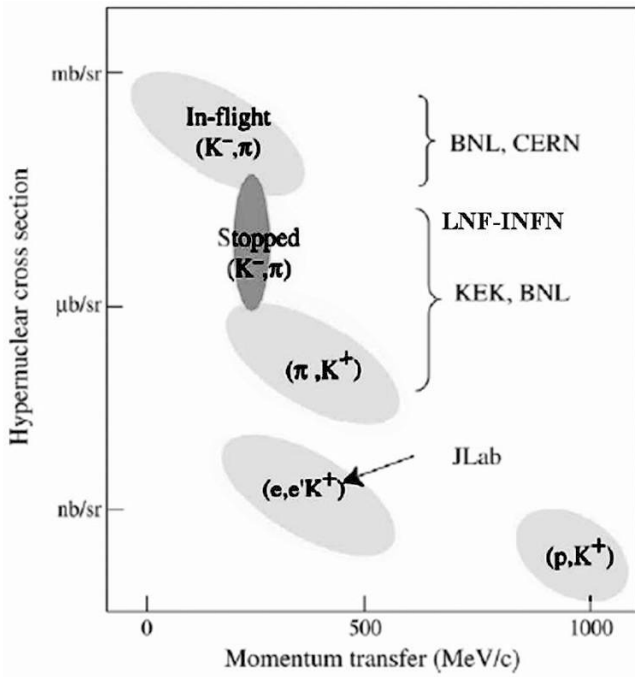
Fig. 2. Hypernuclear production cross-section for typical reactions *versus* momentum transfer. From ref. [5].

KEK with the SKS spectrometer produced a great part of experimental information in the last ten years by means of advanced state-of-art technologies at an old machine, the KEK 12 GeV ProtonSynchrotron. An overview of the measurements done with the SKS can be found in ref. [4].

A special discussion must be given in relation to the use of the (K^-, π^-) reaction at rest. Looking at figs. 1 and 2 this method seems easier to exploit, since no experimental information on the momentum of the incoming particle is needed. The main reason it has not been so widely used stems in point b). Taking again as an example the production of $^{12}_{\Lambda}$C from a ^{12}C target through reaction (2) with K^- at rest

$$K^-_{stop} + {}^{12}C \rightarrow {}^{12}_{\Lambda}C + \pi^-, \qquad (9)$$
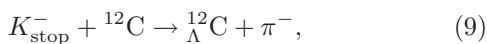
at first sight one could think that the simple spectroscopy of the π^- from (9) should be enough to get information on the excitation spectrum of $^{12}_{\Lambda}$C. The fastest π^- should be those related to the formation of $^{12}_{\Lambda}$C in the ground state. Unfortunately other processes following the capture of K^- at rest produce π^- with momenta even larger than those from reactions like (9). The most dangerous for Hypernuclear spectroscopy is the capture of a K^- by a correlated (np) pair in the nucleus:

$$K^- + (np) \rightarrow \Sigma^- + p, \qquad (10)$$
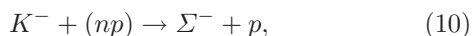
followed by the decay in flight of the Σ^- into $\pi^- + n$. This process leads to the production of π^- with a flat momentum spectrum that extends beyond the kinematics limit due to the two-body production of Hypernuclei. This drawback was clearly understood in the first series of experiments on Hypernuclei with K^- at rest, done at

KEK [41], and the background reasonably modeled by accurate simulations [42]. This circumstance generated ambiguity on the subsequent experiments with K^- at rest, described in the following.

After the visualizing techniques era, in the early '70s the study of Hypernuclei started by means of electronic techniques (magnetic spectrometers), following the progress in the design of new intense K^- beams and pioneering the use of the newly developed multiwire proportional chambers [43]. However, the magnetic spectrometers that were used by the different groups were not designed specifically and optimized for Hypernuclear physics. The first measurement of the π^- spectra emitted from K^- capture at rest by ^{12}C was performed by means of an apparatus dedicated to the measurement of the K_{e2} decay, with some modifications of the target assembly and the trigger [44]. The energy resolution of the Hypernuclear energy levels was 6 MeV FWHM. A similar resolution was attained in the first experiment on the production of Hypernuclei with the reaction (2) in flight, at 390 MeV/c. The apparatus was realized [45] specifically for the study of the production of Hypernuclei, but using pre-existing general purpose magnets. The energy resolution on the Hypernuclear energy levels was about 6 MeV FWHM.

γ-rays spectra emitted from low-lying excited Hypernuclear states were, too, measured from $A = 4$ systems in a pilot experiment performed with NaI detectors [46] at CERN. A double spectrometer for the study of the (K^-, π^-) reaction on some nuclear targets at 900 MeV/c was assembled soon afterwards, always at CERN, again using pre-existing beam elements and magnets, providing a better resolution (5 MeV) and cleaner spectra with higher statistics [47].

The first magnetic spectrometer which was specifically designed for Hypernuclear physics, SPES 2, has quite a funny story. It had quite a sophisticated and nice magnetic optics, it was assembled in 1976 and afterwards used at the proton Synchrotron SATURNE in Saclay in an attempt to produce Hypernuclei by the $(p, p'K^+)$ three-body reaction in the forward direction on a nuclear target. Unfortunately, the experiment failed, due to the overwhelming background, but the spectrometer was so properly designed that, transported at CERN and installed at a K^- beam in 1978, produced an excellent amount of data on Hypernuclear physics by the (K^-, π^-) reaction at 900 MeV/c [48].

A great step of quality in Hypernuclear physics was made possible by these experiments. Production of excited states was observed for several Hypernuclei, mostly in the p-shell, and their quantum numbers determined in some cases. These data constituted the input for several theoretical investigations on the description of the Hypernuclear excited states in terms of microscopic models starting from the ΛN potential. The most important result from this series of measurements is the observation that the spin-orbit term in the Λ-nucleus optical potential is consistent with zero. This conclusion was recently questioned by recent experiments on heavier Hypernuclei, but the original hypothesis of a very small value seems still to be the more valid.

Looking at the very promising results obtained at CERN, the BNL management decided to start a strong effort on Hypernuclear physics. The first step was to set-up a focusing spectrometer system placed on a rotatable platform, called Moby-Dick. A suitable beam line was designed to be operated in connection with the spectrometer.

From the late '70s BNL produced an impressive set of excellent data, practically on all the experimental aspects of Hypernuclear physics. The greater amount of data was obtained by means of the (K^-, π^-) reaction, thanks to the fact that BNL had the better K beams in the world. However, BNL pioneered also to exploit the associated production reaction (3) on nuclei in a very efficient and controlled way. As a matter of fact, the spectra obtained on heavy targets like ^{89}Y showed for the first time, in a very impressive way, the validity of the single-particle model even for the inner shells [49]. It is difficult to enumerate here all the contributions to Hypernuclear physics provided by the BNL experiments, without omissions. They can be found, *e.g.*, in the review by Chrien [50]. BNL pioneered practically all the experimental techniques that are the basis for the present and future installations, but did not perform a systematic study.

At the 12 GeV proton synchrotron of KEK experimental effort started with a series of experiments in which the π spectra emitted following the capture of K^- at rest by several nuclei were measured with a magnetic spectrometer [41]. At the beginning the apparatus was the one used for the study of rare and exotic decays of K^+. In some sense, the situation was similar to that one occurred in 1973 for the first CERN experiment, but the results, immediate and also far reaching, were completely different. Exploiting the better beam quality, the use of dedicated detectors for coincidence measurements and also the physics information gained by more than ten years of experimental results with the in-flight reactions, the KEK results showed that reaction (2) with K^- at rest could provide results on Hypernuclear physics of very high quality, in contrast to the initial perception. The main results from the KEK experiment is summarized in ref. [41].

At the end of the '90s, a powerful detector dedicated to Hypernuclear Physics was approved for installation at KEK. It was based on a large superconducting dipole magnet with a pole gap of 50 cm and a maximum field of 3T, optimized to provide a large solid angle (100 msr) for the reaction (π^+, K^+) on nuclei. A dedicated new beam line, providing $\sim 2 \times 10^6 \pi^+$/spill at about 1 GeV/c was put into operation. The spectrometer, named SKS (acronym for Superconducting Kaon Spectrometer) was equipped with state-of-art drift chambers and detectors for particle identification. Figure 3 shows a sketch of the detector. The final resolution of the device was about 1.5 MeV on the Hypernucleus energy spectrum as shown in fig. 4 [51].

As a first step, excitation energy spectra were measured for $^7_\Lambda$Li, $^9_\Lambda$Be, $^{10}_\Lambda$B, $^{12}_\Lambda$C, $^{13}_\Lambda$C, $^{16}_\Lambda$O, $^{28}_\Lambda$Si, $^{51}_\Lambda$V, $^{89}_\Lambda$Y, $^{139}_\Lambda$La, $^{208}_\Lambda$Pb. It is the more systematic study ever done, and confirmed the previous result on the physical reality of single-particle states deeply located in nuclei as heavy
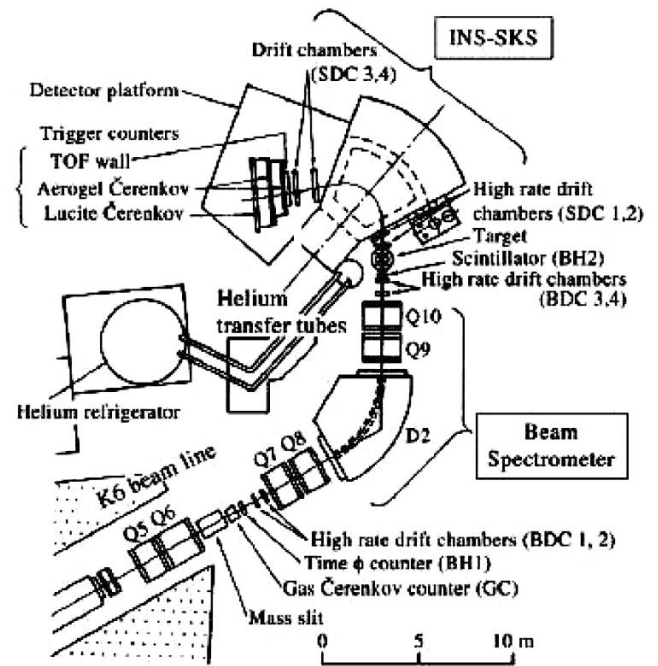
Fig. 3. Schematic drawing of the SKS spectrometer system with the beam line spectrometer. From ref. [4].
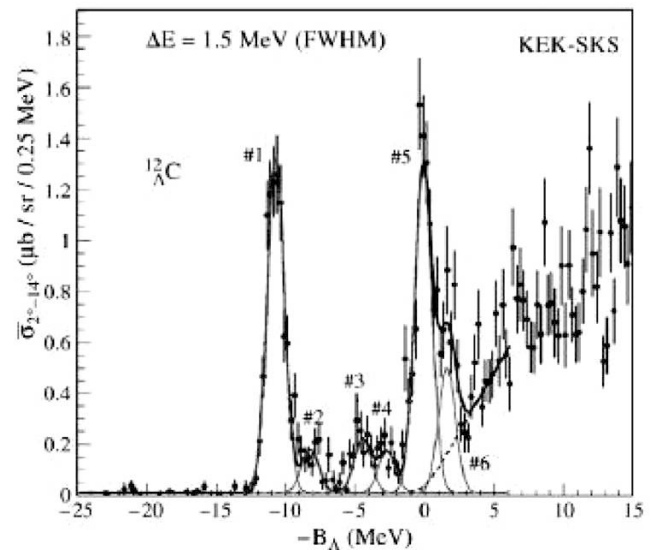
Fig. 4. Missing-mass spectrum of the ^{12}C$(\pi^+, K^+)^{12}_\Lambda$C reaction at the KEK 12 GeV PS using the SKS spectrometer. From ref. [51].

as $A = 208$ systems. This bank of data allowed a reliable determination of the parameters of the potential well seen by the Λ in a Hypernucleus. Furthermore, thanks to the improved energy resolution, a splitting of the peaks corresponding to the Λ in one shell was observed. The splitting seemingly increased with the angular momentum of the observed shell-model orbit, asking then for a non-zero value of the spin-orbit term.

After this series of systematic measurements, the SKS was used to "prepare" Hypernuclei in well defined states

(ground or excited) and study their decay by other arrays of complex detectors. This was possible thanks to the space left free around the targets used in the (π^+, K^+) reaction. The most important of these additional complex detectors was certainly the so-called Hyperball, since it pioneered a new field in Hypernuclear physics, the γ-rays spectroscopy of excited states, allowing the achievement of an energy resolution (of the order of keV) better by about three orders of magnitude than that reached with the magnetic spectrometers. It is important to notice that the device had in any case to be coupled to a magnetic spectrometer in order to prepare, with a resolution of some MeV, the Hypernuclear energy excitation spectrum to be analyzed by means of a further coincidence with the Hyperball detector. Details on the physics results achieved with this technique will be given in sect. 3. The first Hyperball consisted of fourteen n-type coaxial Ge detectors, arranged in a compact geometry. The Ge detectors were surrounded by BGO counters for background suppression (Compton scattering, high-energy electromagnetic showers from π^0 and penetration of high-energy pions and muons). The energy resolution of the detector was $\sim 3\,\mathrm{keV}$ FWHM and the total efficiency was 0.38% for γ-rays of 1 MeV. The system was cooled at $\mathrm{LN_2}$ temperature and equipped with fast-readout electronics, necessary to operate at high rates. The very successful results provided by the first Hyperball led to a continuous improvement of the detector. The last one, named Hyperball-J (J stands for J-PARC) is equipped with a mechanical cooling with a refrigerator instead of $\mathrm{LN_2}$ cooling, PWO counters instead than BGO for background suppression (they have much shorter time for light emission) and new readout electronics.

The second, complex detector fully dedicated to Hypernuclear physics, built taking into account the very interesting results obtained by using K^- at rest, is FINUDA. FINUDA (acronym for FIsica NUcleare a DAΦNE) may be considered the more complete detector built up to now and is completely different from all the other detectors and spectrometers described up to now. It was installed at an (e^+, e^-) collider, DAΦNE, at Laboratori Nazionali di Frascati. Thanks to the large angular coverage for detection of charged and neutral particles from the formation and decay of Hypernuclei, many observables (excitation energy spectra, partial decay widths for mesonic, non-mesonic decay and multi-nucleon absorption), were measured simultaneously and provided a bulk of data of unprecedented completeness, precision and cleanliness. Furthermore, spectra corresponding to different targets were measured simultaneously, avoiding possible systematic errors in comparing the properties of different Hypernuclei. Under this point of view, FINUDA is the modern electronic experiment approaching more closely the original visualizing technique by Danysz and Pniewski.

The idea of performing an experiment on the production and decay of Hypernuclei, which is inherently a fixed target physics, at a collider seems not good at first sight. The main decay channel of the Φ-meson, produced nearly at rest in the collision of 510 MeV electrons and positrons at a rate of $\sim 4.4 \times 10^2\,\mathrm{s^{-1}}$ at the luminosity $\mathcal{L} = 10^{32}\,\mathrm{cm^{-2}\,s^{-1}}$, is (K^+, K^-), BR $\sim 49\%$. Since the Φ-
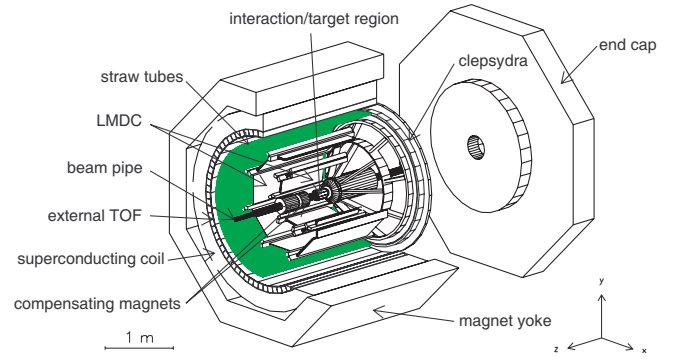
Fig. 5. Global view of the FINUDA detector with the superconducting solenoid and the iron yoke. From ref. [54].

meson is produced at rest, DAΦNE at LNF is a source of $\sim 2.2 \times 10^2$ (K^+, K^-) pairs/s, which are collinear, background free, and, very important, of very low energy ($\sim 16\,\mathrm{MeV}$). The low energy of the produced charged kaons is the key advantage for an experiment on Hypernuclei production and decay by means of the strangeness-exchange reaction with K^- at rest

$$K^-_{\mathrm{stop}} + {}^A Z \to {}^A_\Lambda Z + \pi^-, \qquad (11)$$

in which ${}^A Z$ indicates the nuclear target and ${}^A_\Lambda Z$ the produced Hypernucleus. The K^- can be stopped in very thin targets (a few hundreds of $\mathrm{mg/cm^2}$), in contrast to what happens in experiments with stopped K^- at hadron machines, where from 80% up to 90% of the incident K^- beam is lost in the degraders facing the stopping target. Furthermore, the cylindrical geometry of the interaction region at a collider allows the construction of cylindrical high resolution spectrometers with solid angles for detecting the π^- from (2) very much bigger ($> 2\pi\,\mathrm{sr}$) than those at fixed target machines ($\sim 100\,\mathrm{msr}$). Last but not least, the use of thin targets introduces lower cuts on the measurement of the energy spectra of charged particles (π^-, p, d) from the weak decay of the Hypernuclei produced by (11) and they are detected by the same arrays of detectors with large solid angles ($> 2\pi\,\mathrm{sr}$). These considerations were put forward in 1991 [52] and a proposal was afterwards elaborated [53] and soon accepted by the Scientific Committee of LNF. Figure 5 shows a sketch of the detector, immersed in a superconducting solenoid which provides a homogeneous magnetic field of 1.0 T inside a cylindrical volume of 146 cm radius and 211 cm length. We emphasize that different experimental features relevant to different measurements (*e.g.*, momentum resolution for the different particles *versus* the statistical significance of the spectra) may be optimized out of the same data bank by applying with software different selection criteria. The approach is then quite different from that followed by SKS, in which different hardware layouts were used in subsequent runs in order to obtain excellent results, some of which we will present in the following sections.

Let us now emphasize a peculiar feature of FINUDA, not adopted in the detectors so far mentioned. It is the presence of a powerful vertex detector, composed by two
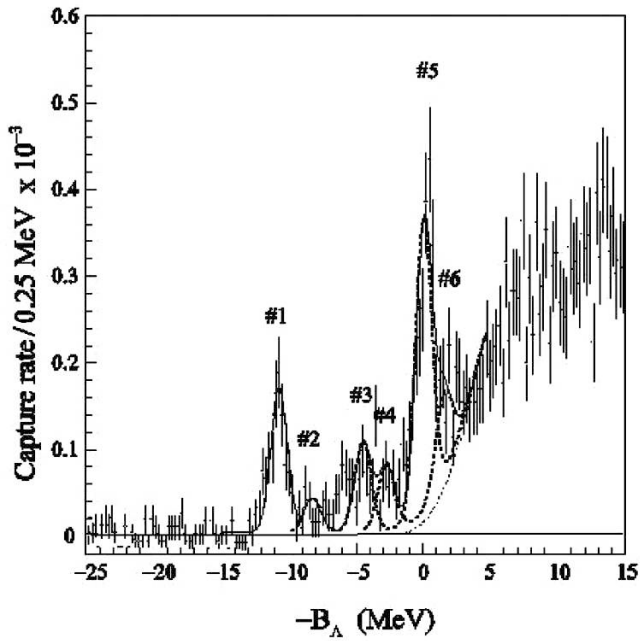
Fig. 6. Λ-binding energy spectrum of $^{12}_{\Lambda}$C measured by FI-NUDA. The solid line represents the best fit obtained with seven Gaussian functions. From ref. [54].

barrel-shaped arrays of Si Microstrip detectors that allow the separation of the primary interaction vertex of reaction (2) from the secondary vertexes from the decay of the produced hyperons, Λ and Σ, to better than 1 mm. For studies of Hypernuclear spectroscopy it is of paramount importance to measure the Hypernuclear energy spectra minimizing the background, that should forbid the observation of states produced with a low strength. As discussed before, the more significant contribution in the bound Hypernuclear states region comes from the absorption of the K^- on a NN pair, producing a $\Sigma^{\pm}$ and a nucleon. The Σ decays in flight into $N + \pi$, and the π from this process has a broad flat spectrum extending beyond the kinematics limit corresponding to the formation of the Hypernucleus in the ground state ($^{12}_{\Lambda}$C in the example).

Thanks to these features FINUDA provided nice results on Hypernuclear spectroscopy featuring the best energy resolution on the Hypernuclear energy levels (1.29 MeV FWHM) so far reached with magnetic spectrometers for meson-induced reactions like (2) and (3). Figure 6 shows the excitation energy spectrum measured for $^{12}_{\Lambda}$C [54].

As mentioned before, only recently reaction (4) has been exploited at JLab for the production of Hypernuclei. Two performing complexes of spectrometers were installed in Hall A and Hall C, respectively. Since reaction (4) leads to three bodies in the final state, two magnetic spectrometers with large acceptance had to be installed for the event-by-event reconstruction. A further difficulty, for the Hall C spectrometer, was represented by the necessity of using a splitter magnet after the target, keeping at minimum the disturbance introduced by such an element in the magnetic optics of the spectrometers. Figure 7 shows
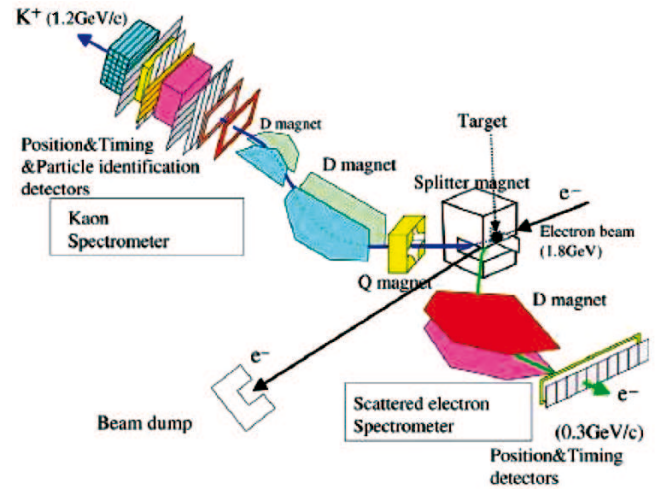
Fig. 7. Hypernuclear spectrometer system in JLab Hall C for E89-009. From ref. [4].
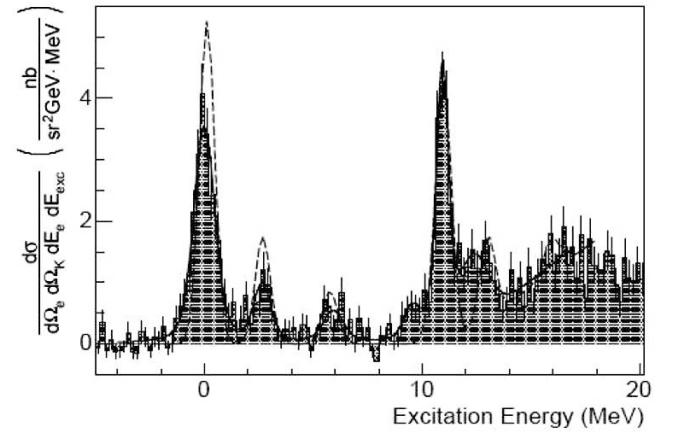
Fig. 8. The $^{12}_{\Lambda}$B excitation-energy spectrum. The best fit (solid curve) and a theoretical prediction (dashed curve) are superimposed on the data. From ref. [55].

a sketch of the spectrometer complex installed in Hall C. The difficulty of spectroscopizing two charged particles in the final state is overcompensated by the fact that spectrometers for electrons offer the best momentum resolution and then the final energy resolution on the Hypernuclear levels is considerably improved. As a matter of fact, a resolution of 0.67 MeV FWHM was very recently attained [55] by using the spectrometry's complex installed in Hall A, in a measurement on a ^{12}C target, with good statistics. Figure 8 shows the obtained $^{12}_{\Lambda}$B excitation-energy spectrum, with peaks corresponding to the Hypernucleus ground state and to both Λ and nuclear core excited states [55].

2.2.2 Other reactions for the production of Hypernuclei

Several projectiles other than mesons and electrons were used in attempts to produce Hypernuclei and measure some observable with a precision better than that reached with the standard reactions of sect. 2.2.1. We recall that

low-momentum $\bar{p}$ from LEAR were used to produce heavy Hypernuclei from Bi and U targets and measure their lifetime by the delayed fission using the recoil shadow method [56,57]. The same method was used some years later [58] using the p of 3 GeV from COSY to produce fissionable heavy Λ-Hypernuclei. Both experiments provided values for the heavy Hypernuclei with errors which at the end were at the same percentage level of those measured in experiments using mesons as projectiles. However, the reported values of the lifetimes for heavy Hypernuclei look too low when compared to those obtained for light-medium A Hypernuclei. We notice that, otherwise than other experiments, the lifetime determination was not direct, but needed some additional hypotheses; a detailed description will be given in sect. 4.1.

With the advent of the relativistic ion beams, some measurements were performed on Hypernuclear observables. The first attempt was the measurement of the lifetime for $^{16}_{\Lambda}$O performed at the LBL Bevalac with a 2.1 GeV/nucleon $^{16}_{\Lambda}$O beam [59]. However, the obtained value was about 3 times lower than the lifetime for neighboring Hypernuclei, indicating that some serious drawback was affecting the measurement. The method was improved at the JINR Synchrophasatron, providing reliable results for the lifetime of light Hypernuclei [60]. More details will be given in sect. 4.1.

Heavy-ion collisions experiments are of extreme importance for exploring the phases of strongly interacting matter as a function of temperature and net baryon density. In heavy-ion collisions at moderate energies, one has access to the high net baryon density region of the QCD phase diagram. Experiments of this kind, where particles with moderate strangeness quantum number are produced, will be performed at FAIR by the Compressed Baryonic Matter (CBM) Collaboration: their main aim is to study the nature of the transition between hadronic and quark matter, the search for a QCD critical endpoint and for a chiral phase transition. Instead, in nuclear collisions at high energy, hot and dense matter with almost vanishing net baryonic density is produced in the early stage of the fireball evolution [61]. High-energy heavy-ion collisions experiments have been carried out at RHIC and, at higher energies, are currently running at LHC. The matter created in such experiments contains an almost equal number of quarks and anti-quarks; it has been interpreted as the signature of the formation of a quark-gluon plasma (QGP) [62] and is suited for the production of Hypernuclei and anti-Hypernuclei in addition to many other particles and their anti-particles with large strangeness content.

The production of $^{3}_{\Lambda}$H Hypernuclei and $^{3}_{\bar{\Lambda}}\bar{H}$ antimatter Hypernuclei was observed by the STAR Collaboration at RHIC in Au + Au collisions at a center-of-mass energy per nucleon-nucleon collision $\sqrt{s_{NN}} = 200$ GeV [63–65]. This is the first observation of an antimatter Hypernucleus.

The lifetime of hypertriton and anti-hypertriton were measured by observing $^{3}_{\Lambda}$H $\rightarrow$ ^{3}He + π^{-} and $^{3}_{\bar{\Lambda}}\bar{H}$ $\rightarrow$ $^{3}\overline{He} + \pi^{+}$ mesonic decays, with a value $\tau = (182^{+89}_{-45} \pm 27)$ ps determined from the combined set of hypertriton and anti-hypertriton data (the separate hypertriton and anti-hypertriton showed no difference within errors, as predicted by the matter-antimatter symmetry). The determined masses, $m(^{3}_{\Lambda}H) = (2.989 \pm 0.001 \pm 0.002)$ GeV and $m(^{3}_{\bar{\Lambda}}\bar{H}) = (2.991 \pm 0.001 \pm 0.002)$ GeV, are consistent with the best value for hypertriton from the literature.

The experiment determined a $^{3}_{\bar{\Lambda}}\bar{H}/^{3}_{\Lambda}H$ ratio between the $^{3}_{\bar{\Lambda}}\bar{H}$ and $^{3}_{\Lambda}H$ production yields of about 0.5. This result is consistent with $^{3}_{\bar{\Lambda}}\bar{H}$ and $^{3}_{\Lambda}H$ production via a hadron coalescence mechanism by the overlapping of the Λ, p, n baryon wave functions for $^{3}_{\Lambda}H$ and $\bar{\Lambda}$, $\bar{p}$, $\bar{n}$ anti-baryon wave functions for $^{3}_{\bar{\Lambda}}\bar{H}$ in the final stage of the collision: in a coalescence picture one has $^{3}_{\bar{\Lambda}}\bar{H}/^{3}_{\Lambda}H \sim (\bar{\Lambda}/\Lambda) \times (\bar{p}/p) \times (\bar{n}/n)$, where with $\bar{B}/B$ ($B = \Lambda, p, n$) we indicate the baryon yield ratios. Relativistic heavy-ion collisions are expected to produce large amounts of hyperons and anti-hyperons with two or three units of strangeness, thus may be regarded as interesting sources of multi-strangeness Hypernuclei and anti-Hypernuclei.

Equilibration between strange and light quarks has been considered as a signature of the formation of a QGP. According to recent studies [66], the evolution of the correlation between the baryon and the strangeness quantum numbers as a function of the collision energy provides information on the onset of deconfinement which separates the QGP and the hadron gas phases. These baryon-strangeness correlations can be measured from the Hypernuclear production yields by introducing the so-called strangeness population factor $S_3 = {^{3}_{\Lambda}H}/(^{3}He \times (\Lambda/p))$. This observable is expected to increase as a function of the collision energy for a deconfined partonic phase while for a systems which remains in a hadronic phase is almost independent of energy [67]. Heavy-ion collision measurements at high energy can thus distinguish between the two phases of matter in the high-temperature regime. Although with large errors, S_3 was measured to be about 1/3 for AGS@BNL collisions at $\sqrt{s_{NN}} = 5$ GeV, and about 1 for RHIC collisions at $\sqrt{s_{NN}} = 200$ GeV [63]. A value of S_3 close to 1 indicates that the phase-space populations for strange and light quarks are similar to each other and favours the formation of a high-temperature matter made up of deconfined partons. New experiments at RHIC and LHC could elucidate this important issue.

3 Hypernuclear structure and the ΛN interaction

As said in sect. 1, the spectroscopic study of Λ-Hypernuclei has become an indispensable tool for the determination of the ΛN interaction. One can distinguish between reaction spectroscopy and γ-ray spectroscopy, which are complementary to each other. Reaction spectroscopy provides the gross features of the ΛN interaction, *i.e.*, the central, spin-independent part of this interaction, through the determination of the Hypernuclear masses, the hyperon binding energies and the production reaction cross-sections. With γ-ray spectroscopy one has access to high-resolution measurements of the Hypernuclear excitation energies (the energy resolution is about three orders of

magnitude better than with reaction spectroscopy), thus opening the possibility to study the fine structure and the hyperon spin-orbit splittings of Hypernuclei and therefore to determine the spin-dependent part of the ΛN interaction.

3.1 Theoretical models of the bare ΛN interaction

Before discussing the empirical results obtained in reaction and γ-ray spectroscopy experiments and their implications on Hypernuclear structure, we wish to briefly summarize the theoretical approaches used to determine the free-space YN and YY interactions which are usually adopted in those Hypernuclear calculations which are compared with the aforementioned experiments.

Various free-space YN and YY meson-exchange potentials have been constructed by the Nijmegen group by extending the NN interaction models using (broken) flavour $SU(3)$ symmetry together with a fitting procedure of the scarce ΛN and ΣN scattering data and the rich body of NN data. The one-boson–exchange picture led to the so-called soft-core interaction models NSC89 [68] and NSC97 [69], while the extended soft-core models ESC04 [70,71] and ESC08 [16,72] consist of one-boson exchange, two-pseudoscalar exchange, meson-pair exchange and multiple-gluon exchange. The Juelich group also proposed meson-exchange YN and YY potentials [73–75] and other potentials based on leading-order chiral effective field theory [76–78]. In ref. [79] a chiral unitary approach is adopted to study the central part of the ΛN and $\Lambda\Lambda$ interactions. Models of the baryon-baryon interactions also including quarks degrees of freedom have been developed, for instance in refs. [17,80,81] within a spin-flavour $SU(6)$ quark-model supplemented by an effective-meson exchange potential. Finally, we mention that Lattice QCD calculations of the baryon-baryon interactions are being developed in recent years [82–84], providing results for the scattering parameters in the strangeness -1 and -2 worlds and the first simulations for the YN potentials. Especially the meson-exchange models differ from each other concerning their spin-isospin structure, which cannot be fixed by the few existing baryon-baryon scattering data. Therefore, often these models provide results in disagreement with each other concerning Hypernuclear observables such as the hyperon-nucleus potential depths, the Hypernuclear energy level structure, etc., as we discuss in sects. 3.2 and 3.3.2.

3.2 Structure of Λ-Hypernuclei from reaction spectroscopy experiments

Since the '70s up to the beginning of the new millennium, many reaction spectroscopy experiments have been performed at CERN, BNL, KEK and LNF with the (K^-, π^-) and $(\pi^\pm, K^+)$ production reactions [4] and more recently at JLab with the $(e, e'K^+)$ reaction [85]. They achieved good energy resolution and provided good quality excitation spectra and the binding energy (1) of the hyperon in Hypernuclei in wide excitation energy and mass ranges, from $^3_\Lambda$H to $^{208}_\Lambda$Pb. In such experiments, the energies of the
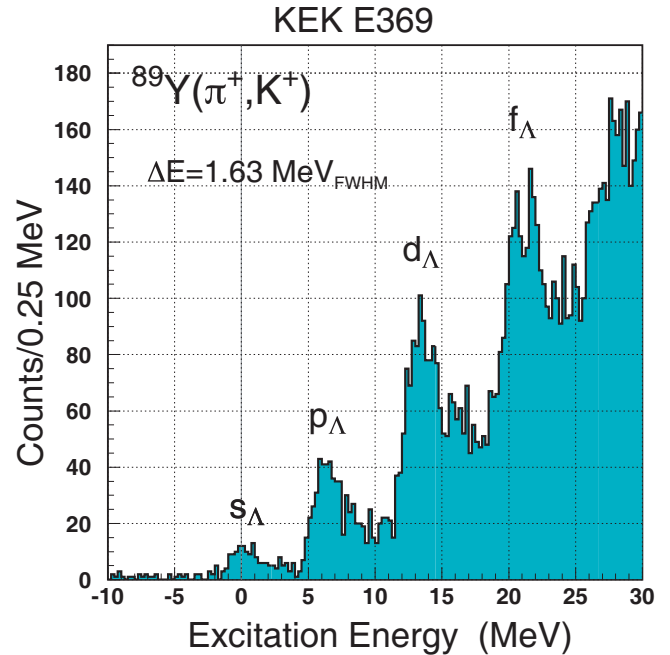
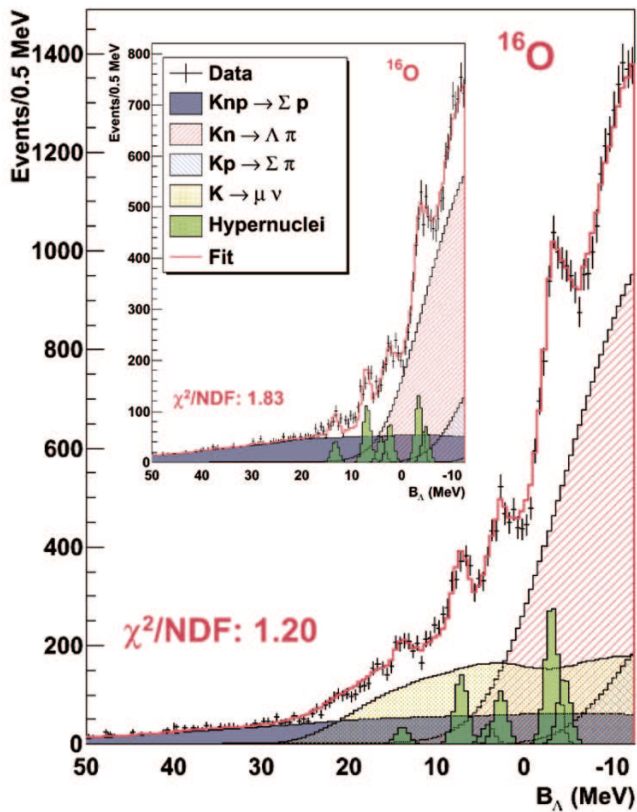**Fig. 9.** Excitation energy spectrum of $^{89}_\Lambda$Y obtained with the (π^+, K^+) reaction at KEK-E369. The peaks shows the s_Λ, p_Λ, etc., Λ single-particle states. From ref. [51].

various s_Λ, p_Λ, etc., Λ levels are directly obtained from the production reaction. Figure 9 clearly shows, through the well-separated peaks, the Λ single-particle levels structure of $^{89}_\Lambda$Y. As a matter of fact, since there is only one Λ, all the single particle states are allowed. This is not the case for nucleons in a nucleus, due to the Pauli principle. One often refers to this case as a textbook example of the Λ independent particle behavior in Hypernuclei.

The observed excitation spectra were rather well explained by DWIA calculations based on the shell model [86]. The observed Hypernuclear states were instead interpreted with shell-model [87] and cluster-model calculations [88].

With the exception of s- and p-shell Hypernuclei, mean field models with Wood-Saxon Λ-nucleus potentials reproduce rather well the Hypernuclear mass dependence of the hyperon binding energies of the various orbits determined by the reaction spectroscopy experiments by using a radius $R = 1.1(A-1)^{1/3}$ fm and a depth of 28–30 MeV [89]: $\mathrm{Re}\,V_\Lambda(\rho_0) \sim -(28\text{–}30)\,\mathrm{MeV}$. The fact that a simple mean field picture turns out to be a fairly accurate description of the bulk Hypernuclear properties means that the hyperon, being a distinguishable particle, maintains its single-particle behavior in the medium; this occurs even for states well below the Fermi surface, a property which is not observed for the nucleons. Due to its position in the inner part of the nucleons' core, on a single-particle level which is forbidden, by the Pauli principle, to the nucleons, the Λ plays the role of stabilizer of the Hypernucleus.

The spectroscopy by the $(K^-_{\mathrm{stop}}, \pi^-)$ reaction performed with the best achieved resolution on ^{12}C (fig. 6) [54] showed new features of relevance for the description of Hypernuclear states. Besides the two wide peaks

Fig. 10. Excitation energy spectrum of $^{16}_{\Lambda}$O obtained with the (K^-_{stop}, π^-) reaction by FINUDA. In the inset the binding energy distribution for a sample free from the K^- in flight decay background is shown. From ref. [90].

corresponding to the formation of $^{12}_{\Lambda}$C with the Λ in the s- and p-states, there is a considerable strength for the production of excited states lying between these two. It is of the same order $(10^{-3}/\text{stopped } K^-)$ of that for the production of the ground state of $^{12}_{\Lambda}$C. These states may be described by mixed L-excited nuclear core configurations and are predicted by some theoretical calculations concerning their energies, not at all, to our knowledge, their production rates. The importance of the excited nuclear core states was confirmed, with a better resolution, by an experiment with the $(e, e' K^+)$ reaction on a ^{12}C target [55] (see fig. 8).

Stimulated by this observation, the FINUDA Collaboration published recently [90] new data on the spectroscopy of $^{7}_{\Lambda}$Li, $^{9}_{\Lambda}$Be, $^{13}_{\Lambda}$C and $^{16}_{\Lambda}$O produced by K^- at rest. The measured pattern of excited states is similar to that obtained with the (π^+, K^+) reaction at $1.05\,\text{GeV}/c$ [4]; this is expected since the two experiment feature a comparable energy resolution and a comparable momentum transfer $(300\,\text{MeV}/c)$. As an example, the spectrum obtained with the ^{16}O target is shown in fig. 10. The only disagreement was found for the binding energy of the ground state of $^{16}_{\Lambda}$O, $13.4 \pm 0.4\,\text{MeV}$, to be compared with $12.42 \pm 0.05\,\text{MeV}$ of ref. [4]. We believe that, in spite of the larger error, the value from FINUDA is more reliable since it agrees with a previous measurement [41] with
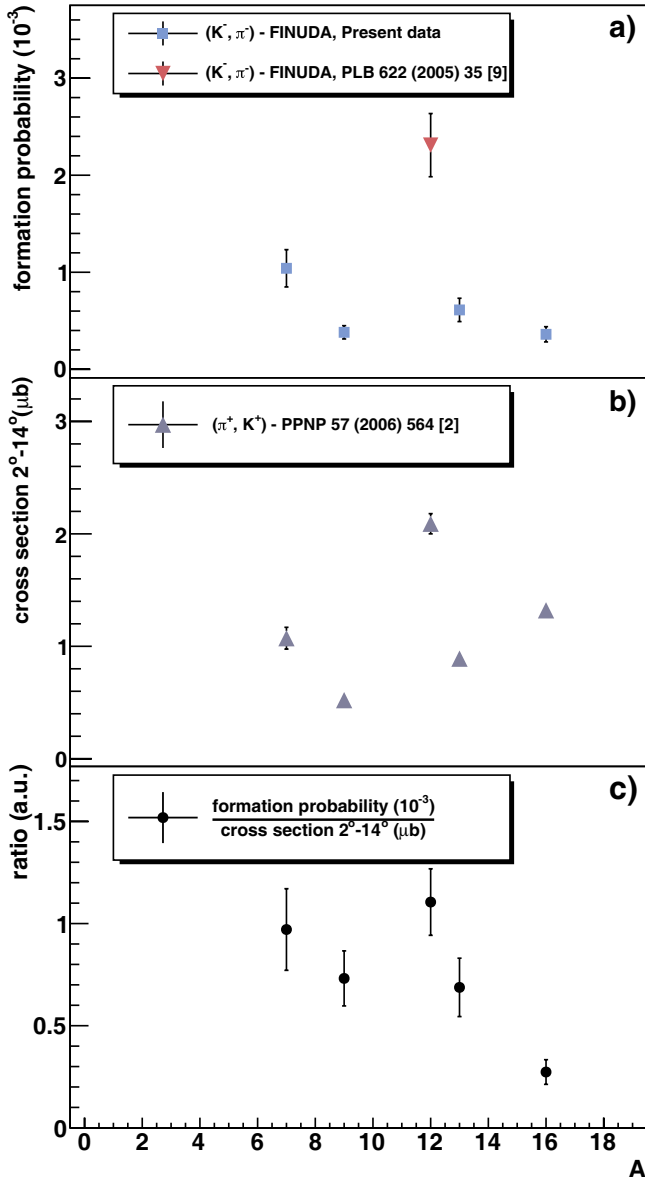
stopped K^- $(12.9 \pm 0.4\,\text{MeV})$ and with a recent result [91] on the $(e, e' K^+)$ electroproduction reaction on ^{16}O leading to the formation of $^{16}_{\Lambda}$N $(13.76 \pm 0.16\,\text{MeV})$. Furthermore, FINUDA had the advantage of a continuous self-calibrating control on the stability on the absolute value of the momenta of the spectroscopized pions by means of the monochromatic μ^+ from the $K_{\mu2}$ decay.

It was not easy to draw from the data on K^- capture probabilities of formation of the different states a simple A-dependence for the examined p-shell Hypernuclei. As a matter of fact, if we consider only their ground states, there are strong differences in the description of the nuclear configurations, and in some cases a not completely clean separation, from an experimental point of view, of the ground state from low-lying excited states (*e.g.*, $^{7}_{\Lambda}$Li or $^{12}_{\Lambda}$C, in which the doublet of states, one of which is the ground state, has a spacing of some hundreds keV). On the other hand, considering all states with binding energy greater than zero, we know that in some cases the states at higher excitation are described by configurations containing a Hypernucleus with a lower A. For these reasons, in order to consider only well-defined Hypernuclides, only excited states with energy below the threshold for the decay by nucleon emission were selected. Figure 11(a) shows a plot of the capture rates chosen following the above criterion as a function of A. A smoothly decreasing behavior appears, with the exception of a strong enhancement corresponding to the formation of $^{12}_{\Lambda}$C bound states. Figure 11(b) shows, for comparison, the differential cross-section integrated in the forward direction $(2°–14°)$ for the production of the same states observed with the (π^+, K^+) reaction [4] and fig. 11(c) the ratio between the two values. This ratio ranges from a large value for $^{7}_{\Lambda}$Li and $^{12}_{\Lambda}$C to a small value for $^{16}_{\Lambda}$O, showing a distinct A-dependence for the two reactions, K^- capture at rest and in flight (π^+, K^+). The strong A-dependence of the (K^-_{stop}, π^-) rates with respect to the weak dependence of the (π^+, K^+) differential cross-sections reflects the sizable difference between the strongly attractive K^--nuclear interaction at threshold and the weakly repulsive K^+-nuclear interaction. This remark was the starting point for an attempt [92] to determine the value of $\mathrm{Re}\,V_{K^-}$, quite important for several items of K-nuclear physics, as it will be discussed with more details in sect. 5.2. Theoretical approaches varying from shallow potentials $(40–60\,\text{MeV})$ at threshold to very deep density dependent potentials $(150–200)\,\text{MeV}$ were in fact proposed. The authors considered only $1s_\Lambda$ capture rates and for this reason they scaled the experimental capture rates given in ref. [90] by appropriate structure functions derived from neutron pick-up spectroscopic fractions in the target nuclei. The comparison of these normalized experimental formation rates with the calculations performed with a shallow or deep potential slightly favored the second one, as shown in fig. 12.

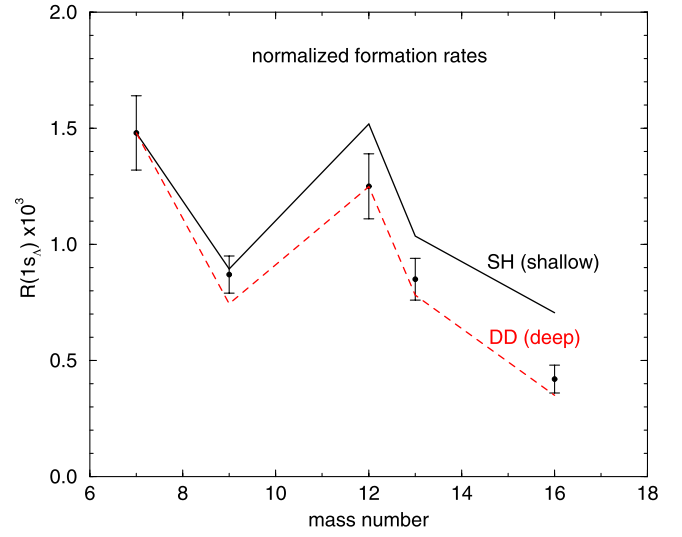### 3.2.1 Theoretical predictions based on ΛN effective interactions

In various calculations, the Λ single-particle potential V_Λ is obtained via a folding procedure from G-matrix ΛN

Fig. 12. Comparison between $1s_\Lambda$ formation capture rates from FINUDA [90] and DWIA calculations normalized to the $1s_\Lambda$ formation rate of $^7_\Lambda$Li for shallow (SH) and deep (DD) K^- nuclear potentials. From ref. [92].

Fig. 11. Formation probabilities from FINUDA (a) and cross-section from E336 [4] (b) for bound states. In (c) the ratio between the two is shown. From ref. [90].

interactions based on free-space YN potential. G-matrix calculations in nuclear matter at normal densities based on the Nijmegen soft-core (NSC97, ESC04 and ESC08) YN potentials [16] can reasonably reproduce the depth of the Λ-nucleus potential, $\mathrm{Re}\,V_\Lambda(\rho_0) \sim -30\,\mathrm{MeV}$, determined phenomenologically and (especially for the "a" version of the ESC08 potential) the Λ binding energies for the s_Λ, p_Λ, d_Λ, etc., single-particle states in medium and heavy Hypernuclei [15] (this is the case, for instance, of $^{89}_\Lambda$Y, see fig. 9). In ref. [93], a ΛN G-matrix interaction is used in a α-α-Λ three-body calculation of $^9_\Lambda$Be. The ΛN-ΣN coupling was introduced effectively. The main purpose was to study the central, spin-independent ΛN interaction by the $B_\Lambda(^9_\Lambda$Be$)$ binding energy. The experimental value of $B_\Lambda(^9_\Lambda$Be$)$ could be reproduced for different versions of the

bare potentials (NSC97, ESC04 and ESC08) by fixing the nuclear Fermi momentum of the ΛN G-matrix interaction to give the experimental Λ binding energy in $^5_\Lambda$He, without the need of any additional ΛNN three-body force. Calculations of the Λ single-particle potential [94] have also been performed via nuclear matter ΛN G-matrices derived from a $SU(6)$ quark model [80]: these calculations tend to overestimate the potential depth at normal density.

Other many-body calculations based on Nijmegen YN potentials were carried out within the extended Skyrme-Hartree-Fock model (a review of these calculations is given in ref. [23]). The adopted YN G-matrix interactions were obtained in a Bruekner-Hartree-Fock approach. The calculations with the NSC89 and NSC97f potentials provided s, p, d, etc., Λ single-particle energies which compare well with data.

In addition, low-momentum ΛN effective interactions $V^\Lambda_{\mathrm{low}\,k}$ have been constructed in ref. [95] starting from Nijmegen bare potentials. In ref. [96] $V^\Lambda_{\mathrm{low}\,k}$ effective interactions have been applied for predicting the momentum and density dependence of the Hypernuclear Λ-nucleus single-particle potential in Hartree-Fock approximation. Reasonable results for $\mathrm{Re}\,V_\Lambda(\rho_0)$ have been obtained for bare NSC97 and chiral effective field theory [76] ΛN interactions, while the use of NSC89 potentials (Juelich potentials of ref. [75]) has led to a strong underestimation (overestimation) of $\mathrm{Re}\,V_\Lambda(\rho_0)$.

Effects beyond the mean field such as three-body interactions and two-body interactions with strangeness exchange are also relevant in Hypernuclei. The ΛNN three-body force is an important ingredient to investigate the structure of Λ-Hypernuclei, especially in light systems. This is due to the ΛN-ΣN strong coupling, which is sizable in the nuclear medium [97], and, on the other hand, leads to a non-negligible second-order tensor force in the ΛN interaction. Especially because of the relatively small

Λ-Σ mass difference, $m_\Sigma - m_\Lambda \sim 78$ MeV, in Hypernuclei the ΛN-ΣN coupling is more important than the NN-ΔN coupling in conventional nuclei, where it plays a very small role in binding few-nucleon systems since $m_\Delta - m_N \sim 293$ MeV. Four-body cluster model calculations based on YN NSC97f interactions have demonstrated the relevance of the ΛN-ΣN coupling in $A = 4$ Hypernuclei ($^4_\Lambda$H and $^4_\Lambda$He) structure calculations [98], although the data for the 1^+ excited states binding energies were underestimated. New calculations with the most recent Nijmegen potentials, ESC08, are in progress [93].

Another signal of the ΛN-ΣN coupling probably comes from the observation that in s-wave relative states the Λp interaction is more attractive than the Λn interaction. This follows from a comparison of the experimental Λ binding energies for the ground states and the first excited states in the $A = 4$, $I = 1/2$ doublet, formed by $^4_\Lambda$He and $^4_\Lambda$H (with separations of 0.35 MeV between the ground states and of 0.24 MeV for the excited states, the latter being determined from the γ-ray spectroscopy experiments discussed in sect. 3.3), which implies an important charge symmetry breaking (CSB) for the ΛN interaction. The origin of this CSB is still not known. Also the relevant experimental data, from old measurements, must be taken with some care. A cluster model study on the CSB was performed for $A = 7$ and $A = 8$ iso-multiplets on the basis of the phenomenological information available for $A = 4$ Hypernuclei [93]. The calculation showed that the few existing emulsion data on $A = 7$ and $A = 8$ Hypernuclei may be inconsistent with the large CSB indicated by the $A = 4$ data. New measurements for $A = 4$, 7, 8 Hypernuclei are thus important.

Another important aspect of the ΛN interaction is its spin-dependence. A qualitative indication of the difference between the singlet ($J = 0$) and triplet ($J = 1$) ΛN interactions comes from the comparison of the Λ binding energy in isobar nuclei not related by charge symmetry. For example, $B_\Lambda(^7_\Lambda$Li$)$ is larger than $B_\Lambda(^7_\Lambda$Be$)$ by about 0.42 MeV. The greater B_Λ value corresponds to the Hypernucleus whose nucleons' core has non-zero spin; the above difference can be explained by the effect of the spin-dependent Λ interaction with the unpaired nucleons, a proton and a neutron, in $^7_\Lambda$Li. Moreover, reaction spectroscopy experiments showed for the first time that the spin-orbit splittings of the Λ in Hypernuclei are small (the evidence came from the splitting between the $p_{1/2}$ and the $p_{3/2}$ Λ states in $^{16}_\Lambda$O [48]). However, as we will discuss in sect. 3.3, a complete study of the spin-dependence of the ΛN interaction requires precision experiments which measure the detailed Hypernuclear excitation spectra.

3.3 Structure of p-shell Λ-Hypernuclei from gamma-ray spectroscopy experiments

To have access to the complete information on the spin-dependence of the ΛN interaction, one has to perform experiments with high energy resolution. One needs to observe the de-excitation, caused by the electromagnetic
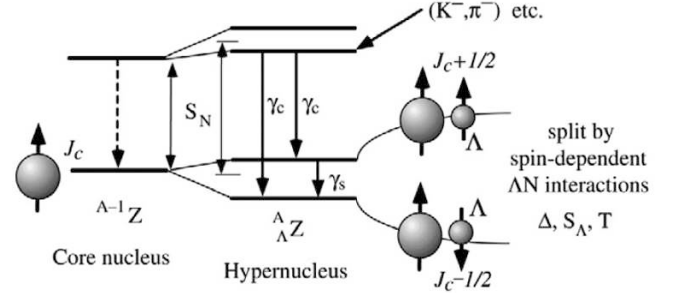
Fig. 13. Schematic low-lying level structure and γ-ray transitions for Λ-Hypernuclei in the weak-coupling limit. With γ_c and γ_s we indicate the core transitions and the Λ spin-flip transitions, respectively. From ref. [4].

interaction, of the Hypernucleus produced in various excited states and study the small (sub-MeV) energy separation of the spin-doublet and the Λ spin-orbit splittings together with the larger non-doublet separations.

γ-ray spectroscopy with Ge detectors is currently the only method to access few tens keV Hypernuclear splittings. Experiments on Hypernuclear γ-ray spectroscopy started in 1998 at KEK by using the Hyperball Ge detector and continued within systematic programs at KEK and BNL with Hyperball and Hyperball2 [4,99–103]: they allowed to measure with a few keV precision various electromagnetic transitions and in some cases their lifetimes and relative intensities.

Studies of the level structure of various p-shell Hypernuclei ($^7_\Lambda$Li, $^9_\Lambda$Be, $^{10}_\Lambda$B, $^{11}_\Lambda$B, $^{12}_\Lambda$C, $^{15}_\Lambda$N and $^{16}_\Lambda$O) with the reactions (π^+, K^+) and (K^-, π^-) have provided us with reliable information on the spin-dependence of the ΛN interaction and some indication on the ΛN-ΣN strong coupling [8,104]. This has been possible by identifying 22 γ-ray transitions for a total of 7 Hypernuclei [4,105], which led to the measure of 9 spin-doublet spacings.

3.3.1 Spin-dependent ΛN effective interaction

In the weak-coupling picture, information on the spin-dependence of the ΛN interaction can be obtained from the energy spacings of the $J = J_c \pm 1/2$ spin-doublets in Λ-Hypernuclei, where the hyperon in the s-shell is coupled to a (ground-state) nuclear core with non-zero spin J_c. A schematic representation of the low-lying Hypernuclear levels together with some γ transition is shown in fig. 13. The weak-coupling scheme turns out to work well for Λ-Hypernuclei with the hyperon in the s state due to the weakness of the ΛN interaction.

Shell-model calculations have been performed to interpret the γ-ray experiments. As input, they use a ΛN interaction parametrized as follows [106–109]:

$$V_{\Lambda N}(r) = V_0(r) + V_\sigma(r)\boldsymbol{s}_N \cdot \boldsymbol{s}_\Lambda + V_\Lambda(r)\boldsymbol{l}_{\Lambda N} \cdot \boldsymbol{s}_\Lambda + V_N(r)\boldsymbol{l}_{\Lambda N} \cdot \boldsymbol{s}_N + V_T(r)S_{12}, \tag{12}$$

where $S_{12} = 3(\boldsymbol{\sigma}_\Lambda \cdot \boldsymbol{r})(\boldsymbol{\sigma}_N \cdot \boldsymbol{r})/r^2 - \boldsymbol{\sigma}_\Lambda \cdot \boldsymbol{\sigma}_N$ is the tensor operator, $\boldsymbol{r} = \boldsymbol{r}_N - \boldsymbol{r}_\Lambda$ is the relative ΛN coordinate, $\boldsymbol{s}_N$
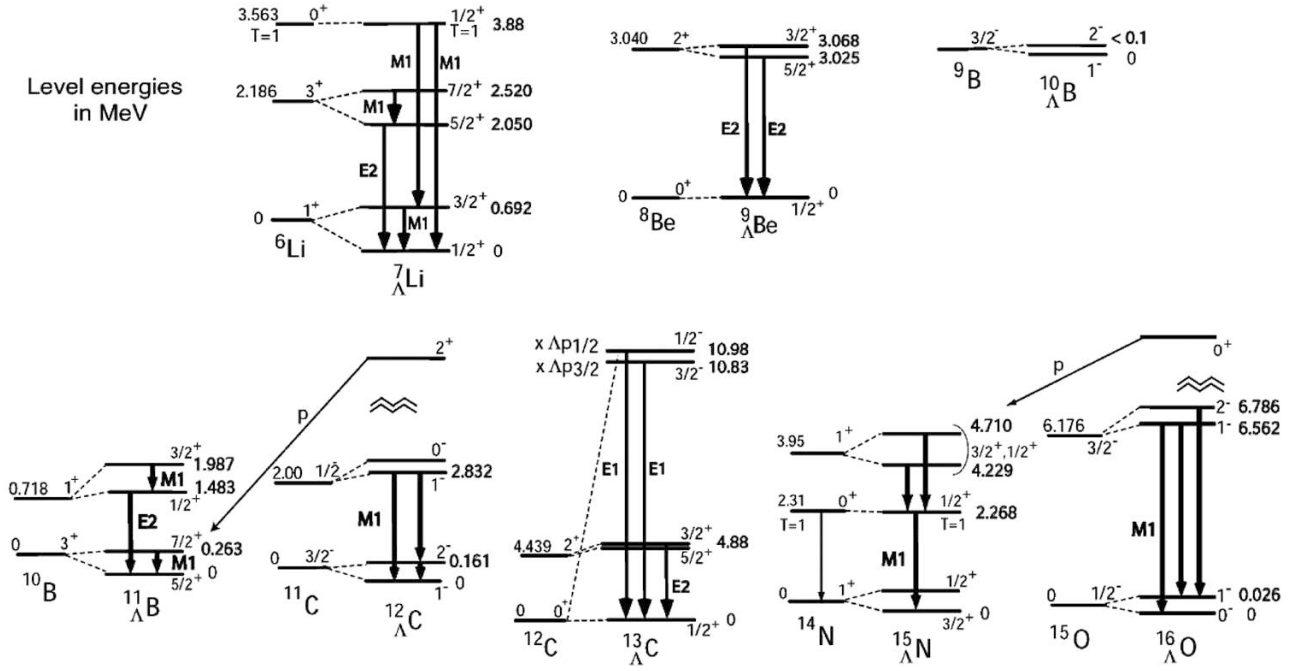
Fig. 14. Energy level scheme and γ-ray transitions observed for p-shell Hypernuclei in γ-ray spectroscopy experiments with Hyperball and Hyperball2 [4] (the scheme for $^{13}_{\Lambda}$C was measured with a NaI detector [112]). Energies are in MeV. From ref. [113].

($\boldsymbol{s}_\Lambda$) is the nucleon (hyperon) spin operator and $\boldsymbol{l}_{\Lambda N}$ is the ΛN relative angular momentum operator. Moreover, $V_0 = (V_1 + 3V_3)/4$ is the spin-averaged central interaction, $V_\sigma = V_3 - V_1$ is the difference between the triplet and the singlet central interactions, $V_\Lambda = V_\Lambda^{\mathrm{LS}} + V_\Lambda^{\mathrm{ALS}}$ ($V_N = V_\Lambda^{\mathrm{LS}} - V_\Lambda^{\mathrm{ALS}}$) is the sum (difference) between the symmetric and antisymmetric spin-orbit interactions and V_T is the tensor interaction. Once Σ degrees of freedoms are introduced, one has similar expressions to eq. (12) for the $\Lambda N \to \Sigma N$ and $\Sigma N \to \Sigma N$ effective interactions.

For the radial form of the effective interaction (12), ΛN multirange Gaussian potentials, *i.e.*, expansions in terms of a number of Gaussian functions, are often used [8]. From these radial potentials, in a shell-model approach one defines two-body matrix elements with respect to a set of ΛN relative wave functions. For Hypernuclei with an s-level Λ coupled with a p-shell nuclear core there are 5 $p_N s_\Lambda$ two-body matrix elements. These matrix elements are determined by 5 radial integrals [8], usually denoted as $\bar{V}$ (spin-independent interaction), Δ (spin-spin interaction), S_Λ (Λ-spin–dependent spin-orbit interaction), S_N (nucleon-spin–dependent spin-orbit interaction) and T (tensor interaction), associated to the V_0, V_σ, V_Λ, V_N and V_T terms of eq. (12), respectively. In a schematic way, for the spin-spin matrix element one has

$$\Delta \sim \int d\boldsymbol{r}\, \phi^\star_{\Lambda N}(\boldsymbol{r}) V_\sigma(r) \phi_{\Lambda N}(\boldsymbol{r}), \qquad (13)$$

where $\phi_{\Lambda N}$ is the ΛN radial relative wave function in the Hypernucleus. Similar equations may be written for the other terms in (12). From eqs. (12) and (13) one thus

obtain the following ΛN effective interaction in the p-shell:

$$V_{\Lambda N} = \bar{V} + \Delta\, \boldsymbol{s}_N \cdot \boldsymbol{s}_\Lambda + S_\Lambda\, \boldsymbol{l}_N \cdot \boldsymbol{s}_\Lambda$$
$$+ S_N\, \boldsymbol{l}_N \cdot \boldsymbol{s}_N + T\, S_{12}. \qquad (14)$$

Note that, since the Λ is in the s level, the angular momentum $\boldsymbol{l}_{\Lambda N}$ in eq. (12) is proportional to the angular momentum $\boldsymbol{l}_N$ in eq. (14).

The spin-independent matrix element $\bar{V}$ contributes to the Λ binding energy B_Λ. It is well known already from emulsion data that B_Λ increases linearly with A with a slope of about $1\,\mathrm{MeV}$/(unit of A) for $6 \lesssim A \lesssim 20$ and then saturates at about $27\,\mathrm{MeV}$ for heavy Hypernuclei. In a first approximation, neglecting three-body ΛNN interaction, for $6 \lesssim A \lesssim 20$ the simple relation $B_\Lambda \sim \bar{V}(A-1)$ (based on a shell-model picture) turns out to fit the data quite well: a value of $\bar{V}$ of about $1\,\mathrm{MeV}$ is thus expected. In the weak-coupling limit of the shell model, the energy separations of the p-shell Hypernuclear spin-doublets for nuclear core states with non-zero spin are linear combinations of the ΛN spin-dependent parameters Δ, S_Λ and T and depend on the ΛN-ΣN coupling (the shell model fixes the coefficients of the different parameters). In the same limit, the parameter S_N does not affect these doublet separations but contributes to the nuclear spin-orbit interaction and is derived from the splittings between Hypernuclear states based on different nuclear core states.

To give an example, the $(3/2^+, 1/2^+)$ and $(7/2^+, 5/2^+)$ spin-doublet splittings in $^7_\Lambda$Li (see fig. 14) are given

by [109]

$$E(3/2^+) - E(1/2^+) = \frac{3}{2}\Delta, \tag{15}$$

$$E(7/2^+) - E(5/2^+) = \frac{7}{6}\Delta + \frac{7}{3}S_\Lambda - \frac{14}{5}T, \tag{16}$$

respectively, in the limit of pure nuclear core configurations, *i.e.*, in the LS coupling limit, which is a fairly good approximation for light systems. However, configuration mixing in the nuclear core modifies these simple relations, and for the above doublet separations ref. [104] found:

$$E(3/2^+) - E(1/2^+) = 1.461\,\Delta + 0.038\,S_\Lambda \\ + 0.011\,S_N - 0.285\,T, \tag{17}$$

$$E(7/2^+) - E(5/2^+) = 1.294\,\Delta + 2.166\,S_\Lambda \\ + 0.020\,S_N - 2.380\,T. \tag{18}$$

A fit of the experimental determinations of the Hypernuclear excitation spectra thus allows one to determine the values of the ΛN interaction parameters. For details on the shell model and the fitting procedure we refer to refs. [8, 109–111]. In the following we only discuss the final results for the fitting parameters and the energy level separations. Figure 14 reports the Hypernuclear level schemes and the transitions determined since 1998 in γ-ray spectroscopy experiments. Three types of γ transitions are possible in the weak-coupling limit: core transitions, Λ spin-flip transitions and Λ inter-shell transitions. Core transitions, denoted by γ_c in fig. 13, connect different doublets and are due to transitions in the nuclear core: it is the case, for instance, of the $E2(5/2^+ \to 1/2^+)$ transition in $^7_\Lambda$Li of fig. 14. Λ spin-flip transitions, denoted by $M1$ in fig. 14 and by γ_s in fig. 13, connect the upper and lower members of the same doublet and are due to a spin-flip of the hyperon spin: it is the case, for instance, of the $M1(3/2^+ \to 1/2^+)$ transition again in $^7_\Lambda$Li. Spin-flip $M1$ transitions are also possible between Hypernuclear doublet members: two of these transitions are shown in fig. 14 for $^7_\Lambda$Li. Finally, in a Λ inter-shell transition, denoted by $E1$ in fig. 14, the hyperon changes the shell orbit from p_Λ to s_Λ: it is the case of the $\Lambda p_{1/2} \to \Lambda s_{1/2}$ and $\Lambda p_{3/2} \to \Lambda s_{1/2}$ transitions in $^{13}_\Lambda$C.

The first experiment with Hyperball, KEK-E419, was performed in 1998 and studied $^7_\Lambda$Li, produced with the (π^+, K^+) reaction. Figure 14 shows that $^7_\Lambda$Li is the best studied Hypernucleus: 5 γ-rays were measured for it, which led to the determination of 2 doublet splittings and 2 core transition separations. Note that here and in the following the considered number of core transition separations does not take into account those ones which are not independent from the other (core or doublet) separations. The $^9_\Lambda$Be Hypernucleus was then studied, again in 1998 and with Hyperball, at BNL-E930 by using the (K^-, π^-) reaction, with the observation of 2 γ-rays, corresponding to 1 doublet splitting and 1 core transition measurement. After including the ΛN-ΣN coupling, a fit of the experimental $^7_\Lambda$Li and $^9_\Lambda$Be energy separations (the 3 doublets and the 3 independent core transitions of fig. 14) has led

to the following determination of the radial matrix elements [104]:

$$A = 7 \div 9:$$
$$\Delta = 0.430, \quad S_\Lambda = -0.015, \quad S_N = -0.390, \quad T = 0.030, \tag{19}$$

where all numbers are in MeV.

$^{13}_\Lambda$C γ-ray measurements were performed in 1998 at BNL-E929 with the (K^-, π^-) reaction and a NaI detector [112], with the determination of 2 Λ inter-shell transitions and 1 core transition. For $^{11}_\Lambda$B, $^{12}_\Lambda$C, $^{15}_\Lambda$N and $^{16}_\Lambda$O Hypernuclei, a total of 6 spin-doublet splittings and 5 core transitions were determined experimentally with the Hyperball and Hyperball2 detectors. $^{15}_\Lambda$N and $^{16}_\Lambda$O were studied at BNL-E930 in 2001 with the (K^-, π^-) reaction and the Hyperball detector, while $^{11}_\Lambda$B and $^{12}_\Lambda$C were investigated in 2005 at KEK-E518 and KEK-E566, respectively, with the (π^+, K^+) reaction and the Hyperball2 detector. The data for Hypernuclei from $^{11}_\Lambda$B to $^{16}_\Lambda$O (the 6 doublets and the $1_2^- \to 0^-$ core transition for $^{16}_\Lambda$O of fig. 14) led to a determination of smaller values for the Λ spin-dependent parameters Δ and T and for the parameter S_N [104]:

$$A = 11 \div 16:$$
$$\Delta = 0.330, \quad S_\Lambda = -0.015, \quad S_N = -0.350, \quad T = 0.024, \tag{20}$$

where again the values are in MeV.

For all the p-shell Hypernuclei, the shell-model approach [104] adopted the following predictions of the ΛN-ΣN interaction parameters

$$\bar{V}' = 1.45, \quad \Delta' = 3.04, \quad S_\Lambda' = S_N' = -0.09, \quad T' = 0.16 \tag{21}$$

(values in MeV), derived from a multirange Gaussian potential fitted to a G-matrix calculation [97] performed with the NSC97a,f potentials.

The γ-ray measurements of the Hypernuclear energy level separations do not allow one to determine the ΛN spin-independent parameter, $\bar{V}$, which is related to the Λ binding energy B_Λ. To have an idea of the magnitude of this parameter, we quote the predictions of the shell-model calculation of ref. [114] derived from the experimental B_Λ values: $\bar{V} = -0.84$ MeV for $^9_\Lambda$Be and $\bar{V} = -1.06 \pm 0.03$ MeV for $^{10}_\Lambda$B, $^{11}_\Lambda$B and $^{12}_\Lambda$C.

The values obtained for the spin-spin parameter Δ inform us that the ΛN singlet central interaction is more attractive than the ΛN triplet central interaction. Some γ transitions turned out to be particularly important in the determination of the various parameters. The $M1(3/2^+ \to 1/2^+)$ transition in $^7_\Lambda$Li mainly contributes to the determination of the spin-spin strength Δ (see eq. (17)). The small value of the Λ-spin-dependent spin-orbit parameter S_Λ and the relatively large value of the nucleon-spin-dependent spin-orbit parameter S_N mean that the symmetric (S^+) and antisymmetric (S^-) spin-orbit interactions have almost the same strength and opposite sign:

$S^+ = (S_\Lambda + S_N)/2 \sim -0.19\,\mathrm{MeV}$ and $S^- = (S_\Lambda - S_N)/2 \sim$ 0.18 MeV. The $3^+ \to 1^+$ transition for the nuclear core in $^7_\Lambda$Li is particularly important to determine S_N. The value of S_Λ mainly originates from the smallness of the $3/2^+$-$5/2^+$ doublet separation, (43 ± 5) keV, in $^9_\Lambda$Be. Information on S_Λ is in principle also given by the spin-orbit splittings of Λ single-particle states, for instance the $(152 \pm 54 \pm 36)$ keV separation between the $(\Lambda p_{1/2})$ and the $(\Lambda p_{3/2})$ states in $^{13}_\Lambda$C. However, a sizable effect of the tensor interaction and a loosely bound p_Λ orbit make it difficult to draw definite conclusions on S_Λ and T starting from the $(\Lambda p_{1/2})$-$(\Lambda p_{3/2})$ spin-orbit splitting [8]. The small tensor parameter T is mainly determined by the small 1_1^--0^- doublet splitting for $^{16}_\Lambda$O, once Δ is fixed from $^7_\Lambda$Li.

The assumption of a mass-independent ΛN interaction is justified for p-shell Hypernuclei if one considers that the rms charge radii of p-shell nuclei is rather constant through the shell. Nevertheless, the spin-dependent parameters of eqs. (19) and (20) exhibit some dependence on the Hypernuclear mass number. However, this is really evident only for the spin-spin parameter: the value of Δ obtained from $^7_\Lambda$Li is considerably larger than the determinations from heavier Hypernuclei. This A-dependence is however not confirmed by calculations of the ΛN interaction parameters based on realistic free-space ΛN potentials [87]. For the future it is thus necessary to clarify the reason of the A-dependence of the shell-model fit.

In table 1 we compare the Hyperball and Hyperball2 experimental data on p-shell level separations (both doublet spacings and core transition separations) with the shell-model predictions of refs. [8,104,114] obtained with the values of eqs. (19), (20) and (21) of the ΛN and ΛN-ΣN interaction strengths. We see that the ΛN-ΣN coupling affects in a non-negligible way the p-shell Hypernuclear spacings, especially the doublet ones. However, we remind the reader that the strongest effect of this coupling has been obtained from the analysis of s-shell Hypernuclei, where its contribution to the 0^+–1^+ doublet splittings in $^4_\Lambda$H and $^4_\Lambda$He is of the same order of the one coming from the spin-spin ΛN interaction [97] and is essential to explain the level structure of all s-shell Hypernuclei. The shell-model calculation well reproduces the data, even for the energy separations not included in the fit, except for the underestimation of a few core transitions separations: the $1/2^+$–$5/2^+$ separation in $^{11}_\Lambda$B and, to a lesser extent, the 1_2^-–1_1^- separation in $^{12}_\Lambda$C and the $3/2^+$–$1/2^+$ separation in $^{13}_\Lambda$C. Apart from these inconsistencies, which deserve further investigation, the spin-dependence of the ΛN effective interaction is rather well understood at present. The interpretation in terms of the shell-model calculation could thus serve to improve the theoretical models of the free-space ΛN interaction.

We conclude this subsection with more detailed comments on the consistency problems arising from the comparison of the shell-model fit results with the γ-ray data. The large value of Δ required in the beginning of the p-shell is unlikely to be simply the effect of a smaller rms radius of the $^7_\Lambda$Li nuclear core size with respect to the other p-shell cores. Given its important role, alternative and improved descriptions of the ΛN-ΣN coupling should be considered in new fits of data. For instance, a contribution of the ΛN-ΣN coupling in the end of the p-shell smaller than the one in the beginning of the p-shell could led to a determination of a value of Δ for $A = 15, 16$ in agreement with the determination for $A = 7, 9$ [105]. In addition, new shell-model calculations should explore the effect of an expansion of the nuclear core basis states beyond the p-shell configurations [114]. A second major problem consists in the fact that for Hypernuclei in the middle of the p-shell (specifically, $^{11}_\Lambda$B, $^{12}_\Lambda$C and $^{13}_\Lambda$C) the parameter S_N does not supply a sufficiently attractive contribution to reproduce the observed splittings for some core transitions (see table 1), which indeed would require more negative values of S_N than in eq. (20). The explicit inclusion of three-body ΛNN interactions, induced by the ΛN-ΣN coupling, could also help in solving this second problem [114], thanks to an antisymmetric spin-orbit ΛNN interaction contribution that has the same effect of the parameter S_N on the core transition splittings. We note that double one-pion–exchange ΛNN interactions were already included long ago [106–108], in an approximated way, in shell-model analyses of the Λ binding energies of p-shell Hypernuclei. Additional experimental γ-ray data for p-shell Hypernuclei will also play an essential role for a deeper understanding of the ΛN interaction.

3.3.2 Theoretical predictions based on ΛN interactions

Various theoretical approaches, mainly based on the YN Nijmegen meson-exchange potentials, have been used for modeling the in-medium ΛN interaction and thus study the structure of Hypernuclei.

In table 2 we summarize the results obtained with some of these approaches for the parametrization of eq. (14) of the ΛN effective interaction in the case of $^7_\Lambda$Li. The reported results are obtained from fixed radial forms of the potentials using Woods-Saxon wave functions and Gaussian [69] or Yukawa [115] representations of ΛN G-matrix elements. The $\Lambda\Sigma$ contributions adopted in the calculations, not shown in the table, are dominated by the central matrix elements $\bar{V}'$ and Δ'. For comparison, in the table we also report the phenomenological values of the parameters determined with the shell-model fit (19) of the γ-ray data. Despite the 6 versions of the NSC97 potentials predict values of the Δ parameter in a rather wide range, only NSC97f provides a prediction for Δ in agreement with the shell-model fit. Unlike the ESC04a interaction, the ESC08a one strongly underestimates the phenomenological Δ value. All the Nijmegen interaction models are inconsistent with the phenomenological determination of the S_Λ and S_N parameters: this indicates that these models need to be revised. Finally, the Nijmegen potentials can approximately explain the small parameter T of the phenomenological determination. The smallness of T is expected on the basis of the absence of π and ρ exchange at tree level in the ΛN interaction.

Table 1. Energy contributions (in keV) to the spacings for the spin-doublet and the core transition separations obtained with the shell-model fitting procedure of refs. [8, 104, 114]. The transitions are indicated with $J^P_{\mathrm{upper}} \to J^P_{\mathrm{lower}}$, J^P_{upper} (J^P_{lower}) indicating the spin-parity of the upper (lower) energy level. The contributions to the energy separation originating from the ΛN-ΣN coupling are indicated in the $\Lambda\Sigma$ column. The theoretical energy separations ΔE^{th} are compared with the experimental determinations ΔE^{exp}. Small contributions from the energies of admixed core states are not shown. ΔE_c is the contribution of the nuclear core level spacing; the values of ΔE_c are taken from experiment.

	Transition	Δ	S_Λ	S_N	T	$\Lambda\Sigma$	ΔE_c	ΔE^{th}	ΔE^{exp}
$^7_\Lambda$Li	$3/2^+ \to 1/2^+$	628	-1	-4	-9	72	0	693	692
$^7_\Lambda$Li	$7/2^+ \to 5/2^+$	557	-32	-8	-71	74	0	494	471
$^7_\Lambda$Li	$5/2^+ \to 1/2^+$	77	17	-288	33	4	2186	2047	2050
$^7_\Lambda$Li	$1/2^+_1 \to 1/2^+_0$	418	0	-82	-3	-23	3565	3883	3877
$^9_\Lambda$Be	$3/2^+ \to 5/2^+$	-14	37	0	28	-8	0	44	43
$^{10}_\Lambda$B	$2^- \to 1^-$	188	-21	-3	-26	-15	0	120	< 100
$^{11}_\Lambda$B	$7/2^+ \to 5/2^+$	339	-37	-10	-80	56	0	267	264
$^{11}_\Lambda$B	$3/2^+ \to 1/2^+$	424	-3	-44	-10	61	0	475	505
$^{11}_\Lambda$B	$1/2^+ \to 5/2^+$	-88	-19	391	-38	5	718	968	1483
$^{12}_\Lambda$C	$2^- \to 1^-$	175	-12	-13	-42	61	0	153	162
$^{12}_\Lambda$C	$1^-_2 \to 1^-_1$	117	17	309	20	49	2000	2430	2834
$^{13}_\Lambda$C	$3/2^+ \to 1/2^+$	-11	22	203	-22	1	4439	4630	4880
$^{15}_\Lambda$N	$1/2^+_1 \to 3/2^+_1$	244	34	-8	-214	44	0	99	> -100
$^{15}_\Lambda$N	$3/2^+_2 \to 1/2^+_2$	451	-2	-16	-10	65	0	507	481
$^{15}_\Lambda$N	$1/2^+; T = 1 \to 3/2^+_1$	86	11	-6	-71	-57	2313	2274	2268
$^{15}_\Lambda$N	$1/2^+_2 \to 3/2^+_1$	-208	13	473	-67	-16	3948	4120	4229
$^{16}_\Lambda$O	$1^-_1 \to 0^-$	-123	-20	1	188	-33	0	23	26
$^{16}_\Lambda$O	$2^- \to 1^-_2$	207	-21	1	-41	92	0	248	224
$^{16}_\Lambda$O	$1^-_2 \to 0^-$	-207	-2	524	170	-70	6176	6582	6562

Table 2. Predictions for the spin-dependent parameters of the ΛN effective interaction (14), in MeV, for $^7_\Lambda$Li obtained from free-space baryon-baryon interactions. The NSC97f prediction is from ref. [69], the ESC04a and ESC08a are from ref. [115], while the phenomenological (Phen.) values are from eq. (19).

Model	Δ	S_Λ	S_N	T
NSC97f	0.421	-0.149	-0.238	0.055
ESC04a	0.381	-0.108	-0.236	0.013
ESC08a	0.146	-0.074	-0.241	0.055
Phen.	0.430	-0.015	-0.390	0.030

We now comment on the general results obtained with the approaches based on free-space baryon-baryon interactions for the energy level splittings in various Hypernuclei. In the next paragraphs we describe the individual frameworks. For $^4_\Lambda$H, $^4_\Lambda$He and $^7_\Lambda$Li, some calculations reproduce the central parameters $\bar{V}$ and Δ as well as the ΛN-ΣN coupling adopted in the shell-model fits. For some of the

YN interaction models, also the predictions for the tensor parameter T agree fairly well with the phenomenological determinations of eqs. (19) and (20). However, although these models provide a wide range of results for the ΛN spin-dependent channels, for most of them the (43 ± 5) keV separation for the $(3/2^+, 5/2^+)$ spin-doublet in $^9_\Lambda$Be and/or the $(152 \pm 54 \pm 36)$ keV splitting between the $(\Lambda p_{1/2})$ and $(\Lambda p_{3/2})$ states in $^{13}_\Lambda$C are overestimated: this implies the incapacity to reproduce the phenomenological value of the parameter S_Λ. This is well established for approaches based on the NSC97 and ESC04 potentials [104, 116], which underestimate the antisymmetric spin-orbit parameter $S^- = (S_\Lambda - S_N)/2 \sim 0.18$ MeV of the shell-model fit; only with the use of the most recent extended soft-core potential, ESC08, which was designed to explain a large amount of Hypernuclear data in addition to NN and YN scattering data [15, 16], one can obtain an improvement of the predictions for the small Λ-nucleus spin-orbit splittings observed experimentally. Nevertheless, the ESC08 potentials predict an incorrect ordering for the ground state spin-doublets in $^{11}_\Lambda$B and $^{12}_\Lambda$C.

Cluster models based on one-range Gaussian ΛN effective interactions have been used since the '80s [117]. Other cluster models were based on G-matrix effective interactions [118] derived from free-space YN meson-exchange potentials (NSC89 [68] and the JA and JB versions of the Juelich potential [73]): none of these approaches could reproduce the $(1^+, 0^+)$ splitting observed for the ground-state spin-doublet in $^4_\Lambda$H and $^4_\Lambda$He. Only with the introduction of the NSC97 Nijmegen potentials [69], cluster model calculations based on YN G-matrix interactions [119] could reproduce the above spin-doublet separation: six versions, a to f, were introduced for the NSC97, each one of them predicting a different ΛN spin-spin interaction, with the NSC97a and NSC97f versions giving the best description of the spin-doublet separations in $^4_\Lambda$H and $^4_\Lambda$He.

After the advent of γ-ray spectroscopy, studies of the spin-dependence of the effective ΛN interaction were performed for p-shell Hypernuclei by comparing the obtained data with three- and four-body calculations based on the Gaussian expansion method, by adopting NSC97, ESC04 and ESC08 YN interactions [93, 120–123].

In ref. [123] the ΛN spin-spin interaction was initially set to reproduce the 1.04 MeV $(1^+, 0^+)$ doublet spacing observed in $^4_\Lambda$H, while the Λ-spin–dependent spin-orbit interaction was fixed to reproduce the 43 keV $(3/2^+, 5/2^+)$ doublet spacing observed in $^9_\Lambda$Be. Then, by an $\alpha+p+n+\Lambda$ four-body cluster model based on a ΛN G-matrix obtained from the NSC97f potential, for the $(3/2^+, 1/2^+)$ and $(7/2^+, 5/2^+)$ spin-doublets in $^7_\Lambda$Li the authors predicted 690 keV and 460 keV separation energies, respectively, in good agreement with the γ-ray data reported in table 1. In ref. [123] it was thus demonstrated that it is possible to explain consistently the ground- and excited-state spin-doublet splittings in $^7_\Lambda$Li and the $(3/2^+, 5/2^+)$ spin-doublet splitting in $^9_\Lambda$Be. However, a similar $3\alpha + \Lambda$ four-body calculation strongly overestimated the spin-orbit splittings of the Λ single-particle states observed in $^{13}_\Lambda$C [88].

In ref. [93] the spin-orbit part of the ΛN interaction was studied with a few-body cluster model for $^9_\Lambda$Be $(2\alpha + \Lambda)$ and $^{13}_\Lambda$C $(3\alpha + \Lambda)$ based on a ΛN G-matrix interaction derived form ESC08 potentials. The G-matrix interaction was fixed to reproduce the empirical values of the Λ binding energies in $^5_\Lambda$He, $^9_\Lambda$Be and $^{13}_\Lambda$C; this required the consideration of density-dependent effects for the interacting hyperon, which were introduced by a phenomenological ΛNN three-body interaction. The best result for the $(3/2^+, 5/2^+)$ spin-doublet separation in $^9_\Lambda$Be was predicted to be of 80 keV with the ESC08a potential (instead of the experimental (43 ± 5) keV), largely improving the predictions based on NSC97 potentials thanks to a less attractive symmetric spin-orbit interaction and a more repulsive antisymmetric spin-orbit interaction. Unfortunately, the best prediction for the splitting between the $(\Lambda p_{1/2})$ and $(\Lambda p_{3/2})$ states in $^{13}_\Lambda$C was obtained as 400 keV (instead of the experimental $(152 \pm 54 \pm 36)$ keV), again with the ESC08a potential.

We can thus summarize the preformed G-matrix calculations as follows. The approaches based on the NSC97

and ESC04 interactions can reproduce the spin-spin strength of the ΛN interaction derived with the shell-model analysis of γ-ray spectroscopy experiments, but strongly overestimate the Λ single-particle spin-orbit splittings. Only with the most recent version of the Nijmegen extended soft-core potentials, ESC08 [16], this overestimation problem can be partially solved [15].

Quark-based models of the baryon-baryon interaction were considered in Hypernuclear structure calculations. Some of them can improve in a natural way the prediction of the (empirically large) antisymmetric spin-orbit strength $S^- = (S_\Lambda - S_N)/2$ of the ΛN effective interaction (they reproduce the small Λ spin-orbit separations) [124–126], but others still have problems in reproducing the phenomenological value of S^- [17, 127].

The Kyoto-Niigata group [17, 127] describes the free-space YN interaction within the QCD inspired spin-flavour $SU(6)$ quark model supplemented by an effective-meson exchange potential (containing scalar, pseudoscalar and vector mesons) acting between quarks. An $\alpha + \alpha + \Lambda$ three-cluster Faddeev calculation was performed in ref. [127] for $^9_\Lambda$Be. While the energies of the $1/2^+$ ground state and the $3/2^+$ excited state could be reproduced, the obtained $(3/2^+, 5/2^+)$ splitting overestimated the γ-ray measurement by a factor ranging from 3 to 5. The authors attribute this result to an inappropriate description of the p-wave ΛN-ΣN coupling. The Λ spin-orbit interaction strengths were previously examined in ref. [94], by a ΛN G-matrix interaction derived from the $SU(6)$ quark model, in a calculation for symmetric nuclear matter at normal density. The results imply a ratio S_Λ/S_N between the Λ-spin–dependent spin-orbit and the nucleon-spin–dependent spin-orbit effective parameters ranging from 0.08 and 0.25, which surely improves the predictions of meson-exchange approaches but overestimates the phenomenological ratio, $S_\Lambda/S_N \sim 0.04$.

Hypernuclear structure studies were also performed with the quark-meson coupling (QMC) model. Within this framework, which is similar to the self-consistent quantum hadrodynamics, the baryon-baryon interactions are described by the exchange of scalar and vector mesons, while the $SU(6)$ quark model is adopted for the bound nucleons and hyperon, with a baryon internal structure modeled by the MIT bag. The first application of the QMC model was done in ref. [124], where the exchange of σ, ω and ρ mesons and a phenomenological ΛN-ΣN coupling were taken into account. Hypernuclei with closed-shell nuclear core were considered. This approach naturally incorporates a weak spin-orbit interaction for the Λ in a Hypernucleus, due to the explicit quark structure of the Λ given by the $SU(6)$ quark model (where non-strange mesons only couple to light u and d quarks of baryons and the Λ spin is carried by the s quark), but the predicted Λ single-particle energies overestimates the experimental data. More recently [125], the QMC model was improved by including the self-consistent effect of the scalar field on the one-gluon–exchange hyperfine interaction between quarks, that in free space leads to the Δ-N and Σ-Λ mass splittings. With the hyperfine interaction, the MIT bag model can reproduce the Δ-N mass

splitting. A single-particle shell model was used and Hypernuclei with closed-shell nuclear cores were considered. Again, the QMC calculation leads to a natural explanation of the small Λ spin-orbit splittings. Moreover, improved predictions are obtained for the Λ single-particle energies, although the calculation tends to overbind the less bound Λ states.

A quark mean field (QMF) model, in which baryons are described by the constituent quark model, was instead considered in ref. [126]. Again, baryon-baryon interactions were given by σ, ω and ρ meson exchange, where the mesons coupled exclusively to light quarks and Hypernuclei consisting of a closed-shell nuclear core were studied. Small Λ spin-orbit splittings were obtained, while the experimental Λ single-particle energies were underestimated. The QMF and QMC models are rather similar to each other. The underbinding in the QMF model and the overbinding in the QMC model can be explained by the different Λ-σ coupling adopted in the two calculations.

Only a recent calculation, with a relativistic energy density functional based on $SU(3)$ chiral effective field theory, predicted both Λ single-particle energies and Λ-nucleus spin-orbit splittings which compare well with data [128]. In $SU(3)$ chiral effective field theory, the ΛN interaction is described as follows: the longest range interactions are described by two-pion exchange diagrams including an intermediate ΣN state and by one-kaon exchange, while the short-range interactions are described by contact terms (scalar and vector mean fields contributions). The mechanism responsible for the improvement of ref. [128] is an almost complete cancellation between the short-range scalar and vector mean fields contributions and the intermediate-range terms originated by the two-pion exchange.

Finally, we note that studies on the spin-dependence of the ΛN interaction can also be performed by mesonic weak decay spectra measurements, which allows one to assign the spin-parity to the decaying Hypernucleus (spin-parity of Hypernuclear states are normally assigned by angular correlations and polarizations of the emitted γ-rays). This will be discussed in sect. 4.2.2.

3.3.3 New-generation γ-ray experiments at J-PARC

The next generation of γ-ray experiments is planned at J-PARC with the Hyperball-J detector, by using intense and pure K^- beams from the 50 GeV proton synchrotron [4, 103]. Improved data for s- and p-shell Hypernuclei ($^4_\Lambda$He, $^{10}_\Lambda$B, and $^{11}_\Lambda$B) are expected from the E13 experiment. They will help in clarifying the present inconsistencies of the shell-model approach. The experiment on the $1^+ \to 0^+$ transition energy in $^4_\Lambda$He is designed to determine the real effect of the charge symmetry breaking in the ΛN interaction. Then, sd-shell Hypernuclei will be considered by E13, starting from $^{19}_\Lambda$N, which requires a shell-model approach with 8 $(sd)s_\Lambda$ additional matrix elements, up to $A = 30$, by using the (K^-, π^-) production reaction. The experiments will allow one to determine the

spin-parity of the observed states and the size of sd-shell Hypernuclei, thus also sheding light on the A-dependence of the spin-spin parameter Δ. At a later stage of E13, studies on medium and heavy Hypernuclei (up to $A = 208$), again with the (K^-, π^-) reaction, could provide information on the p-wave ΛN interaction, through the observation of inter-shell $E1(p_\Lambda \to s_\Lambda)$ transitions.

3.4 Impurity nuclear physics

In a Λ-Hypernucleus the Pauli principle allows the hyperon to occupy the s-level of the Λ-nucleus mean-field potential, thus making the hyperon a good probe of the inner part of the Hypernucleus. A Λ hyperon bound in a Hypernucleus can thus be considered as an impurity for the nuclear core. Some properties of the nuclear core, for instance the size, shape, shell structure and collective motion, are modified by the presence of the strange baryon.

3.4.1 The Λ glue-like role

Theoretical studies predicted a contraction of the nuclear core caused by the presence of the Λ [122,129]: the hyperon plays a glue-like role in Hypernuclei.

This shrinking effect was then confirmed experimentally when the KEK-E419 γ spectroscopy experiment showed that the Λ makes smaller a loosely-bound nuclear core such as ^{6}Li [130]. This was possible by the observation of the $E2(5/2^+ \to 1/2^+)$ core transition in $^7_\Lambda$Li (see fig. 14). The corresponding reduced transition probability was derived from the lifetime (measured with the Doppler shift attenuation method) of the $5/2^+$ Hypernuclear state and the branching ratio of the $E2(5/2^+ \to 1/2^+)$ transition, with the result $B(E2;^7_\Lambda \text{Li}, 5/2^+ \to 1/2^+) = 3.6 \pm 0.5^{+0.5}_{-0.4} \, e^2 \, \text{fm}^4$.

$B(E2)$ turns out to be approximately proportional to the fourth power of the nuclear core radius. The $E2(5/2^+ \to 1/2^+)$ Hypernuclear transition is induced by the $E2(3^+ \to 1^+)$ transition of the ^{6}Li core. In the weak-coupling limit, ref. [122] introduced a size factor

$$S = \left[\frac{9}{7} \frac{B(E2;^7_\Lambda \text{Li}, 5/2^+ \to 1/2^+)}{B(E2;^6 \text{Li}, 3^+ \to 1^+)} \right]^{1/4}, \qquad (22)$$

which provides the change in the ^{6}Li core radius due to the addition of the hyperon. From a previous measurement of $B(E2;^6 \text{Li}, 3^+ \to 1^+)$ a sizable shrinkage of the ^{6}Li core was obtained: $S = 0.81 \pm 0.04$. This result agrees with the cluster model calculation of ref. [129]. By a more recent $\alpha + n + p + \Lambda$ cluster model [122] one can interpret the above size factor as a reduction of the distance between the α cluster and the center of mass of the np pair by $(19 \pm 4)\%$, while the shrinkage of the distance between the proton and the neutron of the np pair is negligible.

The nuclear core compression effect is expected also in heavier Hypernuclei, although generally at a lower level [131,132]. In ref. [133,134] a $3\alpha + \Lambda$ four-body model

was applied to the study of the shrinkage in the nuclear core of $^{13}_{\Lambda}$C. This Hypernucleus has a ^{12}C core with peculiar characteristics: the 0^+_1 ground state has a shell-model–like compact structure, while the 2^+_2 excited state at $E_x = 7.65$ MeV has a loosely bound 3α structure which can hardly be explained in a shell-model approach. Because of this behaviour, for the $^{13}_{\Lambda}$C$(1/2^+_1)$ and ^{12}C(0^+_1) ground states the presence of the hyperon implies a few % shrinkage for the distance between two α clusters, but for $^{13}_{\Lambda}$C$(5/2^+_2)$ a significant compression of the α-α distance, of about 28%, is predicted with respect to the same distance in the ^{12}C(2^+_2) core [133,134].

3.4.2 Deformation of Λ-Hypernuclei

Various open-shell nuclei are deformed in the ground state. This deformation results in the existence of quadrupole transitions and rotational spectra which can be observed experimentally.

Relativistic mean field models [135], non-relativistic Skyrme-Hartree-Fock approaches [136–138] and the framework of non-relativistic nuclear energy density functionals [132] were applied to the study of the collective motion and the deformation properties of Hypernuclei.

The relativistic mean field model of ref. [135] predicted a strong reduction of the deformation for ^{12}C and some of the sd-shell nuclear cores in the presence of a Λ hyperon in the s-orbit: in some cases, the change is from an oblate shape (this is the case of ^{28}Si) to a spherical shape (the ^{28}Si core in the $^{29}_{\Lambda}$Si Hypernucleus). This result does not seem to be corroborated by other studies, for instance by the Skyrme-Hartree-Fock approach of ref. [138], which found that the gross features of the potential energy surfaces in the (β, γ) plane (β and γ being the quadrupole deformation parameters) remain basically unaltered by the addition of the Λ.

These predictions need empirical confirmation. Future γ-ray spectroscopy experiments at J-PARC could help in clarifying the deformation properties and the collective motions in Hypernuclei by measuring the $B(E2)$ values and possibly the excitation energies in the rotational (and vibrational) bands.

3.4.3 Neutron-rich Λ-Hypernuclei

It is well known, from experiments with radioactive nuclear beams, that nuclei produced near the neutron (proton) drip line exhibit a neutron (proton) halo, *i.e.*, a density of weakly bound valence neutron(s) (proton(s)) which extend well beyond the radius of the nuclear core. Neutron-rich nuclei are particularly important in nuclear astrophysics, as they play a role in neutron capture nucleosynthesis.

Since most of the Hypernuclear experiments performed to date with kaon, pion and electron beams used targets of stable nuclei, spectroscopy study of Hypernuclei has been mainly restricted to systems in the β-stability valley.

B $^4_{\Lambda}$He 2.39 Λ	$^5_{\Lambda}$He 3.12 Λ	◇ $^6_{\Lambda}$He 4.18 n 0.17 xxx	◇ $^7_{\Lambda}$He 5.23 n 2.92 halo	$^8_{\Lambda}$He 7.16 n 1.49 xxx	♠ $^9_{\Lambda}$He (8.5) n 3.9 halo
$^3_{\Lambda}$H 0.13 Λ	◇ $^4_{\Lambda}$H 2.04 Λ	$^5_{\Lambda}$H (3.1) n -1.8 xxx	♠ $^6_{\Lambda}$H (4.2) 2n -5 xxx	♠ $^7_{\Lambda}$H (5.2) 3n 0.4 xxx	

Fig. 15. Part of the light Λ-Hypernuclei chart with binding energy and particle instability threshold in MeV. Unstable cores are indicated by xxx; Λ-Hypernuclei produced by the (K^-, π^0) reaction, the so-called mirror Hypernuclei, are indicated by ◇; Λ-Hypernuclei produced by the (K^-, π^+) reaction, neutron-rich Hypernuclei, by ♠. From ref. [139].

However, as a consequence of the modification of nuclear structure introduced by the presence of the hyperon, one can expect that particle bound neutron-rich (proton-rich) Hypernuclei exist even for large (small) values of the neutron to proton ratio [139]. Note that we do not consider as "neutron-rich" Hypernuclei obtained by reaction (4), that are better defined as "mirror" Hypernuclei of those obtained by reactions (2) and (3). Figure 15 shows some of the predicted neutron-rich Hypernuclei.

Various neutron-rich Hypernuclei are in principle accessible to the (K^-, π^+) and (π^-, K^+) double charge-exchange reactions using stable targets. In particular, thanks to the glue-like role of the hyperon, one could produce a Hypernucleus with a neutron halo even by starting from a weakly unbound nuclear core (see the cases of fig. 15 indicated by xxx), thus possibly extending the neutron drip line beyond the standard limits of neutron-rich nuclei [140,141]. We remind that this effect was predicted already in the early days of Hypernuclear physics [142].

Hypernuclei with a neutron or proton excess are suitable systems for studying the ΛN effective interaction, the Λ-nucleus mean field potential and the behaviour of the Λ hyperon in a low density neutron or proton halo matter.

Relevant contributions of the coherent ΛN-ΣN coupling and the associated ΛNN three-body interaction are predicted for Hypernuclei with a neutron excess [143, 144]. Studies of neutron-rich Hypernuclei could thus put constraints on the ΛNN interaction. In a shell-model approach within a perturbation theory framework, the second-order $\Lambda N \rightarrow \Sigma N \rightarrow \Lambda N$ interaction is found to provide a contribution to the spin-doublet separations in neutron-rich Hypernuclei which is of the same order of magnitude of the contribution from the direct $\Lambda N \rightarrow \Lambda N$ interaction [144]. Moreover, the Σ hyperon ad-

mixture in neutron-rich Hypernuclei is found to increase with the isospin, *i.e.* with the neutron excess number $N - Z$ [97, 143, 145], thus it could reveal particularly important also in studies of the composition and equation of state of neutron stars; in various hadronic models, these compact stars indeed have a substantial content of neutrons as well as hyperons, but particularly the effect of Σ hyperons is not yet known.

Since the valence nucleons in Hypernuclei with neutron and proton halos are weakly bound, these systems can be conveniently described by resorting to cluster models. Halo and skin structures were studied theoretically in refs. [146, 147] with a three-body cluster model for $A = 6$ ($^6_\Lambda$He and $^6_\Lambda$Li) and $A = 7$ ($^7_\Lambda$He and $^7_\Lambda$Li and $^7_\Lambda$Be) Hypernuclei. The $\alpha + \Lambda + N$ three-body ($\alpha + \Lambda + N + N$ four-body) model reproduces the binding energies of the ground states observed in $A = 6$ ($A = 7$) Hypernuclei. The case of $^6_\Lambda$He is particularly interesting, as its ground state is only $0.17\,\mathrm{MeV}$ below the $^5_\Lambda$He $+ n$ threshold and the ^{5}He core is unbound. For $^6_\Lambda$He the calculation indeed predicted a structure consisting of three distinct layers of matter: an α nuclear core, a Λ skin and a neutron halo. The halo of the valence neutron is more extended than in the neutron halo nucleus ^{6}He, the Λ density distribution clearly extends beyond the α core but is well confined within the volume of the neutron halo. Analogous three layer structure of matter are exhibited for $A = 7$ Hypernuclei.

Two-body reactions in which neutron-rich Hypernuclei could be produced are

$$K^- + {}^A Z \rightarrow {}^A_\Lambda(Z-2) + \pi^+, \qquad (23)$$
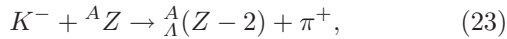
induced on nuclear targets by stopped or in flight K^-, and

$$\pi^- + {}^A Z \rightarrow {}^A_\Lambda(Z-2) + K^+ \qquad (24)$$
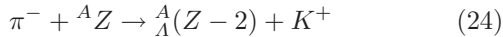
by in flight π^-. In these double charge-exchange reactions, two protons of the target nucleus are replaced by a Λ and a neutron.

The simplest description of the above reactions is a two-step process on two different protons of the same nucleus, converting them into a neutron and a Λ, with the additional condition that the final nuclear system is bound. For (23) it should mean a $K^- p \rightarrow \Lambda \pi^0$ reaction followed by $\pi^0 p \rightarrow n\pi^+$, for (24) a $\pi^- p \rightarrow n\pi^0$ reaction followed by $\pi^0 p \rightarrow K^+ \Lambda$ or $\pi^- p \rightarrow K^0 \Lambda$ followed by $K^0 p \rightarrow K^+ n$. Another mechanism which was proposed [97, 145] is a single-step process such as $\pi^- pp \rightarrow K^+ \Sigma^- p \rightarrow K^+ \Lambda n$ via the Σ admixture in the Λ-Hypernuclear state due to the coherent $\Sigma^- p \rightarrow \Lambda n$ coupling. Owing to these features, both single-step and two-step processes are expected to occur at a much lower rate than the production of normal Λ-Hypernuclei by means of the usual two-body reactions. According to the study of ref. [148], the two-step production reactions have a larger cross-section than the one-step mechanisms even when considering their largest theoretical prediction for the Σ^- admixture probability. Instead, the analysis of ref. [149] favoured one-step reactions over two-step reactions and larger Σ^- admixture probabilities.

The first experimental attempt to produce neutron-rich Hypernuclei by the reaction (23) was carried out at
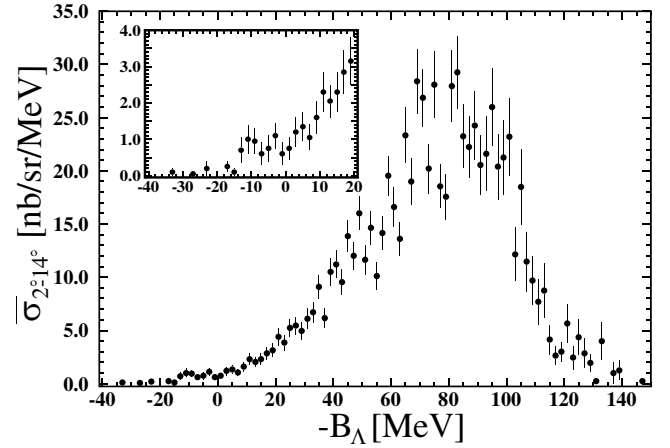
Fig. 16. Binding-energy spectrum in the (π^-, K^+) reaction on a ^{10}B target at $1.2\,\mathrm{GeV}/c$. In the inset an expanded view containing the Λ bound region is shown. From ref. [152].

KEK [150]. An upper limit (per stopped K^-) was obtained for the production of $^9_\Lambda$He, $^{12}_\Lambda$Be and $^{16}_\Lambda$C Hypernuclei: the results are in the range $(0.6$–$2.0) \cdot 10^{-4}/K^-_{\mathrm{stop}}$, while the theoretical predictions [151] for $^{12}_\Lambda$Be and $^{16}_\Lambda$C lie in the interval $(10^{-6}$–$10^{-7})/K^-_{\mathrm{stop}}$, that is at least one order of magnitude lower than the experimental results and three orders of magnitude smaller than the usual $(K^-_{\mathrm{stop}}, \pi^-)$ one-step reaction rates on the same targets $(10^{-3}/K^-_{\mathrm{stop}})$.

Another KEK experiment [152] reported the observation of $^{10}_\Lambda$Li with the (π^-, K^+) double charge-exchange reaction on a ^{10}B target. This experiment was affected by much less background than in the previous one with the $(K^-_{\mathrm{stop}}, \pi^+)$ reaction. Figure 16 shows the binding energy spectrum obtained in ref. [152]: the production cross-section (in nb/sr/MeV) is drawn *versus* the Λ binding energy (in MeV). The results are not directly comparable with theoretical calculations [148] since no discrete structure was observed and the production cross-section was integrated over the whole bound region ($0\,\mathrm{MeV} < B_\Lambda < 20\,\mathrm{MeV}$). Significant production yields were observed in the Λ bound state region, with an integrated cross-section of $11.3 \pm 1.9\,\mathrm{nb/sr}$ ($5.8 \pm 2.2\,\mathrm{nb/sr}$) for a $1.2\,\mathrm{GeV}/c$ ($1.05\,\mathrm{GeV}/c$) incident momentum and a scattering angle in the laboratory system ranging from $2°$ to $14°$. Unfortunately, no clear peak was observed in the Λ bound region, possibly due to the low statistics and resolution. The above results were obtained by assuming that all counts recorded in the Λ bound state region correspond to the formation of the $^{10}_\Lambda$Li Hypernucleus. The measured cross-sections are in disagreement with the theoretical study of ref. [148], which favoured a two-step production mechanism, but agree with the prediction of ref. [149] in the case of a $1.2\,\mathrm{GeV}/c$ incoming momentum. By assuming a dominant one-step production mechanism and a Σ admixture probability of the order of 0.1%, ref. [149] could reproduce the magnitude of the $^{10}_\Lambda$Li production spectrum obtained in ref. [152].

A further attempt to observe neutron-rich Hypernuclei by means of the reaction (23), with K^- at rest, was done at the DAΦNE collider at LNF by the FINUDA experiment [153], on ^{6}Li and ^{7}Li targets. The limited data sample collected during the first run period of the experiment was used to look for the production rates per stopped K^- for $^6_\Lambda$H and $^7_\Lambda$H; the inclusive π^+ spectra from ^{6}Li and ^{7}Li targets were analyzed in momentum regions corresponding, through momentum and energy conservation, to the B_Λ values predicted in ref. [139, 145]. Due to the strong contribution of the background reactions:

$$K^- + p \rightarrow \Sigma^+ + \pi^-$$
$$\downarrow$$
$$n + \pi^+, \qquad (25)$$

and

$$K^- + pp \rightarrow \Sigma^+ + n$$
$$\downarrow$$
$$n + \pi^+, \qquad (26)$$
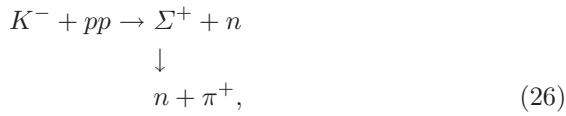
which give the main contributions of the inclusive π^+ spectra for absorption of stopped K^- on nuclei, and to the limited statistics, only upper limits could be evaluated, leading to the values $(2.5 \pm 0.4_{\text{stat}}{}^{+0.4}_{-0.1\,\text{syst}}) \cdot 10^{-5}/K^-_{\text{stop}}$ and $(4.5 \pm 0.9_{\text{stat}}{}^{+0.4}_{-0.1\,\text{syst}}) \cdot 10^{-5}/K^-_{\text{stop}}$ for the production of, respectively, $^6_\Lambda$H and $^7_\Lambda$H; also the production rate of $^{12}_\Lambda$Be was obtained, $(2.0 \pm 0.4_{\text{stat}}{}^{+0.3}_{-0.1\,\text{syst}}) \cdot 10^{-5}/K^-_{\text{stop}}$, lowering by a factor ~ 3 the previous determination of ref. [150].

Very recently, the full statistics collected by FINUDA on ^{6}Li was analyzed by requiring a coincidence between the π^+ signaling the formation of $^6_\Lambda$H and its subsequent decay into ^{6}He $+ \pi^-$ within a very tight energy window [154]. This approach was possible thanks to the very good energy resolution and instrumental stability of the detectors. Three events were found, corresponding unambiguously to the formation and subsequent decay of $^6_\Lambda$H. A very careful analysis showed that they could not be ascribed to possible instrumental or physical backgrounds, mainly coming from reaction (25). The mass of $^6_\Lambda$H deduced from the above events was found to be 5801.4 ± 1.1 MeV, corresponding to a Λ binding energy $B_\Lambda = 4.0 \pm 1.1$ MeV with respect to the mass of the unbound ^{5}H$+\Lambda$. Figure 17 shows the energy level scheme for the ground state of $^6_\Lambda$H deduced by FINUDA. We remark that the measured value of B_Λ compares well with the theoretical evaluation of ref. [139] but is lower by about 1.8 MeV than the theoretical prediction $B_\Lambda = 5.8$ MeV for the ^{5}H $+ \Lambda$ choice of the zero energy level obtained in refs. [97, 145], which also included the effect of the ΛN-ΣN coupling. Note that this 1.8 MeV disagreement is close to the value attributed in refs. [97, 145] to the contribution to $B_\Lambda(^6_\Lambda$H) arising from the ΛNN three-body interaction resulting from the coherent Λ-Σ mixing. From this experiment, which provides the first observation of the hyperheavy hydrogen $^6_\Lambda$H, we may not conclude that the ΛNN force is negligible, but only that its influence looks lower than predicted. The production rate of $^6_\Lambda$H, assuming a 50% probability for the
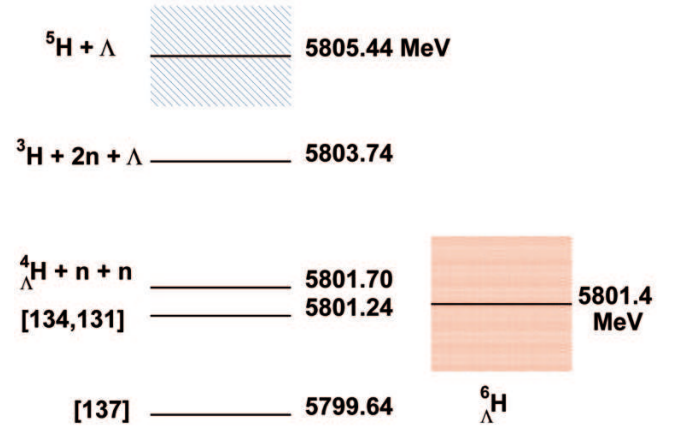
Fig. 17. Energy level scheme for $^6_\Lambda$H ground state. The red box represents the error on the mass mean value obtained by FINUDA [154], the blue box indicates the width of ^{5}H.

$^6_\Lambda$H $\rightarrow \pi^- + {}^6$He decay, fully justified by the measured decay rates of neighbour or similar Hypernuclei ($^4_\Lambda$H, $^7_\Lambda$Li), is $(5.9 \pm 4.0) \cdot 10^{-6}$/stopped K^-, about three orders of magnitude lower than the production rates for bound Λ-Hypernuclei, as expected.

An experiment to produce $^6_\Lambda$H via the (π^-, K^+) reaction on ^{6}Li at 1.2 GeV was recently approved at J-PARC [155] and should run as quickly as the Laboratory will be restored to operation. The expected resolution is 2.5 MeV, on a sample of about 100 events. Further results on neutron- and proton-rich Hypernuclei are expected from the HypHI experiment at GSI and FAIR by using stable heavy-ion beams and rare isotope beams [156].

3.5 In-medium hyperon properties

Hyperon properties in Hypernuclei are influenced by the nuclear medium. A partial restoration of chiral symmetry in the nuclear medium or even a partial quark deconfinement may affect Λ properties such as the mass, size and magnetic moment for an hyperon located in the inner core of the Hypernucleus.

3.5.1 The Λ magnetic moment

The magnetic moment of hadrons provides interesting information on the internal structure of these particles. The magnetic moment of a Hypernucleus is an important observable which is sensitive to the spin and angular momentum structure of this many-body system, to the spin-dependent part of the ΛN effective interaction and to the Σ admixture in the Hypernucleus.

The magnetic moment operator of a Hypernucleus in the weak-coupling limit is given by

$$\boldsymbol{\mu} = \frac{1}{2} \int \mathrm{d}^3 \boldsymbol{r} \, \boldsymbol{r} \times \left[\boldsymbol{j}_c^{\text{em}}(\boldsymbol{r}) + \boldsymbol{j}_\Lambda^{\text{em}}(\boldsymbol{r}) \right], \qquad (27)$$

where $\boldsymbol{j}_c^{\mathrm{em}}$ and $\boldsymbol{j}_\Lambda^{\mathrm{em}}$ are the electromagnetic currents of the nuclear core and of the hyperon, respectively. One can rewrite this definition as

$$\begin{aligned}
\boldsymbol{\mu} &\equiv \boldsymbol{\mu}_c + \boldsymbol{\mu}_\Lambda = (g_c \boldsymbol{J}_c + g_\Lambda \boldsymbol{J}_\Lambda) \mu_N \\
&= \left[g_c \boldsymbol{J} + (g_\Lambda - g_c) \boldsymbol{J}_\Lambda \right] \mu_N,
\end{aligned} \tag{28}$$

$\boldsymbol{J}_c$ ($\boldsymbol{J}_\Lambda$) being the total spin of the nuclear core (hyperon), $\boldsymbol{J} = \boldsymbol{J}_c + \boldsymbol{J}_\Lambda$ the total spin of the Hypernucleus, g_c (g_Λ) the effective g-factor of the nuclear core (hyperon) and μ_N the nuclear magneton.

Already the simple-quark model reproduces quite well the magnetic moments of the stable (non-strange and strange) baryons by fixing the magnetic moments of the u, d and s quarks to reproduce the magnetic moments of neutron, proton and Λ. For free Λ and Σ hyperons the measured values of the g-factors are: $g_\Lambda^{\mathrm{free}} = -1.226 \pm 0.008$, $g_{\Sigma^+}^{\mathrm{free}} = 4.916 \pm 0.020$, $g_{\Sigma^-}^{\mathrm{free}} = -2.320 \pm 0.050$ and $g_{\Sigma\Lambda}^{\mathrm{free}} = 3.22 \pm 0.16$ (the last being the $\Sigma^0 \to \Lambda$ transition g-factor for the $\Sigma^0 \to \gamma\Lambda$ electromagnetic transition) [157]. The change in the quark structure of a Λ bound in the inner core of a Hypernucleus is expected to introduce a variation in the Λ magnetic moment compared to the above free-space value.

Before discussing the important question of a possible deviation of g_Λ in Hypernuclei from the $g_\Lambda^{\mathrm{free}}$ value, a related issue has to be clarified: it concerns the role played by the nuclear core in the Hypernuclear magnetic moments. Relativistic mean field models neglecting the ΛN-ΣN coupling predicted Hypernuclear magnetic moments which are very close to the (non-relativistic) Schmidt values [158] (the Schmidt value is $\mu = \mu_\Lambda = g_\Lambda \mu_N / 2 = -0.613 \mu_N$ for a Hypernucleus with a closed-shell nuclear core and an s-level Λ). Reference [159] showed that the global core contribution to the Hypernuclear magnetic moment is vanishingly small ($\mu_c \sim 0$) due to the large contribution of the $\omega\Lambda\Lambda$ tensor coupling induced by the ω vector field, which almost cancels the $\omega\Lambda\Lambda$ vector coupling contribution.

However, in the presence of an important Σ admixture in Hypernuclei and due to large differences among the above free Λ and Σ hyperons g-factors, the value of the Hypernuclear magnetic moments are expected to deviate from the Schmidt values. This is especially true for p-shell and heavier odd-A Hypernuclei with isospin 1 nuclear cores, as demonstrated in the qualitative treatment of ref. [160] based on perturbation theory. For instance, $\mu(^{15}_\Lambda\mathrm{C}) \sim \mu_\Lambda + \sqrt{2}\,\beta\,\mu_{\Sigma\Lambda}$, where β is evaluated in the range from $+0.03$ to $+0.07$ in ref. [160]. According to this result, the deviation of the Hypernuclear magnetic moments from the Schmidt values can be interpreted as a signal of the relevance of the ΛN-ΣN coupling. More quantitative studies within the shell model are needed to settle this important issue.

The effect of the meson exchange currents on the magnetic moment of light Hypernuclei is studied in ref. [161] with an effective Lagrangian method in the harmonic oscillator shell model. The calculation takes into account the NN and ΛN π- and K-exchange currents and the nuclear core polarization. For $^5_\Lambda\mathrm{He}$ the magnetic moment is reduced in absolute value by 9% from the Schmidt value

$\mu_\Lambda = -0.613\,\mu_N$: $\mu(^5_\Lambda\mathrm{He}) = \mu_\Lambda + 0.054\mu_N = -0.559\,\mu_N$. This change is originated only by the isoscalar ΛN K-exchange currents, as both the Λ and the ^{4}He nuclear core have isospin 0. Smaller variations from the Schmidt values are instead obtained for the ($^6_\Lambda\mathrm{He}$, $^6_\Lambda\mathrm{Li}$) isodoublet, despite in these cases the magnetic moment also has an isovector part.

We come now to the question concerning the in-medium Λ g-factor, g_Λ. Since it is impossible to directly measure g_Λ, due to the very short lifetime for spin precession in a magnetic field, an indirect method consists in the measurement of the reduced transition probability $B(M1)$ for the strengths of Λ spin-flip transitions $M1$, which in the weak-coupling limit is related to g_Λ by [109]

$$B(M1) = \frac{3}{8\pi} \frac{2J_{\mathrm{down}}+1}{2J_c+1} (g_\Lambda - g_c)^2 \mu_N^2, \tag{29}$$

where J_{down} is the spin of the lower state of the doublet.

$B(M1)$ can be obtained experimentally by measuring the γ-ray energy for the Λ spin-flip transition ΔE and the lifetime τ of the excited state (determined with the Doppler shift attenuation method): $B(M1) \propto 1/(\tau\,\Delta E^3)$. A few measurements of $B(M1)$ have already been performed, at BNL and KEK, but with insufficient accuracy to establish the modification of the Λ g-factor in a Hypernucleus: the most precise determination is indeed $g_\Lambda = -1.04 \pm 0.41$ [103].

A future measurement of $B(M1)$ for the $M1(3/2^+ \to 1/2^+)$ transition in $^7_\Lambda\mathrm{Li}$ will be carried out at J-PARC E13 with a 5% level accuracy [103]. In order to study the density- and isospin-dependence of g_Λ, experiments on the $B(M1)$ values will be performed at J-PARC for heavier Hypernuclei. In experiments with heavy-ion beams such as HypHI [156] Hypernuclei are produced with large velocities and fly in free-space for tens of centimeters before decaying, thus enabling direct measurements of the Λ magnetic moment by observing the spin precession in strong magnetic fields.

4 Weak decay of Hypernuclei

Λ-Hypernuclei are produced in the ground state or in an excited state of the Λ-particle neutron-hole configuration. When a Λ-Hypernucleus is excited above the particle emission threshold it decays dominantly by the strong interaction, through nucleon or cluster emission; the remaining strange nuclear system then de-excites to its ground state via electromagnetic transitions.

A Λ-Hypernucleus in the ground state decays to non-strange nuclear systems through the mesonic (MWD) or non-mesonic (NMWD) weak decay mechanisms.

In MWD the Λ hyperon decays into a nucleon and a pion in the nuclear medium, similarly to the weak decay mode in free space

$$\Lambda_{\mathrm{free}} \to p + \pi^- + 37.8\,\mathrm{MeV} \qquad (B.R. = 64.2\%), \tag{30}$$

$$\Lambda_{\mathrm{free}} \to n + \pi^0 + 41.1\,\mathrm{MeV} \qquad (B.R. = 35.8\%), \tag{31}$$

in which the emitted nucleon carries a momentum $q \approx 100\,\text{MeV}/c$, for a decay at rest, corresponding to a Q-value of about $40\,\text{MeV}$. The branching ratios of the channels (30) and (31) are consistent with the empirical $\Delta I = 1/2$ rule, valid for all non-leptonic strangeness-changing processes, like the Σ hyperon decay and pionic K decays.

Inside a Hypernucleus the binding energy of the Λ (~ 3 MeV for $^5_\Lambda$He, $\sim 11\,\text{MeV}$ for $^{12}_\Lambda$C, $\sim 27\,\text{MeV}$ for $^{208}_\Lambda$U) further reduces the energy available to the final-state particles; MWD is thus suppressed in Hypernuclei with respect to the free-space decay due to the Pauli principle, since the momentum of the emitted nucleon is by far smaller than the nuclear Fermi momentum ($k_F \sim 270\,\text{MeV}/c$) in all nuclei except for the lightest, s-shell ones.

In NMWD the Λ-Hypernucleus decays through processes which involve a weak interaction of the constituent Λ with one or more core nucleons. If the pion emitted in the hadronic vertex $\Lambda \to \pi N$ is virtual, then it can be absorbed by the nuclear medium, resulting in a non-mesonic decay of the following types:

$$\Lambda n \to nn \quad (\Gamma_n), \tag{32}$$

$$\Lambda p \to np \quad (\Gamma_p), \tag{33}$$

$$\Lambda NN \to nNN \quad (\Gamma_2), \tag{34}$$

where in parentheses we indicate their decay rates. The channels (32) and (33) are globally indicated as *one-nucleon induced decays*, in particular one-neutron induced decay (32) and one-proton induced decay (33). The channel (34), referred to as *two-nucleon induced decay* and suggested in ref. [162], can be interpreted by assuming that the pion from the weak vertex is absorbed by a pair of nucleons (np, pp or nn), correlated by the strong interaction. Note that the non-mesonic processes can also be mediated by the exchange of mesons more massive than the pion.

The NMWD mode is possible only in nuclei; the Q-value of the elementary reactions (32)–(34) ($\sim 175\,\text{MeV}$) is high enough to avoid any Pauli blocking effect, being the outgoing nucleons momenta as high as $\sim 420\,\text{MeV}/c$ for the one-nucleon induced process and $\sim 340\,\text{MeV}/c$ for a two-nucleon induced process, if the available energy is equally distributed among the final-state particles; the final nucleons thus have a great probability to escape from the nucleus. Indeed, the NMWD dominates over the MWD for all but the s-shell Hypernuclei and only for very light systems ($A \leq 5$) the two decay modes are competitive.

The NMWD is a four-fermion, $\Delta S = 1$, baryon-baryon weak interaction and represents the only practical way to obtain information on the weak process $\Lambda N \to nN$, which represents the first extension of the weak, $\Delta S = 0$, $NN \to NN$ interaction to the strange baryon sector. We recall that the short Λ lifetime prevents from producing hyperon targets or beams of suitable intensity and only scarce ΛN scattering data are presently available. Moreover, the four-body $\Delta S = 1$ interactions (32) and (33) are the best candidate to allow the investigation of the parity-conserving part of the weak interaction, which is completely masked by the strong component in the $NN \to NN$ reaction [6,163,164].

The total decay width of a Λ-Hypernucleus $\Gamma_\text{T}(^A_\Lambda Z)$ is given by the sum of the mesonic and the non-mesonic decay widths,

$$\Gamma_\text{T} = \Gamma_\text{M} + \Gamma_\text{NM}, \tag{35}$$

where the first term can be further expressed as the sum of the decay widths for the emission of negative (Γ_{π^-}) and neutral (Γ_{π^0}) pions,

$$\Gamma_\text{M} = \Gamma_{\pi^-} + \Gamma_{\pi^0}, \tag{36}$$

and the second term can be written as the sum of the one-nucleon (Γ_1) and two-nucleon induced (Γ_2) decay widths,

$$\Gamma_\text{NM} = \Gamma_1 + \Gamma_2, \tag{37}$$

with $\Gamma_1 = \Gamma_p + \Gamma_n$. The total decay width $\Gamma_\text{T}(^A_\Lambda Z)$ is expressed in terms of the Hypernuclear lifetime by

$$\Gamma_\text{T}(^A_\Lambda Z) = \hbar/\tau(^A_\Lambda Z). \tag{38}$$

The decay observables which can be directly measured are the Hypernucleus lifetime, τ_Λ, the branching ratios and decay rates for the MWD channels, Γ_{π^-} and Γ_{π^0}, and the spectra of both MWD and NMWD light decay products (pions and nucleons). The total non-mesonic rate can thus be obtained in an indirect way as $\Gamma_\text{NM} = \Gamma_\text{T} - \Gamma_\text{M}$. The partial decay rates for the NMWD channels (Γ_n, Γ_p, Γ_{np}, etc.) cannot be directly determined from the data due to presence of final state interactions (FSI) for the weak decay nucleons; these rates are not quantum-mechanical observables [165]. Each one of the possible elementary non-mesonic decays occurs in the nuclear environment, thus subsequent FSI modify the quantum numbers of the weak decay nucleons and new, secondary nucleons are emitted as well. Daughter nuclei can hardly be detected.

A complete review of the experimental results and theoretical models describing the weak decay of Hypernuclei before 1990 can be found in ref. [166]; more recent review papers on the results obtained from 1990 on and on the development of the theoretical interpretations can be found in refs. [6,163,164,167].

4.1 Hypernuclear lifetimes

Among the experimental observables, the Hypernucleus lifetime τ, or equivalently the total decay width Γ_T, is the one which can be measured with the highest accuracy and is free from all the distortions and corrections connected to final-state interactions of the emitted particles. Being an inclusive quantity, for its measurement one has to detect any of the possible products of either mesonic or non-mesonic decays (typically protons from non-mesonic decays) as a function of time and then fit the observed distribution with an exponential decay law. The lifetime measurement, moreover, is the starting point for obtaining, from the measured MWD branching ratios, the Γ_NM rates as well as the ratio Γ_n/Γ_p between the one-neutron induced and the one-proton induced NMWD rates. However, one has to note that for the determination of the

the "experimental" value of Γ_n/Γ_p (the same occurs for the individual rates Γ_n and Γ_p) one needs 1) a measurement of the nucleon emission spectra and 2) a theoretical model of nucleon FSI. Indeed, the nucleon spectra turn out to strongly depend on these FSI effects: the experimental Γ_n/Γ_p ratio must thus be obtained by a deconvolution of the nucleon FSI effects contained in the measured spectra.

The weak decay of Λ-Hypernuclei has been studied since their discovery in 1953; the first determinations of τ date back to the sixties when visualizing techniques were used, by exposing, mainly, photographic emulsions and, less frequently, LH_2 filled bubble chambers to the worldwide available K^- beams (Argonne ZGS, BNL AGS and Bevatron). In emulsions, Hypernuclei were produced as Hyperfragments on the emulsion components, like hydrogen, carbon, nitrogen, oxygen, silver and bromine, with a strong prevalence of the lighter nuclei; in bubble chambers, the helium was an active target. Only events with unambiguously identified Hyperfragments were used to determine the lifetime, and both decays at rest and in flight were considered. A maximum-likelihood method was developed in order to extract $\tau(^A_\Lambda Z)$ from the measurements of moderation times or flight times of the selected events. Meager samples (1–30 events each) were typically collected due to the reduced intensity of the beams and, consequently, big statistical errors were obtained, ranging from 15% to more than 100%. Lifetimes of s-shell Hypernuclei were measured for $^3_\Lambda$H [168–172], $^4_\Lambda$H [168,169,173], $^4_\Lambda$He [169] and $^5_\Lambda$He [168–170,173]. The obtained values are all consistent with the free Λ lifetime within errors.

Obvious limitations of the visualizing techniques prevent from performing a complete study of the Hypernucleus decay. Concerning lifetime, since the decay timing information cannot be obtained, only indirect determinations of $\tau(^A_\Lambda Z)$ were available, as discussed before. Moreover, concerning the study of the different decay modes, visualizing devices are blind to neutral particles, such as γ and neutrons; thus the study was limited to the weak decay modes with charged particles in the final state. Finally, the apparatuses were not able to count the number of formed Hypernuclei, obstructing the determination of the decay branching ratios.

As described in sect. 2.2, starting from the eighties, the counter experiments at BNL AGS and at the 12 GeV PS at KEK opened a new era in the study of Hypernuclear weak decay, overcoming the difficulties of the visualizing techniques. These experiments used the (K^-, π^-) and (π^+, K^+) reactions to copiously produce Hypernuclei, thus allowing to perform coincidence measurements for the study of weak decay. Actually, the counter experiments dedicated to Hypernuclear spectroscopy started in the early seventies, but high intensity K^-/π^+ beams and large solid angle spectrometers for the high statistics (10^3–10^5 events) production of Λ-Hypernuclei, needed for the decay coincidence study, became available only about ten years later.

For a direct determination of the lifetime it is necessary to measure the delay in the emission of the decay products from the ground state of the Hypernucleus. In counter experiments this normally requires the detection of a particle emitted in the decay in coincidence with a particle originating from the production reaction, π^- or K^+, which tags the formation of the ground state or of a low-lying excited state which is known to de-excite to the ground state by electromagnetic decay; in this way it is possible to identify uniquely the decaying system.

The typical apparatuses operated both at BNL and at KEK and consisted of double spectrometers to measure with high precision the momenta of the incident (K^- or π^+) and scattered (π^- or K^+) mesons and to determine, by simple momentum and energy conservation, the mass of the produced Hypernuclear state. Around the reaction target, coincidence detectors were placed to detect charged and neutral decay particle and to measure the decay time; for charged particle the identification was performed by specific ionization and range measurements and the energy was determined by the range, while for neutrals both the identification and the energy evaluation were performed by time-of-flight measurements. For lifetime determination, the formation time was given by a fast detector located in front of the target and the delay in the emission was determined by the difference between decay and formation time. Lifetimes of light- and medium-A Hypernuclei were extracted from the measured delay time distributions for $^4_\Lambda$H [174, 175], $^4_\Lambda$He [175–177], $^5_\Lambda$He [178, 179], $^9_\Lambda$Be [178], $^{11}_\Lambda$B [178, 180, 181], $^{12}_\Lambda$C [178–181], $^{27}_\Lambda$Al, $^{28}_\Lambda$Si and $_\Lambda$Fe [181], with statistical errors ranging from 3% to 20%. BNL and KEK values, when available for the same Hypernuclear specie, are consistent within errors.

Figure 18, from ref. [181], shows the mass number dependence of Hypernuclear lifetime for $A < 60$ obtained by various counter experiments at BNL and KEK (open and full circles), from 1985 to 2000. The data indicate that the lifetime is quite stable from light- to medium-A Hypernuclei and is rather constant above $A = 20$, at ~ 210 ps, which corresponds to $\sim 80\%$ of the free Λ lifetime. This smoothly decreasing behaviour is sign of an anticorrelation between the MWD and NMWD modes: the rapid decrease of the MWD, due to Pauli blocking effect, seems to be balanced by the NMWD decay mechanism and the asymptotic behaviour of the lifetime indicates the presence of saturation properties for the $\Lambda N \rightarrow nN$ weak interaction for increasing A analogous to those of the finite range NN strong interaction.

In fig. 18 the dot-dashed line shows calculations by ref. [182], where $2\pi/\rho$ and $2\pi/\sigma$ exchange terms were added to the one-pion–exchange potential for the NMWD. These calculations reproduce Hypernuclear lifetime quite well, with a slight underestimation of the saturation value for $^{28}_\Lambda$Si and $^{56}_\Lambda$Fe. The dashed line represents lifetime calculations by ref. [183] in which a one-pion–exchange model approach is used, including the two-nucleon induced decay modes on strongly correlated np pairs, to evaluate lifetimes for medium and heavy Hypernuclei from $^{12}_\Lambda$C to $^{208}_\Lambda$Pb. The calculated values are short by a 30–40% with respect to the measured values. By a detailed study of baryon-baryon short-range correlations and of the Λ wave function in Hypernuclei, which was obtained by
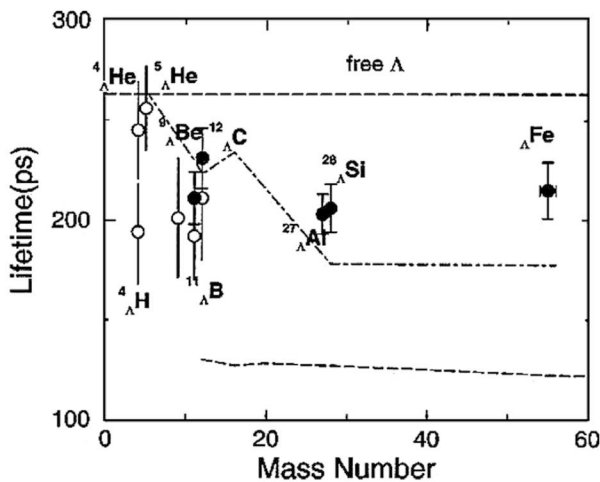
Fig. 18. Mass-dependence of Hypernuclear lifetime, from ref. [181]. Full circles: KEK-E307 results [181]; open circles: previous counter experiments [175, 178, 180]. The dot-dashed line shows the calculations by ref. [182] and the dashed line the calculations by ref. [183].

reproducing the data on s and p Λ level energies with Woods-Saxon Λ-nucleus potentials, this calculation was then updated in ref. [184]. It was then possible to reproduce the experimental lifetimes from light to heavy Hypernuclei (see fig. 4 in ref. [184]).

In the medium mass region, a lifetime measurement was also performed for $A \sim 16$ Hypernuclei ($_{\Lambda}^{16}Z$) [59] using a 2.1 GeV/nucleon ^{16}O beam and a polyethylene target at the LBL Bevalac. The trigger for the Hypernuclear production was given by the decay at rest of K^+ produced together with K^- by the associated production reaction, but the Hypernuclear mass spectrum could not be reconstructed and the Hypernuclear specie could not be identified. The lifetime was extracted from the recoil distance distribution, measured by spark chambers. Only 22 decay events were identified and the lifetime from the maximum-likelihood fitting of the recoil distance was ~ 86 ps, much smaller than the value for neighbor $_{\Lambda}^{12}$C and $_{\Lambda}^{28}$Si reported in fig. 18. The datum on ^{16}O, however, is very likely to be affected by some experimental drawback due to the presence of a very strong instrumental background and, unfortunately, the measurement was not repeated so that no reliable value is available for $A = 16$.

More recently, the lifetimes of $_{\Lambda}^{3}$H and $_{\Lambda}^{4}$H were obtained with relativistic ions beams (^{3}He, ^{4}He, ^{6}Li and ^{7}Li ions with 2.2–5.1 GeV/nucleon energies) and ^{12}C targets, at JINR [60]; the technique used at LBL was improved by means of a more effective trigger system for the Hypernuclear production, able to identify events in which a Hypernucleus of charge Z decays, through π^- MWD, to a nucleus with charge $Z + 1$. The lifetime was determined by measuring the Hypernucleus recoil distance distribution with a Ne streamer chamber. Values of 220 ps were reported for $_{\Lambda}^{4}$H with errors at 20% level and of 240 ps for $_{\Lambda}^{3}$H with errors of $\sim 60\%$.

In the heavy mass region, Hypernucleus lifetimes have been measured, between 1985 and 2003, in electroproduc-

tion experiments on ^{209}Bi targets [185], in low momentum $\bar{p}$-A annihilation at CERN on ^{209}Bi [56] and ^{238}U [57] targets and in p-A collisions at COSY on ^{197}Au, ^{209}Bi and ^{238}U [58] targets. For heavy Hypernuclei the application of direct timing methods, as adopted for light and medium-A systems, is not feasible due to the huge background of the light particles produced. This problem is overcome by detecting heavy fragments from fission processes, induced by the high energy release due to the NMWD of the heavy Hypernucleus. A common feature of both $\bar{p}$-A and p-A reactions is that the Hypernucleus is produced with a sizable energy, in particular for high-momentum p-A collisions and recoils over a distance of some mm before decaying; the recoil shadow method [186], used in nuclear physics for the measurement of fission isomers, can thus be applied with good sensitivity to evaluate the lifetime. The determination, however, is not direct and depends strongly on theoretical models which describe the time evolution of the system during the reaction: transport calculations for the initial fast non-equilibrium phase and statistical calculations for the final evaporation phase. These calculations give the mass (A) and charge (Z) distribution of the Hypernuclei which undergo delayed fission together with their individual, A- and Z-dependent, velocity distribution in the laboratory frame; a fit of the recoil distance distribution allows to extract the lifetime.

Following this procedure, from $\bar{p}$-A experiments $\tau(_{\Lambda}^{A}Z)$ values of 180 ± 40 ps have been obtained for the ^{209}Bi target and 130 ± 30 ps for ^{238}U target [57], and from p-A experiments values of 130 ± 20 ps for ^{197}Au target, 161 ± 16 ps for ^{209}Bi target and 138 ± 18 ps for ^{238}U target were reported [58]. It must be noted that, unlike (K^-, π^-) and (π^+, K^+) reactions, both $\bar{p}$-A and p-A production mechanisms do not allow to identify the decaying system; the A and Z values of the produced Hypernuclei are, indeed, obtained from the calculated (Z, A) distributions which span over 35–40 mass units and 8–10 charge units [58]. Considering the overlapping of the individual (A, Z) distributions for the three targets used in p-A experiments, it is possible to average over them to obtain a mean lifetime for Hypernuclei with masses $A \sim 180$–225, with a dispersion in charge $\Delta Z \sim 3$ for fixed A, of $\tau(_{\Lambda}^{Z}A) = 145 \pm 11$ ps, while, by averaging over the results obtained in $\bar{p}$-A experiments on Bi and U, the value $\tau(_{\Lambda}^{Z}A) = 143 \pm 36$ ps can be quoted.

The value from p-A collisions, figuring a global 8% error, shows an uncertainty level only a factor two worse than that obtained in recent very high statistics (π^+, K^+) experiments on $_{\Lambda}^{12}$C at KEK [179], 212 ± 6 ps. Both $\bar{p}$-A and p-A averaged values represent about the 55% of the free Λ lifetime and suggest a very different behaviour of the Λ when bound in heavy nuclei with respect to the case of medium-A nuclei. Indeed, if in nuclei with $A = 12$–56 the lifetime seems to saturate at about the 80% of the free particle value, indicating the short-range nature of the weak decay interaction, the presence of a much more massive nuclear system seems to produce a stronger interaction of the Λ with the core nucleons, as if the range of the weak four-body NMWD interaction could increase considerably between $A = 56$ and $A = 180$ to include large

part of the nucleons. On the other hand, in $\bar{p}$-A and p-A collision experiments, the production of Λ-Hypernuclei is not identified by the detection of a particle which undoubtedly signs the formation of a bound strange nuclear system; the complexity of systems with 180–225 components leads to suppose the presence of other interaction mechanisms which could open for some threshold A value, higher than 60 mass units, and could explain the strong enhancement of the interaction rate for $A > 180$. It is worth to remind, however, that the lifetime determination is indirect and relies on calculated, model dependent, A, Z and velocity distributions, which take into account the interaction dynamics during all the development of the process. The big difference between the lifetime values obtained with the recoil shadow method and those obtained directly in (K^-, π^-) and (π^+, K^+) reactions suggests that the first method could be affected by sources of systematic errors, possibly connected to the nature of the process which causes the fission, that need to be carefully considered; anyway, further experimental work in the $A \sim 200$ region is necessary, with an explicit tagging of the strange nuclear system formation.

4.2 Mesonic weak decay

In MWD, light- and medium-A Hypernuclei are converted to non-strange nuclei through the reactions

$$^A_\Lambda Z \rightarrow {}^A(Z+1) + \pi^- \quad (\Gamma_{\pi^-}), \tag{39}$$

$$^A_\Lambda Z \rightarrow {}^A Z + \pi^0 \quad (\Gamma_{\pi^0}), \tag{40}$$

corresponding to the elementary reactions (30) and (31) for bound Λ; the final nuclear states in (39) and (40) are not necessarily particle stable.

The theory of Hypernuclear MWD was initiated by Dalitz [187–192], based on a phenomenological Lagrangian describing the elementary decay processes (30) and (31), and motivated by the observation of MWD reactions in the pioneering Hypernuclear physics experiments with photographic emulsions that provided means of extracting Hypernuclear ground-state spins and parities. The J^π assignment for $^3_\Lambda$H, $^4_\Lambda$H, $^4_\Lambda$He, $^8_\Lambda$Li, $^{11}_\Lambda$B and $^{12}_\Lambda$B [189–195] was done by applying the recently established properties of the free Λ mesonic decay ($\Delta I = 1/2$ rule; prevalence of the s-wave, parity-violating, spin–non-flip amplitude; π angular distribution dependence on Λ spin axis) to Λ bound in nuclear systems; see ref. [196] for a recent summary.

Following the development of counter techniques for use in (K^-, π^-) and (π^+, K^+) reactions in the 1970s and 1980s, a considerable body of experimental data on Γ_{π^-} and/or Γ_{π^0} is now available on light Λ-Hypernuclei up to $^{15}_\Lambda$N: $^4_\Lambda$H [174], $^4_\Lambda$He [175], $^5_\Lambda$He [178,179,197,198], $^7_\Lambda$Li [198], $^{11}_\Lambda$B [178,198–201], $^{12}_\Lambda$C [178,199–201] and $^{15}_\Lambda$N [198].

Comprehensive calculations of the main physical properties of MWD were performed during the 1980s and 1990s for s-shell [202, 203], p-shell [203–205] and sd-shell Hypernuclei [203, 205]. The basic ingredients of the calculations are the Pauli suppression effect, the enhancement of

MWD owing to the pion polarization effect in the nuclear medium [206–209], the sensitive final-state shell-structure dependence and the resulting charge-dependence of the decay rates.

An important ingredient of MWD calculations is the pion-nucleus potential which generates pion distorted waves that strongly affect the magnitude of the pionic decay rates. Indeed, for low-energy pions, the pion-nucleus potential has been studied so far through π-nucleus scattering experiments [210] and measurements of X-rays from pionic atoms [211]; the study of MWD in which a pion is created by the decay of a Λ hyperon deep inside the nucleus offers important opportunities to investigate in-medium pions and to discriminate between different off-shell extrapolations inherent in potential models. For this reason, MWD continues to be an interesting item of Hypernuclear physics, and precise and systematic determinations of Γ_{π^-} and Γ_{π^0} are very welcome.

In the following two subsections s-shell and p-shell Hypernuclei MWD will be discussed separately.

### 4.2.1 MWD of s-shell Hypernuclei and the ΛN potential

As discussed before, due to the short Λ lifetime, the production of Λ-Hypernuclei and the investigation of their structure is the only practical way to study the ΛN interaction. To date, the theory of few-body systems is able to calculate directly up to five-body systems starting from the elementary two-body ΛN interaction; on the other hand, to construct a reliable ΛN interaction model, the basic requirement is to reproduce the measured binding energy values of all s-shell Hypernuclei.

In the determination of a realistic ΛN phenomenological potential, a long-standing problem was that potentials determined by fits to $B_\Lambda(^3_\Lambda$H$)$, $B_\Lambda(^4_\Lambda$H$)$ and $B_\Lambda(^4_\Lambda$He$)$, together with low-energy Λp scattering data, lead to overestimate data on $B_\Lambda(^5_\Lambda$He$)$. A better agreement with data is obtained by explicitly incorporating the ΛN-ΣN coupling [121].

The possible existence of a central repulsion in the hyperon-nucleus mean potential has been discussed by several authors by starting from the realistic two-body YN interaction: the strength of the long-range attraction of the YN interaction is much weaker than that of the NN interaction and it would be almost counterbalanced by the short-range repulsion. Consequently, inner repulsion would be present also in the Y-nucleus potentials constructed from the YN interaction with the folding procedure. The effect would be seen most clearly for very light Hypernuclei ($A = 4, 5$): the hyperon would be pushed outward the nucleus due to this repulsion and consequently the overlap of the hyperon wave function with the nucleus would be much reduced.

The existence of such a repulsive core is established experimentally for $^4_\Lambda$He, where the $\Sigma N \rightarrow \Lambda N$ conversion is suppressed thanks to the expulsion of the Σ outward the nuclear core due to the inner repulsion. This mechanism is considered to be responsible for the narrow width of the $^4_\Sigma$He system [212–215].
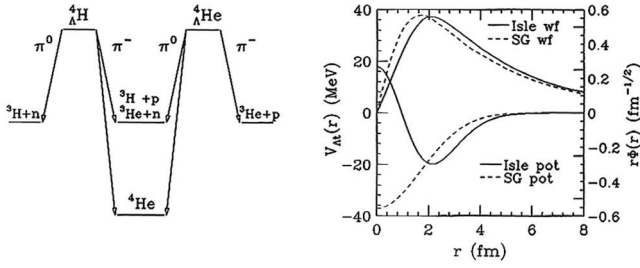
Fig. 19. Left: mesonic weak decay scheme for $^4_\Lambda$H and $^4_\Lambda$He. Right: Λ radial wave functions and α-Λ folding potentials for $^4_\Lambda$H, calculated by the SG and Isle interactions. From ref. [218].

Moreover, the experimental evidence for the presence of a central repulsion in the Λ-nucleus potential can be obtained from the Hypernuclear decay observables, which provide significant information on the Λ single-particle behaviour. In particular, the MWD rate, influenced by Pauli suppression, is sensitive to the overlap between the wave functions of the Λ and of the nuclear core; this overlap, in turn, reflects the potential shape felt by the Λ in nuclei.

A repulsive core in the ΛN interaction was introduced in ref. [216, 217] to lead to a repulsion in the α-Λ potential: the Λ wave function is spread outward the nucleus and the MWD rate is enhanced as a consequence of the Pauli suppression relaxation, since on the Hypernuclear surface the local nuclear Fermi momentum is smaller than in the nuclear core. The α-Λ potential is expressed by a two-range Gaussian function, indicated as Isle, and yields a 30% larger MWD rate than the single-Gaussian α-Λ potential, indicated as SG, without the repulsive central part. In the calculations, the strength parameters of both Isle and SG potentials are determined to reproduce $B_\Lambda(^5_\Lambda\mathrm{He})$ and only MWD rate measurements can distinguish between them.

Other authors too suggested a central repulsion in the Λ-nucleus potential and evaluated MWD rates for s-shell Hypernuclei [202, 218]. In fig. 19 the left part shows the decay scheme for $^4_\Lambda$H and $^4_\Lambda$He; the charge symmetry features of $A = 4$ Hypernuclei can be observed by comparing the two mesonic decays. In the right part of the figure, the Λ radial wave functions and the α-Λ folding potentials for $^4_\Lambda$H, calculated by the SG and Isle interactions, are shown. Two-body decays are allowed only for reactions producing ^{4}He in the final state, being the residual nuclei of the other two-body channels only loosely bound. A Λ-nucleus potential for $A = 4$ with a central repulsion gives a two-body decay rate smaller than that of a SG potential, due to the reduction of the overlap of the Λ and final nucleon wave functions. This produces an enhancement of the three-body decay rates and hence the total MWD rate should not change so much, whereas the ratio between two- and three-body decays is very sensitive to the potential shape and is thus useful to investigate the nature of the short-range part of the ΛN interaction.

From the experimental side, a precise measurement of the Hypernuclear decay rates requires as a pre-requisite a precise measurements of both lifetime and branching ratios of reactions (39) and (40). The E167 experiment at

Table 3. MWD rates of $^4_\Lambda$H in units of the free Λ decay rate (Γ_Λ) measured by the KEK-E167 experiment [175]. The values are compared with theoretical estimates obtained with SG and Isle ΛN potentials [218].

Decay Rate	Data	SG	Isle
$\Gamma_\mathrm{T}/\Gamma_\Lambda$	$1.03^{+0.12}_{-0.10}$		
$\Gamma_{\pi^0}/\Gamma_\Lambda$	0.53 ± 0.07	0.49	0.51
$\Gamma_{\pi^-}/\Gamma_\Lambda$	0.33 ± 0.05	0.25	0.31
$\Gamma_{\pi^0}/\Gamma_{\pi^-}$	1.59 ± 0.20	2.02	1.59

Table 4. MWD rates of $^4_\Lambda$He in units of the free Λ decay rate (Γ_Λ) measured by the KEK-E167 experiment [175] and by refs. [193, 194]. The values are compared with theoretical estimates obtained with SG and Isle ΛN potentials [218].

Decay Rate	Data	SG	Isle
$\Gamma_\mathrm{T}/\Gamma_\Lambda$	$1.36^{+0.21}_{-0.15}$		
$\Gamma_{\pi^0}/\Gamma_\Lambda$		0.16	0.19
$\Gamma_{\pi^-}/\Gamma_\Lambda$	$1.00^{+0.18}_{-0.15}$	0.93	0.88
$\Gamma_{\pi^-\ ^4\mathrm{He}}/\Gamma_\Lambda$	$0.69^{+0.12}_{-0.10}$	0.71	0.61
$\Gamma_{\pi^-\ ^4\mathrm{He}}/\Gamma_{\pi^-}$	0.69 ± 0.02	0.76	0.69

KEK measured the MWD and NMWD rates of $^4_\Lambda$H and $^4_\Lambda$He [175] produced with the $(K^-_\mathrm{stop}, \pi^-)$ reaction on a liquid He target, measuring the momentum of the outgoing formation π^- with a large acceptance (~ 100 msr) magnetic spectrometer with a resolution of 1–2% FWHM. π^0, π^- and p coming from decay reactions were detected by a system of NaI(Tl) counters covered by thin plastic scintillators for energy deposition measurement and particle identification. The MWD rates obtained by the experiment are summarized in tables 3 and 4 together with theoretical calculations from [218]. In table 4 results of older visualizing techniques experiments [193, 194] are also reported for $^4_\Lambda$He.

From the comparison between the experimental results and the theoretical calculations of ref. [218] it is possible to observe that the Isle ΛN potential is able to reproduce the data within $\pm 1\sigma$ error, while SG calculations figure a disagreement at 2σ level for the $\Gamma_{\pi^0}/\Gamma_{\pi^-}$ ratio of $^4_\Lambda$H. This allows to conclude that the existence of a repulsive core in the Λ-nucleus mean potential seems to be experimentally established.

More recently, the E462 and E508 experiments at KEK measured with very high statistics both π^- [179] and π^0 [197] MWD rates of $^5_\Lambda$He in (π^+, K^+) measurements on ^{6}Li target with the SKS magnetic spectrometer. The results are reported in table 5 and compared with SG and Isle based calculations [202, 219]. For BR(π^-) the calculations with the Isle potential are in good agreement with the measured decay rates, whereas the SG potential gives a significant underestimation [219]. For $\Gamma_{\pi^0}/\Gamma_\Lambda$ the experimental value is located between Isle and SG calculations

Table 5. MWD branching ratios and rates of $^5_\Lambda$He in units of free Λ decay rate (Γ_Λ) measured by the KEK-E462 and KEK-E508 experiments [179, 197]. The values are compared with theoretical estimates obtained with SG and Isle ΛN potentials for $\Gamma_{\pi^-}/\Gamma_\Lambda$ [219] and for $\Gamma_{\pi^0}/\Gamma_\Lambda$ [202].

Decay Rate	Results	SG	Isle
$\Gamma_{\rm T}/\Gamma_\Lambda$	0.947 ± 0.038		
BR(π^-)	0.359 ± 0.009		
$\Gamma_{\pi^-}/\Gamma_\Lambda$	0.340 ± 0.016	0.271	0.354
BR(π^0)	0.212 ± 0.008		
$\Gamma_{\pi^0}/\Gamma_\Lambda$	0.201 ± 0.011	0.177	0.215

of ref. [202], but the Isle value reproduces the experimental result within 1σ, while the SG one differs of more than 2σ. Thank to the very small value of the errors on the measured BR's, this fact strongly supports the presence of the central repulsion in the α-Λ potential, independently of the considered specific theoretical calculation.

The last conclusion is representative of the deep interplay between particle and nuclear physics that is realized in Hypernuclear physics. Indeed, being at the frontier between the two fields, Hypernuclei can be studied exploiting experimental techniques and models typical of both approaches; in particular we can see here how, from measurement of typical nuclear physics observables, like decay rates, it is possible to obtain information on the baryon-baryon potentials, a typical subject of particle physics.

4.2.2 MWD of p-shell Hypernuclei and the π nuclear polarization effect

In Hypernuclei MWD is disfavoured by the Pauli principle, particularly in heavy systems. It is strictly forbidden in normal infinite nuclear matter, where the nucleon Fermi momentum is about $270\,{\rm MeV}/c$, while in finite nuclei it can occur because of three important effects: 1) in nuclei the hyperon has a momentum distribution, being confined in a limited spatial region, that allows larger momenta to be available to the final nucleon; 2) the final pion feels an attraction by the nuclear medium, due to the p-wave part of the optical π-nucleus potential, which modifies the pion dispersion relation; for a fixed momentum, the pion carries an energy smaller than if it was free and the energy conservation increases the chance of the final nucleon to lie above the Fermi surface; indeed, it has been shown that the pion distortion increases the MWD width by more than one order of magnitude for very heavy Hypernuclei ($A \sim 200$) with respect to the value obtained without the medium distortion [220]; 3) at the nuclear surface the local Fermi momentum can be smaller than $270\,{\rm MeV}/c$ and the Pauli blocking is less effective in forbidding the decay.

In any case, the MWD rate rapidly decreases as the Hypernucleus mass number increases. Table 6 reports the actual experimental knowledge of both Γ_{π^-} and Γ_{π^0} for p-shell Hypernuclei. For the sake of completeness, also $^5_\Lambda$He,

Table 6. MWD rates Γ_{π^-} and Γ_{π^0} in units of free Λ decay rate Γ_Λ for p-shell Λ-Hypernuclei obtained in recent counter experiments. $^5_\Lambda$He, $^{27}_\Lambda$Al and $^{28}_\Lambda$Si results are also reported for comparison.

Hypernucleus	$\Gamma_{\pi^-}/\Gamma_\Lambda$	$\Gamma_{\pi^0}/\Gamma_\Lambda$	Ref.
$^5_\Lambda$He	0.44 ± 0.11	0.14 ± 0.19	[178]
	0.340 ± 0.016		[179]
		0.201 ± 0.011	[197]
	0.332 ± 0.069		[198]
$^7_\Lambda$Li	0.353 ± 0.059		[198]
$^9_\Lambda$Be	0.178 ± 0.050		[198]
$^{11}_\Lambda$B	0.22 ± 0.05		[221]
		0.192 ± 0.056	[199]
	0.23 ± 0.06		[200]
	0.212 ± 0.036		[201]
	0.249 ± 0.051		[198]
$^{12}_\Lambda$C	$0.052^{+0.063}_{-0.035}$		[178]
		0.217 ± 0.073	[199]
	0.14 ± 0.07		[200]
	0.113 ± 0.014		[201]
$^{15}_\Lambda$N	0.108 ± 0.038		[198]
$^{27}_\Lambda$Al	0.041 ± 0.010		[201]
$^{28}_\Lambda$Si	0.046 ± 0.011		[201]

$^{27}_\Lambda$Al and $^{28}_\Lambda$Si counter experiments results are included. A significant part of the available data comes from experiments at KEK [179, 197, 199, 201] and are affected by relative errors of about 20–25%, which diminish significantly in high-statistics measurements [179] to about 5%.

Very recently, the FINUDA experiment has performed a systematic study of the charged MWD channel of p-shell Hypernuclei [198], $^7_\Lambda$Li, $^9_\Lambda$Be, $^{11}_\Lambda$B and $^{15}_\Lambda$N, and of $^5_\Lambda$He with errors ranging between 15% (for $A = 5$) and 35% (for $A = 15$). Very thin target materials were used to stop the low momentum ($\sim 127\,{\rm MeV}/c$) K^-'s coming from the $\Phi \to K^- K^+$ decay; moreover the high transparency of the FINUDA tracker and the very large solid angle ($\sim 2\pi\,{\rm sr}$) covered by the detector ensemble make the FINUDA apparatus suitable to study the formation and the decay of Λ-Hypernuclei by means of high-resolution magnetic spectroscopy of the charged particles emitted in the processes. In particular, a π^- of about 250–280 MeV/c momentum has been required to identify the Hypernucleus bound state production on p-shell nuclear targets, in coincidence with a second π^- of momentum less than $120\,{\rm MeV}/c$ to detect the MWD.

It must be stressed that the information available before the FINUDA measurements on the charged MWD of light Hypernuclei consisted almost entirely of $\Gamma_{\pi^-}/\Gamma_\Lambda$
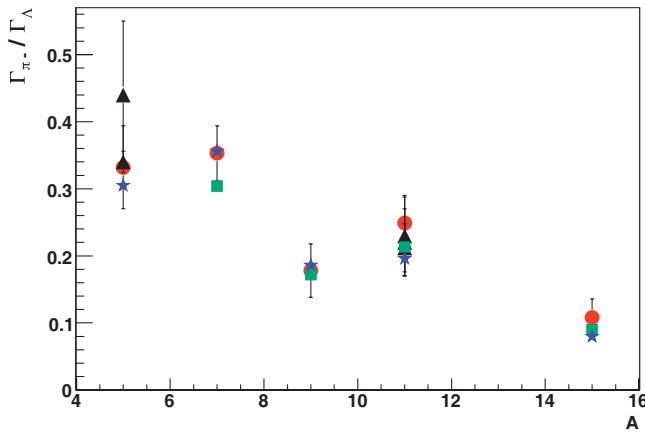
Fig. 20. The $\Gamma_{\pi^-}/\Gamma_\Lambda$ ratios obtained by the FINUDA experiment (red circles) [198], compared with previous measurements (black triangles) [178, 179, 200, 201, 221] and with theoretical calculations [204, 205] (green squares) and [223] (blue stars). See ref. [198] for more details.

and $\Gamma_{\pi^0}/\Gamma_\Lambda$ values obtained by means of counting measurements in coincidence with the Hypernuclear formation π^- detection, with no magnetic analysis of the decay meson; π^- kinetic energy spectra were reported for $^{12}_\Lambda$C MWD only [201]. The π^- spectra of ref. [198], on the other hand, allow one to have a more careful confirmation of the elementary mechanism that is supposed to underlie the decay process, through the determination of the decay rates, as well as to have information on the spin-parity of the initial Hypernuclear ground state through the analysis of their energy dependence. In this respect, the study of pion spectra from MWD can be regarded as an indirect spectroscopic investigation tool.

In particular, the ratios $\Gamma_{\pi^-}/\Gamma_\Lambda$ were obtained from the measured branching ratios, using available $\Gamma_{\rm T}/\Gamma_\Lambda$ values or relying on a linear fit to the known values of all measured Λ-Hypernuclei in the mass range $A = 4$–12 [222]. Figure 20 reports the values obtained by the FINUDA experiment (red circles) compared with previous experimental data (black triangles) and theoretical calculations (green squares and blue stars) for $^5_\Lambda$He, $^7_\Lambda$Li, $^9_\Lambda$Be, $^{11}_\Lambda$B and $^{15}_\Lambda$N.

Being characterized by a small Q-value, the MWD mode is strongly affected by the details of both the Hypernucleus and the daughter nucleus structure. Indeed, the theoretical calculations of refs. [204, 205] evaluate the p-shell Hypernuclei total and partial MWD decay rates by incorporating the pion final-state interaction using pion-nuclear distorted waves and by describing the structure of the nuclear core with the Cohen-Kurath spectroscopic approach [224, 225]. The authors found that for p-shell Hypernuclei the total π^- decay rate is dominated by $\Lambda_{1s} \rightarrow p_{1p}$ transitions, while only little contributions are given by higher energy configurations of the final nuclear system, mainly through $\Lambda_{1s} \rightarrow p_{2s,1d}$ transitions.

Recently, in ref. [223] these calculations were revisited, following the same approach, and a new sum rule was introduced to encapsulate the suppressive effect of the Pauli

principle on the total and partial π^- decay rates. In fig. 20, both calculations of refs. [204, 205] (green squares) and ref. [223] (blue stars) are reported, for ground-state spin-parity $1/2^+$ for $^5_\Lambda$He and $^7_\Lambda$Li, $5/2^+$ for $^{11}_\Lambda$B and $3/2^+$ for $^{15}_\Lambda$N. A good agreement holds among the FINUDA results and previous measurements (black triangles), when existing, and among the FINUDA results and the theoretical calculations. The total decay rates for the other choice of ground state spin-parity calculated in refs. [204, 205, 223] ($3/2^+$ for $^7_\Lambda$Li, $7/2^+$ for $^{11}_\Lambda$B and $1/2^+$ for $^{15}_\Lambda$N) are substantially lower and disagree with the experimentally derived values; an exception is given by $^{15}_\Lambda$N, for which the calculated values reported in ref. [205] does not allow one to fix the ground-state spin-parity, as will be discussed in the following.

The agreement between experimental data and calculations supports the correctness of the hypotheses on which the theoretical descriptions are based. It clearly indicates the possibility to evaluate typical nuclear physics observables, like the rates of the MWD of Hypernuclei, starting from the knowledge of the elementary phenomenological Hamiltonian which describes the decay of the free Λ; it also gives a confirmation of the presence of the distortion of the outgoing π^- wave function due to the polarization effect of the nuclear medium and of the effectiveness of the Cohen-Kurath spectroscopic calculations in describing both the Hypernucleus core and the daughter nucleus, allowing to account naturally for the strong final state shell-structure dependence and charge dependence of the measured decay rates.

The decay π^- kinetic energy spectra obtained by the FINUDA experiment for MWD of $^7_\Lambda$Li, $^9_\Lambda$Be, $^{11}_\Lambda$B and $^{15}_\Lambda$N [198] show interesting structures which can be directly related to the excitation function of the daughter nucleus calculated by refs. [204, 205, 223], allowing to determine the spin-parity configuration of the Hypernucleus ground state.

In fig. 21 the π^- spectrum from MWD of $^7_\Lambda$Li is shown (upper part) and compared with the calculated decay ratios $\Gamma_{\pi^-}/\Gamma_\Lambda$ to final ^{7}Be states [223] (lower part). These calculated rates are close to those obtained in ref. [205]. The correspondence of the structures observed in the experimental spectra with the rates for decays to different excited states of the daughter nucleus, assuming a $1/2^+$ initial spin-parity state, is clear. The peak structure corresponds to the production of ^{7}Be in its $3/2^-$ ground state and in its only bound $1/2^-$ excited state, at $429 \, {\rm keV}$, not resolved due to the FINUDA experimental resolution (4.2 MeV FWHM). The part of the spectrum at lower energies is due to three-body decays. The shape of the spectrum confirms the spin assigned to the Hypernuclear ground state of $^7_\Lambda$Li [222]. Indeed, only a $1/2^+$ spin-parity for $^7_\Lambda$Li ground state, shown by red bars, reproduces the fitted peak at $\sim 36 \, {\rm MeV}$ due to the ^{7}Be ground state and excited state at $429 \, {\rm keV}$. A $3/2^+$ spin-parity for $^7_\Lambda$Li ground state would imply a radically different spectral shape [205, 223], as indicated in fig. 21 by the blue bars.

In fig. 22 the spectrum for $^9_\Lambda$Be is shown in the upper part and compared with calculated decay ratios $\Gamma_{\pi^-}/\Gamma_\Lambda$
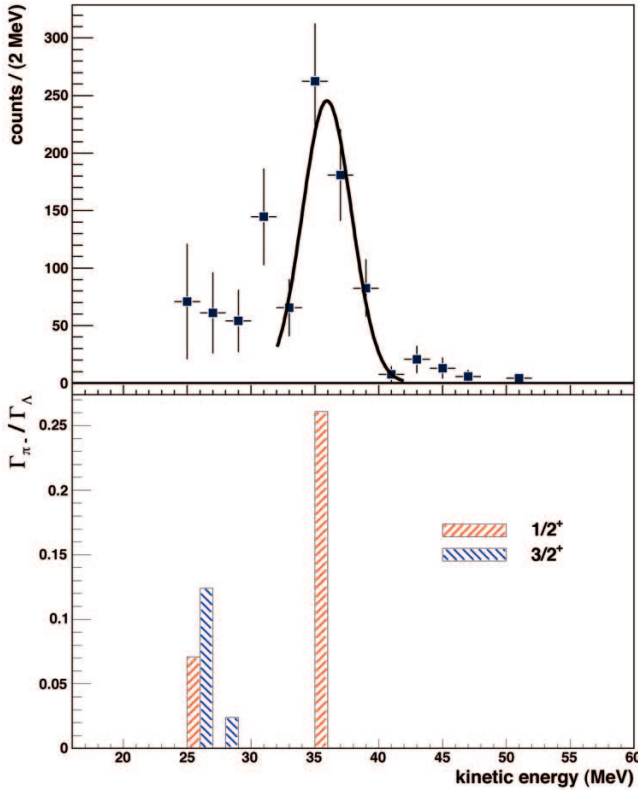
Fig. 21. Top: kinetic energy spectrum of MWD π^- from $^7_\Lambda$Li; the solid line is a Gaussian fit to compare with theoretical calculation. Bottom: calculated major decay rates to ^{7}Be final states [223] for $^7_\Lambda$Li $1/2^+$ (red bars) and $3/2^+$ (blue bars) ground-state spin-parity. From ref. [198].
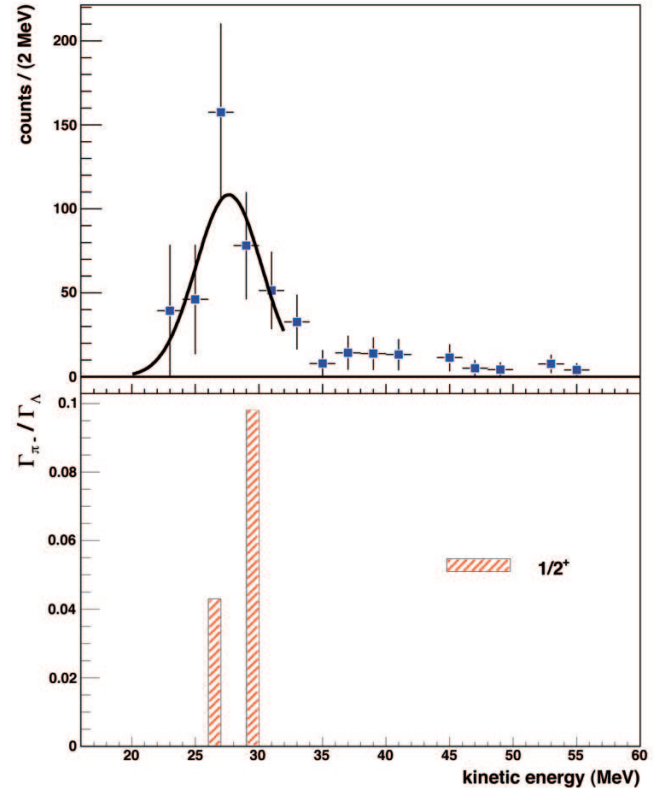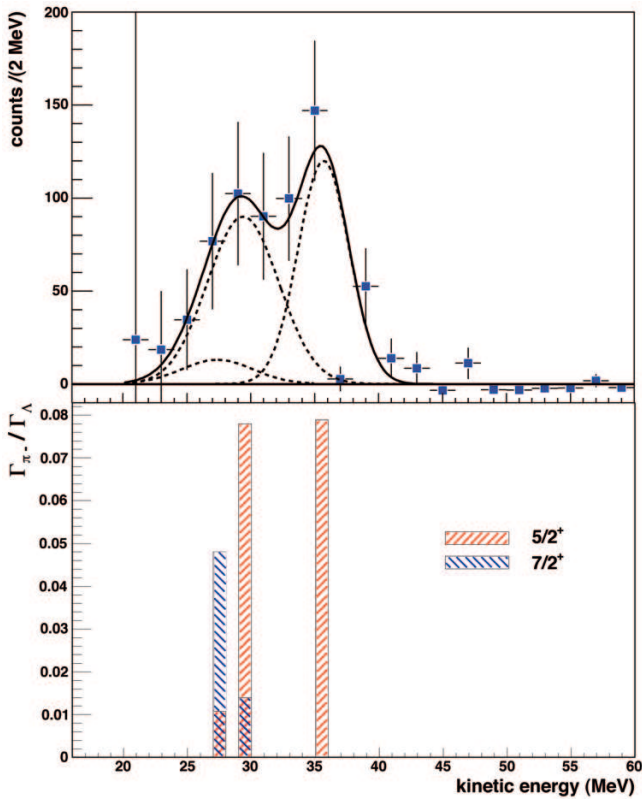

Fig. 22. Top: kinetic-energy spectrum of MWD π^- from $^9_\Lambda$Be; the solid line is a Gaussian fit to compare with the theoretical calculation. Bottom: calculated major decay rates to ^{9}B final states [223] for $^9_\Lambda$Be $1/2^+$ ground state (red bars). From ref. [198].

to ^{9}B final states [223] shown in the lower part. These calculated rates too are close to those predicted by ref. [205]. In the $^9_\Lambda$Be spectrum the energy resolution does not allow a separation between the two components predicted to dominate the spectrum [205,223], the $3/2^-$ ^{9}B ground state and the $1/2^-$ excited state at 2.75 MeV. The correspondence between the experimental spectrum and the calculated rates of decay to different excited states of the daughter nucleus is clear. The spectrum is consistent with the interpretation from (π^+, K^+) reactions [4, 226], according to which the $^9_\Lambda$Be ground state is dominantly a $1s$ Λ coupled to the ^{8}Be(0^+) ground state.

In fig. 23 the spectrum for $^{11}_\Lambda$B is shown and compared with calculated decay rates to ^{11}C final states [223]. By assuming a $5/2^+$ ground state, it is possible to identify two major contributions in the $^{11}_\Lambda$B spectrum due to a $3/2^-$ ^{11}C ground state and its $7/2^-$ excited state at 6.478 MeV, both shown by red bars. It is clear from the figure that the shape of the spectrum is well reproduced by assigning a $5/2^+$ spin-parity to $^{11}_\Lambda$B ground state, while by assuming a $7/2^+$ ground state, the ^{11}C ground-state peak is missing and the dominant decay is to the $5/2^-$ excited state at 8.420 MeV, shown by a blue bar. A $5/2^+$ assignment for $^{11}_\Lambda$B ground state, first made by Zieminska by studying emulsion spectra [227], was experimentally confirmed by the KEK measurement [201], comparing the

derived value of the total π^- decay rate with the calculation of ref. [203]. The FINUDA measurement of the decay spectrum shape provides a confirmation of the fact that $J^\pi(^{11}_\Lambda B_{g.s.}) = 5/2^+$ by a different observable.

In fig. 24 the spectrum for $^{15}_\Lambda$N is shown and compared with calculated decay rates to ^{15}O final states [223]. In the experimental spectrum, the ^{15}O $1/2^-$ ground-state contribution stands out clearly, along with a hint for a secondary structure separated by about 6 MeV. The fit to the lower-energy secondary structure is strongly influenced by the substantial error affecting the data point at the lowest energy. According to refs. [204,223], this secondary structure derives most of its strength from sd states scattered around 6 MeV excitation, while the contribution of the $p_{3/2}^{-1}p_{1/2}$ ^{15}O excited state at 6.176 MeV is negligible. Before the FINUDA measurement, the ground-state spin of $^{15}_\Lambda$N was not determined experimentally. The most recent theoretical study of Hypernuclear spin-dependence [228] predicts $J^\pi(^{15}_\Lambda N_{g.s.}) = 3/2^+$, setting the $1/2^+$ excited state of the ground-state doublet about 90 keV above the $3/2^+$ state. The spin ordering, however, could not be determined from the γ-ray de-excitation spectra measured recently on a ^{16}O target at BNL [105]. The prominence of ^{15}O$_{g.s.}$ in the spectrum of fig. 24 supports this $3/2^+$ theoretical assignment. Moreover, as already observed, the total π^- decay rate of $^{15}_\Lambda$N agrees with calculations by

Fig. 23. Top: kinetic-energy spectrum of MWD π^- from $^{11}_\Lambda$B; the solid line is a Gaussian fit to compare with the theoretical calculation. Bottom: calculated major decay rates to ^{11}C final states [223] for $^{11}_\Lambda$B $5/2^+$ (red bars) and $7/2^+$ (blue bars) ground states. From ref. [198].
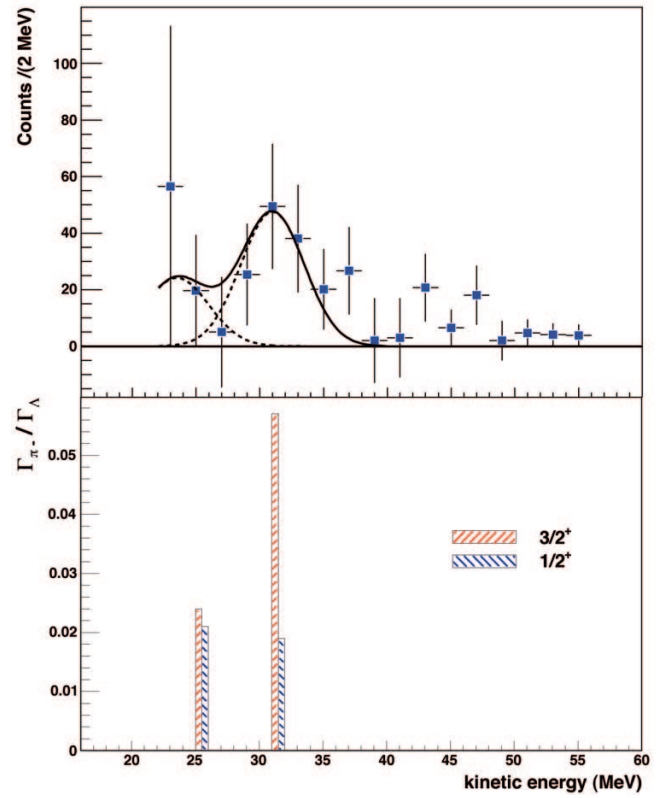
Fig. 24. Top: kinetic-energy spectrum of MWD π^- from $^{15}_\Lambda$N; the solid line is a Gaussian fit to compare with the theoretical calculation. Bottom: calculated major decay rates to ^{15}O final states [223] for $^{15}_\Lambda$N $3/2^+$ (red bars) and $1/2^+$ (blue bars) ground states. From ref. [198].

refs. [205,223] by assuming a $3/2^+$ ground-state spin-parity assignment. These two calculations disagree for a $1/2^+$ spin-parity assignment, and, following the new calculation [223] for $^{15}_\Lambda$N, which corrects the older calculations of refs. [204,205], a $1/2^+$ spin-parity is excluded and the assignment $J^\pi(^{15}_\Lambda\mathrm{N}_{\mathrm{g.s.}}) = 3/2^+$ is made based mainly on the decay rate and the shape of the MWD spectrum.

It is thus evident that the study of the MWD spectra has strong potentialities for the determination of the ground state spin-parity for s- and p-shell Hypernuclei; for sd-shell strange nuclear systems, too, the spectroscopy of particles emitted in the decay processes can help in fixing the spectroscopic configuration of the ground state, although the MWD branching ratios diminish below 10% for these Hypernuclei and the errors become consequently very sizable. The MWD spectra analysis has thus demonstrated its reliability as light- and medium-A Hypernuclei spectroscopic tool, complementary to the γ-ray spectroscopy of low-lying excited states [4] when the spin ordering cannot be determined; it represents a new version of the old technique based on the study of the angular distribution of the MWD π^-, which allowed the ground state spin-parity determination of light Hypernuclei from emulsion experiments [189–195], based on the known properties of the free Λ weak decay.

As a matter of fact, very recently plans for performing high resolution ($\sim 100\,\mathrm{keV}$) spectroscopy of π^- from MWD of Hyperfragments produced by electroproduction at JLab and MAMI-C were put forward [229]. Figure 25 shows a schematic view of the experimental layout proposed for operation at JLab, Hall A. However, it is difficult from such experiments to determine the spin-parity of the Hypernuclear ground states, since the quantum numbers of the initial state are difficult, if not impossible, to determine.

4.3 Non-mesonic weak decay

In NMWD, Hypernuclei are converted into non-strange nuclei through the reactions

$$^A_\Lambda Z \rightarrow {}^{A-2}Z + n + n, \tag{41}$$

$$^A_\Lambda Z \rightarrow {}^{A-2}(Z-1) + p + n, \tag{42}$$

corresponding to the elementary neutron- and proton-induced reactions (32) and (33); as for MWD, the final nuclear states in (41) and (42) are not necessarily particle stable and are actually not detectable, so that only inclusive measurements can be performed.

The possibility of NMWD of Λ-Hypernuclei was suggested for the first time in 1953 [230] and interpreted in
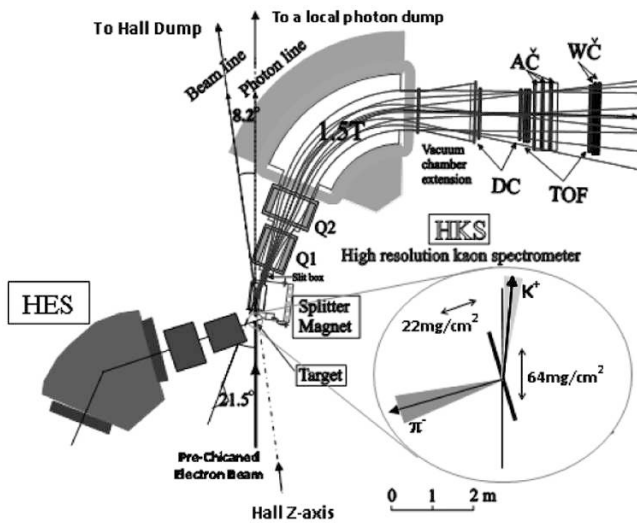
Fig. 25. Schematic view of the experimental layout proposed at JLab Hall A for performing high-resolution spectroscopy from MWD of Hyperfragments produced by electroproduction. From ref. [229].

terms of the free space $\Lambda \to N\pi$ decay, where the pion was considered as virtual and then absorbed by a bound nucleon, as already mentioned before. In the '60s, Block and Dalitz [231] developed a phenomenological model of NMWD, which was recently updated (see, for instance, ref. [232]). Within this approach, some important characteristics of the NMWD of s-shell Hypernuclei, mainly the degree of validity of the $\Delta I = 1/2$ rule on the isospin change, can be reproduced in terms of elementary spin-dependent branching ratios for the processes (32) and (33), by fitting the available experimental data.

After the first analysis by Block and Dalitz, microscopic models of the $\Lambda N \to nN$ interaction began to be developed. The first of these approaches adopted a one-pion-exchange (OPE) model [233]. This model is based on a $\Delta I = 1/2$ $\Lambda N\pi$ vertex, with the absorption of the virtual pion by a second nucleon of the nuclear medium. The results of the decay width calculation for the one-nucleon induced NMWD were not realistic also because the employed $\Lambda N\pi$ coupling was too small to reproduce the free Λ lifetime.

Since the NMWD channel is characterized by a large momentum transfer, the details of the Hypernuclear structure should not have a substantial influence, thus providing useful information directly on the four-baryon, strangeness changing, $\Lambda N \to nN$ weak interaction from nuclear physics measurements, analogously to what occurs in the description of the MWD observables starting from the free Λ decay knowledge. The large momentum transfer implies that NMWD probes short-distance interactions and might, therefore, elucidate the effect of heavy-meson exchange or even the role of the explicit quark/gluon substructure of baryons in baryon weak interactions.

In order to improve the OPE model, mesons heavier than the pion were thus introduced as mediators of the $\Lambda N \to nN$ interaction. McKellar and Gibson [234] evaluated the width for a Λ in nuclear matter, adding

the exchange of the ρ-meson and taking into account the ΛN relative s-states only. They used a $\Delta I = 1/2$ $\Lambda N\pi$ vertex and made the calculation by using the two possible relative signs (being at that time unknown and not fixed by their model) between the pion and the ρ potentials. It is important to note that, for mesons heavier than the pion, no experimental indication supports the validity of the $\Delta I = 1/2$ isospin rule in $\Lambda N \to nN$ (transitions with $\Delta I = 3/2$ are also possible). Some years later, Nardulli [235] determined the relative sign $(-)$ between ρ- and π- exchange by implementing the available information from weak non-leptonic and radiative decays. References [234,235] obtained a NMWD width in the $(\rho+\pi)$ exchange model smaller than the OPE one. In 1986, Dubach *et al.* [236] extended the OPE to a one-meson-exchange (OME) model, in which the π, ρ, K, K^*, ω and η mesons were considered, in a nuclear matter calculation. Shell-model approaches were then considered [237,238] in terms of OME models including the mesons of the pseudoscalar and vector octets and, more recently, also uncorrelated and correlated two-pion-exchange (TPE) were added to the OME potentials [239, 240]. For most of the OME and OME+TPE calculations performed up to date, the $\Delta I = 1/2$ rule is assumed as valid, although this is justified only for the $\Lambda N\pi$ weak vertex. In sect. 4.4 we shall discuss in detail the status of the studies performed on the $\Delta I = 1/2$ rule in NMWD.

Another theoretical approach to the short-range part of the $\Lambda N \to nN$ weak interaction is provided by the quark model. Cheung, Heddle and Kisslinger [241, 242] considered an hybrid quark-hadron approach for the NMWD in which the decay is explained by two separate mechanisms with different interaction ranges: the long-range term ($r \geq 0.8$ fm) was described by the OPE with the $\Delta I = 1/2$ rule, while the short-range interaction was described by a six-quark cluster model including both $\Delta I = 1/2$ and $\Delta I = 3/2$ contributions. More recently, Inoue *et al.* [243] calculated the NMWD widths with a direct-quark (DQ) model combined with the OPE description. In the DQ model, the ΛN and NN short-range repulsion originates from quark exchange between baryons and gluon exchange between quarks. The effective weak Hamiltonian for quarks was obtained from the so-called operator product expansion, which contains perturbative QCD effects and, by construction, both $\Delta I = 1/2$ and $\Delta I = 3/2$ transitions. It was found that the DQ mechanism gives a significant $\Delta I = 3/2$ contribution in the $J = 0$ $\Lambda N \to nN$ channel. The approach was then extended to incorporate a OME model containing π, K and σ exchange [244, 245].

A method alternative to the finite-nucleus shell-model approach makes use of a nuclear matter formalism. This is a many-body technique, first introduced in ref. [208, 209], in which the calculation is performed in infinite nuclear matter and then it is extended to finite nuclei through the local density approximation. It provides a unified picture of both mesonic and non-mesonic decay channels. In nuclear matter one has to evaluate the Λ self-energy Σ, which provides the various mesonic and non-mesonic decay widths through the relation $\Gamma_i = -2 \operatorname{Im} \Sigma_i$ ($i = n$,

p, np, etc.). The Λ self-energy is derived from a diagrammatic approach.

Shell-model– and quark-model–based calculations restricted their analyses to one-nucleon induced NMWD. In the first nuclear-matter calculations proposed for the evaluation of the two-nucleon induced decay rates, a phenomenological approach was used [162, 183]. In these works, the Feynman diagrams contributing to the two-nucleon induced NMWD were not explicitly evaluated, but an approximate calculation was done by using data on pion absorption in nuclei. In the work by Ramos *et al.* [183], additionally, an argument for the phase-space available for the $2p2h$ configurations was introduced. This resulted in a non-negligible contribution of the two-nucleon induced rate to the total NMWD rate. According to a quasi-deuteron approximation, the rate was assumed to be due to a decay induced by a neutron-proton pair: $\Gamma_2 = \Gamma_{np}$.

More recently, a program was started for a microscopic calculation of the one- and two-nucleon induced decays [246]. A nuclear-matter formalism extended to finite Hypernuclei by the local density approximation is adopted. All isospin channels of the two-nucleon stimulated decay, nn-, np- and pp-induced, are included in this diagrammatic approach. In particular, Pauli exchange (ground-state correlation) contributions were recently evaluated [247] ([165]): the results showed that Pauli exchange terms and ground-state correlations are very important for a detailed calculation of all the NMWD rates and that, as expected, the two-nucleon stimulated decay width is dominated by the np-induced process. In ref. [31], the microscopic diagrammatic approach was then applied to the calculation of the nucleon spectra emitted in Hypernuclear NMWD.

For a long period of time, all these theoretical efforts were mainly devoted to the solution of an important question concerning the weak decay rates. In fact, the study of the NMWD was characterized by a long-standing disagreement between theoretical estimates and experimental determinations for the Γ_n/Γ_p ratio between the neutron- and proton-induced decay widths: this became known as the Γ_n/Γ_p *puzzle*.

It is worth to remind here that, up to a few years ago, all theoretical calculations appeared to strongly underestimate the available data measured in several Hypernuclei for the Γ_n/Γ_p ratio. Concerning measured values, the situation can be summarized by the following inequalities:

$$\left\{\frac{\Gamma_n}{\Gamma_p}\right\}^{\text{theory}} \ll \left\{\frac{\Gamma_n}{\Gamma_p}\right\}^{\text{exp}}, \qquad 0.5 \lesssim \left\{\frac{\Gamma_n}{\Gamma_p}\right\}^{\text{exp}} \lesssim 2 \quad (43)$$

(only for $^4_\Lambda$He the experimental value of this ratio is less than 0.5), although the large experimental error bars did not allow to reach any definite conclusion.

Nowadays, it is widely recognized that a solution has been found to the Γ_n/Γ_p puzzle. This achievement was possible mainly by a rapid development of the experiments, which measured a variety of NMWD nucleon emission spectra, and, from the theoretical side, thanks to: 1) the inclusion in the $\Lambda N \to nN$ transition potential of

mesons heavier than the pion (two-meson-exchange was also considered), 2) the description of the short-range ΛN and NN correlations in terms of quark degrees of freedom, 3) the analysis of the effect of the two-nucleon induced decay mechanism and (especially) 4) the accurate study of the nucleon FSI following the elementary one- and two-nucleon induced decays (32)-(34). In sect. 4.6 we shall describe these recent advances in detail.

The experimental observables in NMWD are: the total NMWD width Γ_{NM}, the spectra of the nucleons emitted in the decay (from which one can determine, via some theoretical model, the partial decay rates Γ_n, Γ_p, Γ_{np}, etc.) and the asymmetry of protons from NMWD of polarized Hypernuclei. A theory which aims to explain the NMWD reaction mechanisms must account coherently for the description of the experimental behaviour of all these observables.

In the next sections, the most important topics related to NMWD are discussed: in sect. 4.4, the present status on the $\Delta I = 1/2$ isospin rule in NMWD is concerned; in sect. 4.5, measurements and calculations of the total decay are described; in sect. 4.6, the present status of the experimental and theoretical results on the Γ_n/Γ_p ratio is reported, with particular attention to the latest results from the FINUDA experiment; in sect. 4.7, the existence of the two-nucleon induced mechanism is discussed and different methods for the determination of its strength are described; in sect. 4.8, recent measurements of branching ratios for two-body rare decays of s-shell Hypernuclei are reported; in sect. 4.9 the asymmetry in the spatial distribution of protons from NMWD of polarized Hypernuclei is discussed.

4.4 NMWD and the $\Delta I = 1/2$ rule

The $\Delta I = 1/2$ isospin rule is valid to a good degree of approximation in various non-leptonic strangeness changing processes, for instance in free Λ and Σ hyperon and pionic kaon decays. While this is a well-established empirical rule, it is still unknown whether the large suppression of the $\Delta I = 3/2$ transition amplitudes with respect to the $\Delta I = 1/2$ amplitudes holds as a universal feature of all non-leptonic weak processes. Also, different mechanisms seem to be responsible for the above isospin rule in the various hadronic processes.

A possible relevance of $\Delta I = 3/2$ terms in the Hypernuclear NMWD would represent the first evidence for a $\Delta I = 1/2$ rule violation in non-leptonic strangeness changing interactions. One should note that the $\Lambda N \to nN$ process has an important short-range part which is not accessible to those non-leptonic strangeness changing particle physics processes that respect the $\Delta I = 1/2$ rule. Indeed, while the MWD only involves $\Lambda \pi N$ vertex, which in free space respects the $\Delta I = 1/2$ rule, the NMWD also calls into play mesons different from the pion in the Λ vertexes and is thus a complex source of information. Nowadays, no experimental indication supports nor excludes the validity of the $\Delta I = 1/2$ rule for these couplings with heavy mesons. Indirect information could thus come from Hypernuclear NMWD.

Table 7. Amplitudes for the $\Lambda N \to nN$ decay in s-shell Hypernuclei. The spectroscopic notation $^{2S+1}L_J$ is used. I_f is the isospin of the final NN pair. With PC and PV we denote parity-conserving and parity-violating channels, respectively.

Amplitude	Channel	I_f	Parity
a_p, a_n	$^1S_0 \to {}^1S_0$	1	PC
b_p, b_n	$^1S_0 \to {}^3P_0$	1	PV
c_p	$^3S_1 \to {}^3S_1$	0	PC
d_p	$^3S_1 \to {}^3D_1$	0	PC
e_p	$^3S_1 \to {}^1P_1$	0	PV
f_p, f_n	$^3S_1 \to {}^3P_1$	1	PV

A possible violation of the $\Delta I = 1/2$ rule in the NMWD was studied within a shell model framework in ref. [248]. In this work, a one-meson–exchange model with hadronic couplings evaluated in the factorization approximation was adopted. The conclusion reached by the authors is that only large $\Delta I = 3/2$ factorization terms (of the order of the $\Delta I = 1/2$ ones) have a relevant effect on the decay rates (and also on the asymmetry parameter) for $^{12}_{\Lambda}$C.

Tests of the $\Delta I = 1/2$ rule in NMWD are customarily discussed by adopting a model by Block and Dalitz [231]. Such an approach allows one to easily extract information on the spin-isospin dependence of the $\Lambda N \to nN$ process directly from data on s-shell Hypernuclei. The neutron- and proton-stimulated decay widths of s-shell Hypernuclei are obtained in terms of a few spin- and isospin-dependent rates for the elementary process $\Lambda N \to nN$. The relationship among the elementary rates is strongly affected by the isospin change experienced in the NMWD, both $\Delta I = 1/2$ and $\Delta I = 3/2$ transitions being in principle possible.

Within the Block-Dalitz approximation, the width $\Gamma_{\text{NM}} = \Gamma_n + \Gamma_p$ of the Hypernucleus $^A_{\Lambda}Z$ turns out to be factorized as follows into a density-dependent factor and a term incorporating the dynamics of the decay [231]:

$$\Gamma_{\text{NM}}(^A_{\Lambda}Z) = \bar{R}(^A_{\Lambda}Z)\rho_A, \tag{44}$$

$$= \frac{N\bar{R}_n(^A_{\Lambda}Z) + Z\bar{R}_p(^A_{\Lambda}Z)}{A}\rho_A, \tag{45}$$

where

$$\rho_A \equiv \int \mathrm{d}\boldsymbol{r}\,\rho_A(\boldsymbol{r})|\psi_\Lambda(\boldsymbol{r})|^2,$$

is the average nucleon density at the position of the Λ baryon, $\psi_\Lambda(\boldsymbol{r})$ is the Λ wave function in the Hypernucleus and the nuclear density $\rho_A(\boldsymbol{r})$ is normalized to the mass number $A = N + Z$. Moreover, $\bar{R}$ denotes a rate (per unit nucleon density at the Λ position) averaged over spin and isospin and is given in the second equality in eq. (44) in terms of the spin-averaged rates $\bar{R}_n$ and $\bar{R}_p$.

For s-shell Hypernuclei the ΛN initial pair is in the $L = 0$ relative orbital angular momentum state and the possible $\Lambda N \to nN$ transition channels are given in table 7 together with their main properties.

In terms of the amplitudes of table 7, the rates R_{NJ} for the spin-singlet (R_{n0}, R_{p0}) and spin-triplet (R_{n1}, R_{p1})

elementary $\Lambda N \to nN$ interactions are given by

$$R_{n0} = |a_n|^2 + |b_n|^2,$$
$$R_{p0} = |a_p|^2 + |b_p|^2,$$
$$R_{n1} = |f_n|^2,$$
$$R_{p1} = |c_p|^2 + |d_p|^2 + |e_p|^2 + |f_p|^2. \tag{46}$$

The NMWD widths of s-shell Hypernuclei are thus derived in the following form [231]:

$$\Gamma_{\text{NM}}(^3_{\Lambda}\text{H}) = (3R_{n0} + R_{n1} + 3R_{p0} + R_{p1})\frac{\rho_3}{8}, \tag{47}$$

$$\Gamma_{\text{NM}}(^4_{\Lambda}\text{H}) = (R_{n0} + 3R_{n1} + 2R_{p0})\frac{\rho_4}{6}, \tag{48}$$

$$\Gamma_{\text{NM}}(^4_{\Lambda}\text{He}) = (2R_{n0} + R_{p0} + 3R_{p1})\frac{\rho_4}{6}, \tag{49}$$

$$\Gamma_{\text{NM}}(^5_{\Lambda}\text{He}) = (R_{n0} + 3R_{n1} + R_{p0} + 3R_{p1})\frac{\rho_5}{8}. \tag{50}$$

The isospin-dependence of the Block-Dalitz rates can be summarized by the following relation:

$$\frac{R_{n1}}{R_{p1}} \leq \frac{R_{n0}}{R_{p0}} = 2, \tag{51}$$

which holds for pure $\Delta I = 1/2$ transitions. Instead, for pure $\Delta I = 3/2$ transitions one has

$$\frac{R_{n1}}{R_{p1}} = \frac{R_{n0}}{R_{p0}} = \frac{1}{2}. \tag{52}$$

Various equalities and inequalities among the Hypernuclear decay rates can be obtained from eqs. (47)–(51) in the limit of pure $\Delta I = 1/2$ transitions. The most interesting relation reads

$$\frac{R_{n0}}{R_{p0}} \equiv \frac{\Gamma_n(^4_{\Lambda}\text{He})}{\Gamma_p(^4_{\Lambda}\text{H})} = 2. \tag{53}$$

Predictions of this kind turn out to be relevant for an experimental refutation of the $\Delta I = 1/2$ rule.

In various works, the Block-Dalitz rates were determined phenomenologically by fitting existing data on s-shell Hypernuclei for Γ_{NM} and Γ_n/Γ_p. We consider here in some detail the work by Schumacher [249]. He examined the existing data on NMWD of s-shell Hypernuclei to obtain a quantitative estimate of the relative strength of the two isospin channels of the Λ decay. He observed that the NMWD approaches available at that time were able to achieve reasonable agreement with the data on the total NMWD rates, by assuming the validity of the $\Delta I = 1/2$ rule, but no framework had succeeded in reproducing the measured Γ_n/Γ_p ratios. To further test the isospin rule for the less understood parity-conserving part of the weak interaction, he examined the available data on Γ_n/Γ_p for $^4_{\Lambda}$He and $^5_{\Lambda}$He and the ratio $\Gamma_{\text{NM}}(^4_{\Lambda}\text{He})/\Gamma_{\text{NM}}(^4_{\Lambda}\text{H})$ from refs. [178,231]. In the calculations, the $^1S_0$ ΛN initial state was isolated because it leads to isospin $I_f = 1$ final states, populated by both neutron- and proton-induced processes, while the $^3S_1$ ΛN initial state leads to $I_f = 0$ final states

that can be produced only by the proton-induced reaction, being the neutron-induced transition forbidden by the Pauli principle. From the data, Schumacher determined $R_{n0}/R_{p0} = 0.23 \pm 0.17$, to be compared with the value 2 predicted by pure $\Delta I = 1/2$ $\Lambda N \to nN$ transitions (see eq. (51)). This seems to suggest a rather large violation of the $\Delta I = 1/2$ rule for s-shell Hypernuclei NMWD. Due to the quite large errors affecting the experimental values of refs. [178, 231], ranging from 38% to 59%, this result, however, cannot be considered as definitive.

An analysis of more recent experimental data on s-shell Hypernuclei was performed in ref. [232], again with the phenomenological Block-Dalitz model. It was concluded that the large error bars in the data do not allow to draw definite conclusions about the possible violation of the $\Delta I = 1/2$ rule and the spin-dependence of the Block-Dalitz transition rates. The data turned out to be consistent with the hypothesis of validity of the $\Delta I = 1/2$ rule at the level of 60%. In other words, the $\Delta I = 1/2$ rule could be excluded only at the 40% confidence level. This result is not changed much if present data are used.

The usual outcome of all investigations is that more precise measurements of Γ_n for $^4_\Lambda$He and Γ_p for $^4_\Lambda$H (see eq. (53)) are needed to reach reliable conclusions on the possible violation of the $\Delta I = 1/2$ rule. At present, we known that $\Gamma_n(^4_\Lambda\text{He})$ is very small [175], compatible with zero within the experimental error, while there is no experimental data available for $\Gamma_p(^4_\Lambda\text{H})$: this prevents any further study for the possible violation of the isospin rule in the sector of s-shell Hypernuclei with the Block-Dalitz model. New and more precise experiments are thus necessary. In particular, for a measurement of the $^4_\Lambda$H NMWD one needs to tag the formation of the Hypernucleus through the detection of a neutral meson, like in (K^-, π^0) or (π^-, K^0) reactions, and so very intense beams are necessary. Such beams will be available very soon at the J-PARC accelerator complex, where the NMWD rates of $A = 4$ Hypernuclei will be determined with improved precision [250].

4.5 NMWD: Total decay width

The total NMWD rate, Γ_{NM}, can be determined experimentally from the lifetime and the MWD width measurements: $\Gamma_{\text{NM}} = \Gamma_T - \Gamma_{\pi^-} - \Gamma_{\pi^0}$. In fig. 26, taken from ref. [201], results obtained in the $4 \leq A \leq 238$ mass number range before 2001 are reported. The full circles are data from the KEK-E307 experiment [201], the open circles are previous data from counter experiments in which the formation of the Hypernucleus was explicitly identified [174, 175, 178], the open diamonds are data obtained at COSY on heavy nuclei, Bi and U, [251, 252], the solid, dot-dashed and dashed lines correspond, respectively, to calculations by Itonaga *et al.* [253], Ramos *et al.* [183] and Alberico *et al.* [184]. The open square shows a result from the direct quark mechanism [244, 245] for a Λ in nuclear matter. The experimental data up to $A = 56$ clearly indicate an increasing trend up to $A \sim 30$, followed by a saturation of Γ_{NM} around 1.2–1.3 Γ_Λ, which mainly affects
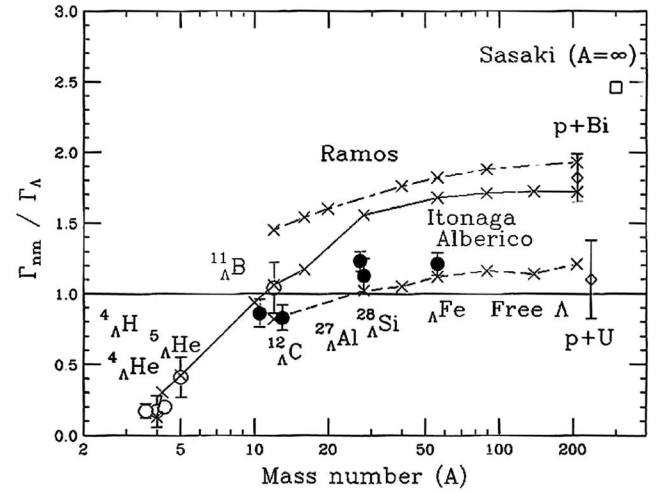
Fig. 26. Mass number dependence of the NMWD rate measured before 2001. Full circles are data from the KEK-E307 experiment [201], open circles are previous data from counter experiments in which the formation of the Hypernucleus was explicitly identified [174, 175, 178], open diamonds are data obtained at COSY on heavy nuclei, Bi and U, [251, 252]. Solid, dot-dashed and dashed lines correspond, respectively, to calculations by refs. [183, 253] and [184]. The open square shows a result from direct quark exchange by refs. [244, 245] for a Λ bound in nuclear matter. From ref. [201].

the Hypernucleus lifetime A-dependence. In ref. [183], the OPE potential was considered with pion renormalization effects in the nuclear medium, while the local density approximation was used to study finite Hypernuclei. The results for Γ_{NM} are sensibly larger than the experimental data. Recently, the calculation of ref. [183] was updated in ref. [184], which obtained values of Γ_{NM} in agreement with data by tuning the Landau-Migdal parameters which fixes the short-range part of the ΛN and NN interactions and by using more realistic in-medium Λ wave functions.

More recently, the KEK high statistics experiments E462 and E508 measured the lifetime, Γ_{π^-} and Γ_{π^0} for $^5_\Lambda$He and $^{12}_\Lambda$C with errors reduced to the 4–5% level [179, 197]; the resulting values of Γ_{NM}, in units of the free Λ decay rate Γ_Λ, are: $\Gamma_{\text{NM}}(^5_\Lambda\text{He}) = 0.406 \pm 0.020$ and $\Gamma_{\text{NM}}(^{12}_\Lambda\text{C}) = 0.953 \pm 0.032$, which adhere completely to the trend indicated by the previous data in fig. 26.

In the high mass number region, the very low values of lifetime obtained by ref. [58] for $A = 180$–225, give a very high value of the total NMWD rate, $\Gamma_{\text{NM}}/\Gamma_\Lambda = 1.82 \pm 0.14$, being the MWD mechanism completely negligible in this region. However, we have to remind the reader that, as discussed in sect. 4.1, this result was obtained from delayed fission experiments with the recoil shadow method, by detecting nuclear fragments which are supposed to originate from Hypernuclear fission, induced by NMWD. This method does not allow the identification of the produced Hypernucleus and requires model-dependent assumptions.

In table 8 we summarize the theoretical and experimental determinations of the total NMWD rate for $^5_\Lambda$He and $^{12}_\Lambda$C. We only list works which also determined the

Table 8. Theoretical and experimental results for the NMWD rate Γ_{NM} in units of the free Λ decay rate Γ_Λ.

Ref. and model	$^5_\Lambda$He	$^{12}_\Lambda$C
Sasaki *et al.* [244, 245]	0.52	
$\pi + K + $ DQ		
Jido *et al.* [239]		1.04
$\pi + K + 2\pi/\sigma + 2\pi + \omega$		
Parreño and Ramos [254]	0.43	0.73
$\pi + \rho + K + K^* + \omega + \eta$		
Itonaga *et al.* [253]	0.42	1.06
$\pi + 2\pi/\sigma + 2\pi/\rho + \omega$		
Barbero *et al.* [255]	0.69	1.17
$\pi + \rho + K + K^* + \omega + \eta$		
Bauer and Garbarino [165]		0.98
$\pi + \rho + K + K^* + \omega + \eta$		
BNL [178]	0.41 ± 0.14	1.14 ± 0.20
KEK [200]		0.89 ± 0.18
KEK [256]	0.50 ± 0.07	
KEK-E307 [201]		$0.828 \pm 0.056 \pm 0.066$
KEK-E462 [179]	0.404 ± 0.020	
KEK-E508 [197]		0.953 ± 0.032

Γ_n/Γ_p ratio. We note that only the theoretical works of refs. [165, 239] include two-nucleon induced weak decays. Most of the theoretical predictions agree with data. However, we have to note that with the most recent and precise KEK-E462 and KEK-E508 data one is able to distinguish among the different theoretical approaches. Moreover, within a particular approach, one could also determine the weak transition potential which better reproduce the KEK-E462 and KEK-E508 data.

4.6 NMWD: The Γ_n/Γ_p puzzle

Table 9 summarizes, in chronological order of publication, the results of measurements on NMWD of $A = 5$–56 Hypernuclei, performed from 1991 on: they represent the subsequent steps toward the solution of the Γ_n/Γ_p puzzle from the experimental side.

As can be seen from the table, the major part of the data have been obtained at KEK on $^5_\Lambda$He and $^{12}_\Lambda$C, which are the best known Hypernuclei as for NMWD, and were published from 1995 to 2009 [25–27, 200, 201, 257–260]. BNL experiments explored NMWD of $^4_\Lambda$He, $^5_\Lambda$He and $^{12}_\Lambda$C during the '90s [177, 178]. Recently, the FINUDA experiment performed a systematic study of the spectra of protons emitted in NMWD of $^5_\Lambda$He and the complete set of p-shell Hypernuclei [28, 29, 261].

Concerning the Γ_n/Γ_p ratio, the first counter experiments studying the NMWD processes detected only protons [178, 200, 256] and determined the Γ_p value for $^5_\Lambda$He, $^{11}_\Lambda$B and $^{12}_\Lambda$C; the Γ_n values were obtained by subtraction of all the other decay rates. Thus, the results might have been affected by an underestimation of the number of

emitted protons due to the rescattering of the proton inside the residual nucleus, *i.e.* the nucleon FSI, and/or to the existence of two-nucleon induced decay modes (34), which at that time had been suggested by ref. [162], but was not yet observed. In this way, missing protons could be considered as neutrons and resulted in an artificial increase of the Γ_n/Γ_p ratio, contributing, from the experimental side, to the birth of the Γ_n/Γ_p puzzle. $\Gamma_n/\Gamma_p = 0.93 \pm 0.55$ for $^5_\Lambda$He, $1.04^{+0.59}_{-0.48}$ for $^{11}_\Lambda$B and $1.33^{+1.12}_{-0.81}$ for $^{12}_\Lambda$C were reported by ref. [178], while ref. [200] obtained $\Gamma_n/\Gamma_p = 2.16 \pm 0.58^{+0.45}_{-0.95}$ for $^{11}_\Lambda$B and $1.87 \pm 0.59^{+0.32}_{-1.00}$ for $^{12}_\Lambda$C and ref. [256] reported $\Gamma_n/\Gamma_p = 1.97 \pm 0.67$ for $^5_\Lambda$He; the quite big statistical errors, varying from about 25% to about 50%, were due to the limited statistics of the data samples. On the contrary, smaller values of Γ_n/Γ_p, between 0.3 and 0.5, were predicted by the most realistic theoretical approaches for all these Hypernuclei.

4.6.1 Single nucleon spectra analyses

It must be stressed that nucleon rescattering in the residual nucleus strongly modifies the shape of the emitted nucleon distributions. FSI affect not only the energy and direction of nucleons, through scattering processes, but also their charge, through charge-exchange processes, and number, through knock-out reactions: FSI thus tend to enhance (decrease) the low-energy (high-energy) region in the nucleon energy spectra.

The highest-statistics experiment measuring single proton spectra were carried out at KEK-E307 [201, 257]. They measured the number of protons emitted in the

Table 9. NMWD measurements for $A = 5$–56 Hypernuclei after 1991, listed in chronological order of publication. In the first column details of the experiment are reported, in column two the reference is given and in column three details of the measurement are reported.

Experiment	Ref.	Measurement
BNL AGS, LESB I (K^-, π^-), 800 MeV/c	[178]	$^5_\Lambda$He: p spectrum, Γ_p, Γ_n, Γ_{NM}; $^{12}_\Lambda$C: Γ_{NM}, Γ_n/Γ_p
KEK PS E160 (π^+, K^+), 1.05 GeV/c	[200]	$^{12}_\Lambda$C: p spectrum; $^{11}_\Lambda$B and $^{12}_\Lambda$C: Γ_p/Γ_Λ, $\Gamma_{NM}/\Gamma_\Lambda$, Γ_n/Γ_p
KEK PS E278 (π^+, K^+), 1.05 GeV/c	[256]	$^5_\Lambda$He: Γ_{NM}, Γ_n/Γ_p
KEK PS E307 (π^+, K^+), 1.05 GeV/c	[257]	$^{12}_\Lambda$C and $^{28}_\Lambda$Si: p spectrum, Γ_n/Γ_p
KEK PS E369 (π^+, K^+), 1.05 GeV/c	[258]	$^{12}_\Lambda$C and $^{89}_\Lambda$Y: n spectrum $^{12}_\Lambda$C: Γ_n/Γ_p
KEK PS E462, E508 (π^+, K^+), 1.05 GeV/c	[259]	$^5_\Lambda$He and $^{12}_\Lambda$C: p and n spectra, Γ_n/Γ_p
KEK PS E307 (π^+, K^+), 1.05 GeV/c	[201]	$^{11}_\Lambda$B, $^{12}_\Lambda$C, $^{27}_\Lambda$Al, $^{28}_\Lambda$Si, $_\Lambda$Fe: p spectrum, $\Gamma_{NM}/\Gamma_\Lambda$
KEK PS E462 (π^+, K^+), 1.05 GeV/c	[25]	$^5_\Lambda$He: nn and np spectra, Γ_n/Γ_p
KEK PS E508 (π^+, K^+), 1.05 GeV/c	[26]	$^{12}_\Lambda$C: nn and np spectra, Γ_n/Γ_p
KEK PS E462, E508 (π^+, K^+), 1.05 GeV/c	[260]	$^5_\Lambda$He: p and n spectra $^{12}_\Lambda$C: p and n spectra, Γ_n/Γ_p
BNL AGS, LESB II (K^-, π^-), 750 MeV/c	[177]	$^4_\Lambda$He: p spectra, Γ_p, Γ_n, Γ_n/Γ_p
LNF DAΦNE, FINUDA (K^-_{stop}, π^-)	[261]	$^5_\Lambda$He, $^7_\Lambda$Li, $^{12}_\Lambda$C: p spectra
KEK PS E508 (π^+, K^+), 1.05 GeV/c	[27]	$^{12}_\Lambda$C: nn and np spectra, Γ_n, Γ_p, Γ_2
LNF DAΦNE, FINUDA (K^-_{stop}, π^-)	[28]	$^5_\Lambda$He, $^7_\Lambda$Li, $^9_\Lambda$Be, $^{11}_\Lambda$B, $^{12}_\Lambda$C $^{15}_\Lambda$N, $^{16}_\Lambda$O: p spectra, Γ_2
LNF DAΦNE, FINUDA (K^-_{stop}, π^-)	[29]	$^5_\Lambda$He, $^7_\Lambda$Li, $^9_\Lambda$Be, $^{11}_\Lambda$B, $^{12}_\Lambda$C $^{15}_\Lambda$N, $^{16}_\Lambda$O: np spectra, Γ_2
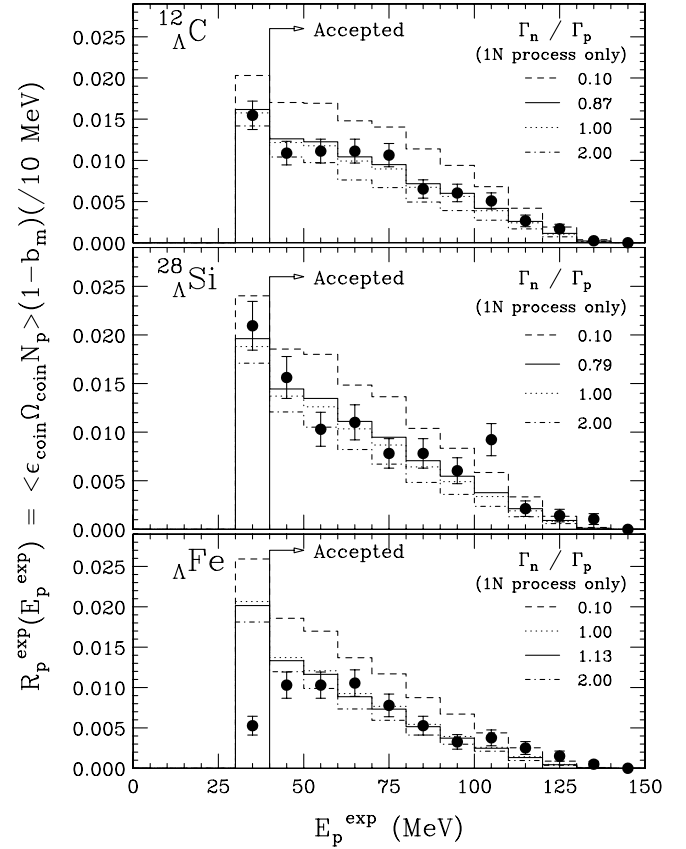
Fig. 27. Protons spectra from NMWD of $^{12}_\Lambda$C, $^{28}_\Lambda$Si and $_\Lambda$Fe as a function of the measured proton kinetic energy. The histograms superimposed to the data represent the simulated spectra from refs. [262, 263] for different values of the Γ_n/Γ_p ratio; the continuous line histograms refer to the best reproduction of the experimental spectra. From ref. [201].

NMWD of $^{12}_\Lambda$C, $^{28}_\Lambda$Si and $_\Lambda$Fe (a mixture of $^{56}_\Lambda$Fe, $^{55}_\Lambda$Fe and $^{55}_\Lambda$Mn), formed in the (π^+, K^+) reaction with the SKS spectrometer and a coincidence detector, located below and above the reaction target, consisting of timing and veto scintillators, range counters made up of stacks of scintillators and drift chambers to detect the charged decay products, to make particle identification (p.id.) between π^- and p and to measure their energy. The proton yield R_p^{exp} was measured as a function of the detected proton kinetic energy E_p and normalized to the number of produced Hypernuclei, giving $R_p^{exp} = Y_{coinc}(E_p)/Y_{hyp}$, where Y_{coinc} is the number of protons detected in coincidence with the K^+ identifying Hypernucleus production and Y_{hyp} is the number of produced Hypernuclei.

Figure 27 shows the raw proton spectra, normalized per NMWD and not corrected for the detector acceptance and efficiency, as a function of the measured proton energy; a lower cut at about 30 MeV, due to the target thickness, is visible. The R_p^{exp} spectra were then compared with those from theoretical calculations obtained by describing the one-nucleon induced NMWD processes (32) and (33) through OPE models, using the local density approxima-
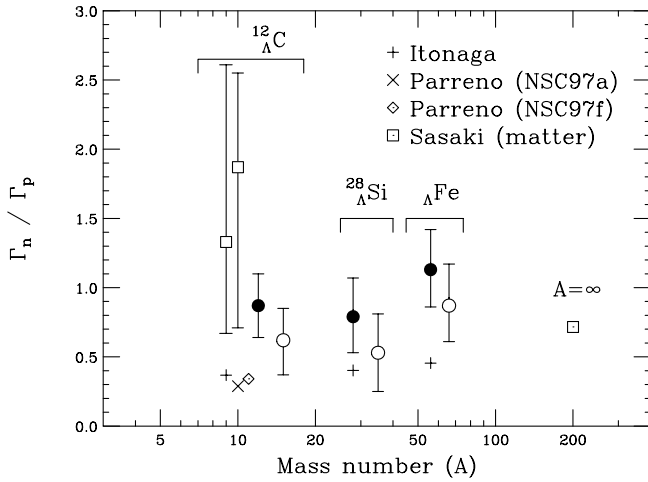
Fig. 28. Γ_n/Γ_p values for the Hypernuclei studied by refs. [178, 200], open squares, and by ref. [201], full (with only one-nucleon induced decays) and open (with the inclusion of two-nucleon induced decays) circles. Theoretical calculations by refs. [244, 245, 253, 254] are also indicated. From ref. [201].

tion [262, 263] and taking into account nucleon FSI effects in the residual nucleus by an intranuclear cascade (INC) calculations and FSI effects in the target material by the GEANT simulation [264]. The Γ_n/Γ_p values for the three targets were obtained in an indirect way, by a comparison between the calculated spectra and the experimental ones. The theoretical calculations are reported in fig. 27 as histograms superimposed to the experimental data, for different values of the Γ_n/Γ_p ratio. The final values of Γ_n/Γ_p are given in the same figure and correspond to the continuous line histograms; in fig. 28 they are reported as a function of the mass number together with the results of refs. [178, 200] and the calculations of refs. [244, 245, 253, 254]. Although all available experimental data agree within 1σ level, the values of ref. [201] are in the region around 0.5–1.0, whereas the previous ones are significantly larger. It turns out that there is no theoretical calculation able to reproduce simultaneously the measured values of Γ_n/Γ_p and Γ_{NM}. This is the core of the Γ_n/Γ_p puzzle.

The single-proton experiments show evident drawbacks in the determination of Γ_n/Γ_p. In particular, to obtain sufficient statistics, thick targets have to be used, in which protons strongly suffer from energy losses and an important deformation of their spectrum is produced. Nucleon FSI inside the nucleus reduce the population of the higher energy part of the spectrum and have to be taken into account in the theoretical calculations with a weight which is not known experimentally. Moreover, if neutrons are not directly counted, the MWD branching ratio has to be used, that contributes with its uncertainty to the total error. Finally, the proton energy threshold of the experimental apparatus produces a loss in the low-energy proton region, which is populated not only by one-nucleon induced decays but also by FSI and two-nucleon induced

processes, giving a systematically higher value for Γ_n/Γ_p if these last processes are ignored in the analysis.

It is thus clear that the measurement of the NMWD neutrons is mandatory for a reliable measurement of Γ_n/Γ_p. The detection of neutrons provides cleaner data than for protons: neutral particles, indeed, do not undergo energy loss in the target material; moreover, if neutrons are counted, it is no more necessary to use MWD branching ratios in the analysis. As for FSI, the effect on neutrons and on protons can be assumed to be similar, due to the charge symmetry of the NN scattering cross-section, and cancel out, at least at the first order, if one considers the ratio between neutron and proton spectra. Neutron spectra from NMWD of $^{12}_{\Lambda}$C and $^{89}_{\Lambda}$Y were measured with high statistics by the KEK-E369 experiment [258], as a by-product of the Hypernuclear spectroscopy measurements. For $^{12}_{\Lambda}$C the yield of neutrons from ref. [258] was compared to that of protons from ref. [201]; the N_n/N_p ratio between the neutron and proton numbers, corrected for acceptance and efficiency, was found to be slightly less than 2; this suggests, through the simple relation $N_n/N_p \sim 2(\Gamma_n/\Gamma_p)+1$ that holds considering the neutron and proton multiplicities in (32) and (33), that $\Gamma_n/\Gamma_p \sim 0.5$, improving the agreement with the most realistic theoretical predictions ranging from 0.3 to 0.5. The dominance of the proton-induced decay channel over the neutron-induced one was thus shown experimentally for the first time.

A very-high-statistics measurement of NMWD proton and neutron spectra was performed by the KEK-E462 experiment for $^{5}_{\Lambda}$He and by the KEK-E508 experiment for $^{12}_{\Lambda}$C [197, 259]. Protons and neutrons were identified by a decay coincidence system analogous to that of ref. [201], but figuring a larger angular acceptance and detection efficiency and a clear separation capability between $\pi/p/d$ for charged particles and γ/n for neutral particles. The kinetic energy detection threshold was 30 MeV for protons and 15 MeV for neutrons. The number of nucleons emitted per NMWD was determined as a function of the measured kinetic energy; the spectra are reported in fig. 29. It is possible to observe that the neutron spectra of both $^{5}_{\Lambda}$He and $^{12}_{\Lambda}$C have a shape similar to those of protons above the proton energy threshold. To evaluate the Γ_n/Γ_p ratio, a threshold was set at 60 MeV on both nucleons spectra, to reduce the contribution from FSI and two-nucleon induced processes; the values of $N_n/N_p = 2.17 \pm 0.15 \pm 0.16$ and $N_n/N_p = 2.00 \pm 0.09 \pm 0.14$ were obtained for $^{5}_{\Lambda}$He and $^{12}_{\Lambda}$C, respectively, leading to $\Gamma_n/\Gamma_p = (N_n/N_p - 1)/2 \sim 0.5$–0.6.

By comparing the proton and neutron spectra from ref. [197] with the neutron spectrum for $^{89}_{\Lambda}$Y from ref. [258] of fig. 29(c), it is possible to see the suppression of the high-energy neutron yield with the mass number and the enhancement of the low-energy region in the heavy Hypernuclei, which can be naturally interpreted as an effect of the FSI. If one-nucleon induced processes dominate and FSI can be neglected, the neutron energy spectrum is expected to show a broadened peak, due to the Fermi motion, at about one half of the reaction Q-value: this should be the case of $^{5}_{\Lambda}$He, due to its small mass number. On the other hand, the shape of the KEK $^{5}_{\Lambda}$He neutron spectrum
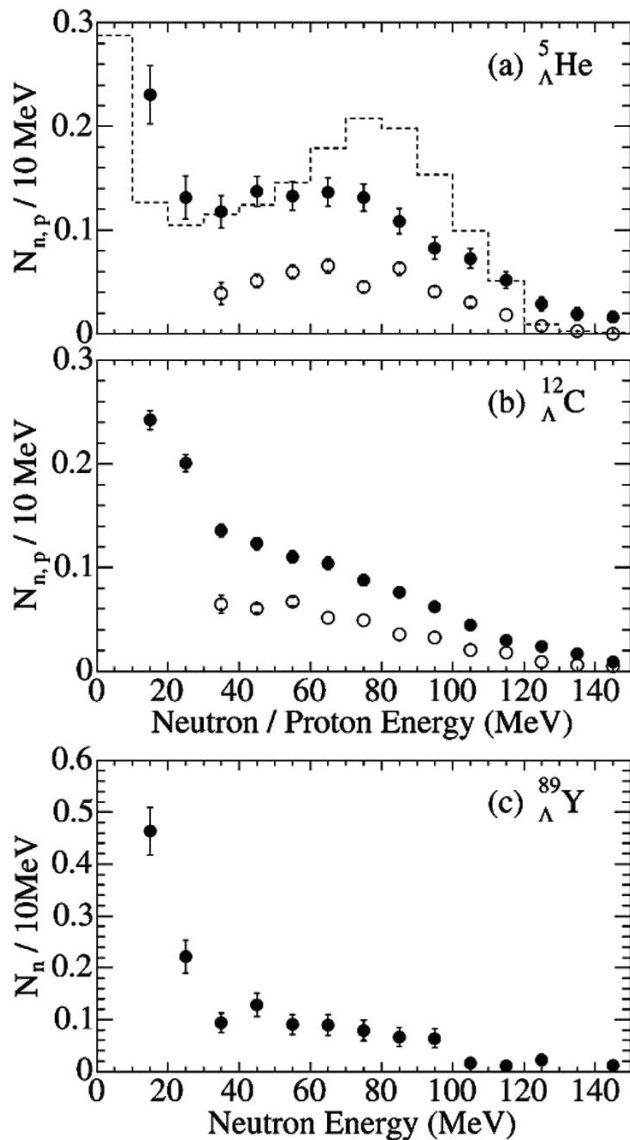
Fig. 29. Neutron (filled circles) and proton (open circles) kinetic energy spectra of (a) $^5_\Lambda$He and (b) $^{12}_\Lambda$C [197]; (c) neutron spectrum for $^{89}_\Lambda$Y [258]. The spectra are normalized per NMWD. The dashed histogram in the upper figure shows the neutron spectrum calculated in ref. [265]. From ref. [259].

of fig. 29 shows a strong increase below 30 MeV, so that FSI and two-nucleon induced processes are supposed to give an important contribution even in such a light Hypernucleus.

The first theoretical analysis of the $^5_\Lambda$He and $^{12}_\Lambda$C nucleon spectra was performed in refs. [265, 266], where a OME model for the $\Lambda N \rightarrow nN$ transition in finite nuclei was incorporated in the INC code of refs. [262, 263] to take into account nucleon FSI. The two-nucleon stimulated channel was also included, using the phenomenological approach of ref. [183]. This approach predicts $\Gamma_n/\Gamma_p = 0.46$ and $\Gamma_2/\Gamma_1 = 0.20$ for $^5_\Lambda$He and $\Gamma_n/\Gamma_p = 0.34$ and $\Gamma_2/\Gamma_1 = 0.25$ for $^{12}_\Lambda$C. Neutron and proton spectra were calculated and compared with the KEK data

for $^5_\Lambda$He and $^{12}_\Lambda$C of fig. 29, which are normalized per NMWD. For $^{12}_\Lambda$C, the KEK neutron spectrum could be explained, while the proton spectrum was overestimated, although the shape of the experimental distribution was qualitatively reproduced. For $^5_\Lambda$He, the theoretical neutron spectrum is overlaid on fig. 29 by the dashed histogram and looks significantly different from the observed one (both in shape and magnitude), which shows a maximum at about $Q/2$ but levels off in the region from 20 to 80 MeV. The theoretical spectrum for protons from $^5_\Lambda$He instead has the same shape of the KEK one, but overestimates the data. A calculation of the ratio between the neutron and proton spectra, N_n/N_p, in the KEK experimental conditions was also performed in ref. [265]. By applying a 60 MeV kinetic-energy threshold for both neutrons and protons, the results are: $N_n/N_p = 1.98$ for $^5_\Lambda$He and $N_n/N_p = 1.42$ for $^{12}_\Lambda$C, to be compared with the KEK determinations: $N_n/N_p = 2.17 \pm 0.15 \pm 0.16$ for $^5_\Lambda$He and $N_n/N_p = 2.00 \pm 0.09 \pm 0.14$ for $^{12}_\Lambda$C.

Recently, the FINUDA experiment obtained single proton energy spectra from NMWD of $^5_\Lambda$He, $^7_\Lambda$Li and $^{12}_\Lambda$C [261]. Exploiting the very good momentum resolution of the magnetic spectrometer (0.6% FWHM for π^- of ~ 270 MeV/c, 2% FWHM for p of ~ 400 MeV/c), the thinness of the targets (~ 0.2 g/cm^2 for ^{6}Li and ^{7}Li, ~ 0.4 g/cm^2 for ^{12}C) in which the low momentum K^-'s from Φ decay are stopped and interact at rest, the large angular coverage, $\sim 2\pi$ sr, and the very good p.id. capabilities of the detector ensemble, the energy spectra of NMWD protons were measured, in coincidence with a π^- identifying the formation of the ground state of the Hypernuclei, with an energy threshold as low as 15 MeV.

The FINUDA proton spectra from NMWD of $^5_\Lambda$He, $^7_\Lambda$Li and $^{12}_\Lambda$C are given in fig. 30. They all show a similar shape, *i.e.*, a peak around 80 MeV, corresponding to about a half the Q-value for the $\Lambda p \rightarrow np$ weak reaction, with a low-energy rise, due to the FSI and/or to two-nucleon induced weak decays [6,30,163,265,266], in spite of the large mass number difference of these nuclei. If the low energy rises were predominantly due to FSI effects, one should naturally expect that the broad peak structure at 80 MeV (coming from clean $\Lambda p \rightarrow np$ weak processes broadened by the Fermi motion of nucleons) would be smeared out for the heavier nuclei. As for the second effect, as already discussed, if the weak decay Q-value is shared by three nucleons, a low-energy rise may exist even for the very light s-shell Hypernuclei. The FINUDA data, thus, seem to agree with the hypothesis of a substantial contribution of the two-nucleon induced NMWD.

Figure 31 shows the comparison of the FINUDA spectrum for $^5_\Lambda$He with the KEK-E462 one [197]. The two spectra were normalized beyond 35 MeV (the proton-energy threshold of ref. [197]) and are compatible at a CL of 75%. Figure 32 shows the comparison of the FINUDA proton spectrum with the theoretical one calculated by ref. [265], which considered both two-nucleon induced decays and nucleon FSI. The two spectra were normalized to have the same area beyond 15 MeV (the FINUDA proton energy threshold). A compatibility test between the two
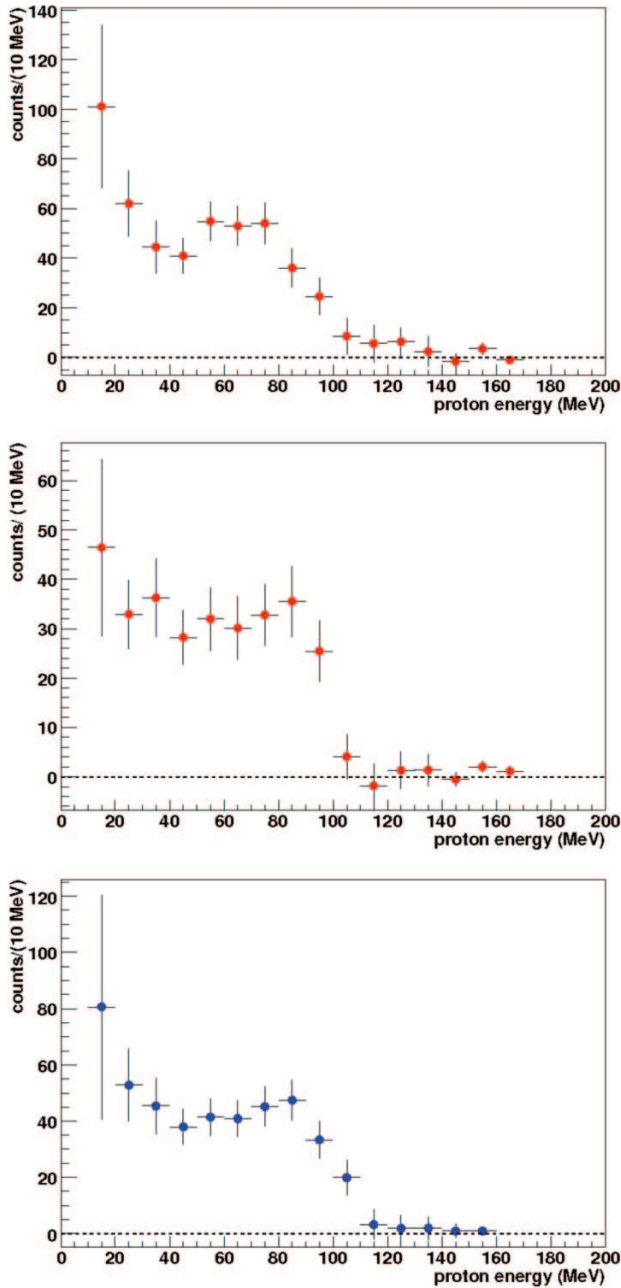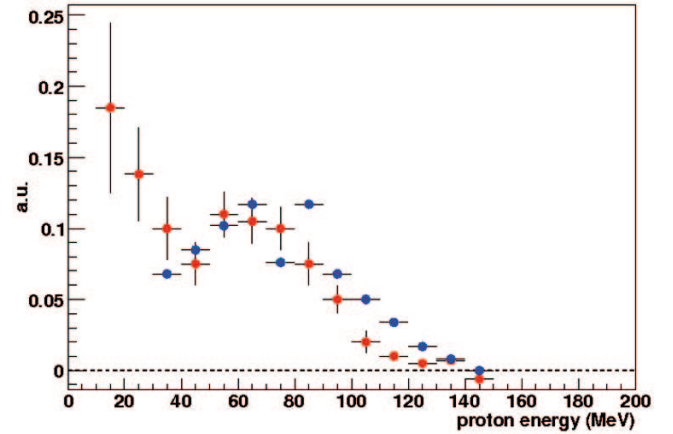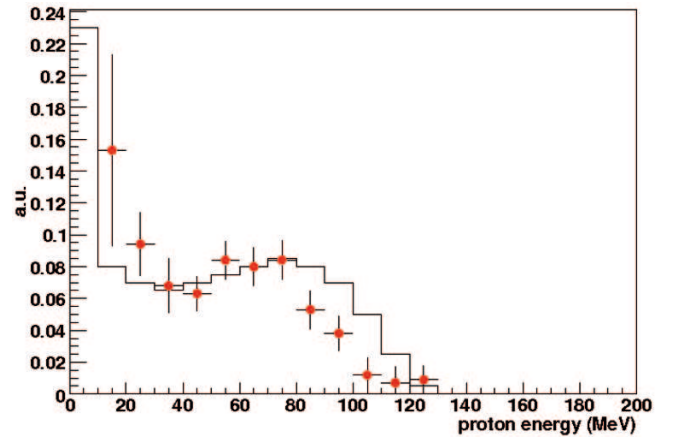
Fig. 30. Proton-energy spectrum of $^{5}_{\Lambda}$He (top), $^{7}_{\Lambda}$Li (center) and $^{12}_{\Lambda}$C (bottom) obtained by the FINUDA experiment. From ref. [261].

Fig. 31. FINUDA (red dots) [261] and KEK (blue dots) [197] proton spectrum from NMWD of $^{5}_{\Lambda}$He. The two spectra are normalized to have the same area beyond 35 MeV. From ref. [261].

Fig. 32. FINUDA (red dots) [261] and theoretical (continuous histogram) [265] proton spectrum from NMWD of $^{5}_{\Lambda}$He; The two spectra are normalized to have the same area beyond 15 MeV. From ref. [261].

spectra provides a CL of 80%, indicating that there is a disagreement between the two experiments, and also with theory. However, these incompatibilities are not so severe.

The situation for $^{12}_{\Lambda}$C is completely different. Figure 33 shows the comparison of the FINUDA and KEK [197] proton spectra: the spectra were normalized to the same area beyond 35 MeV. A compatibility test between the two data sets provides a CL of 20%. Figure 34 shows the comparison of the FINUDA proton spectrum with the calculated one by ref. [265]. The two spectra were normalized to the same area beyond 15 MeV. The compatibility

test between the theoretical and experimental spectra of fig. 33 provides a CL of 5%. The conclusion is that there is a strong disagreement between the two experiments and with theory.

Concerning the discrepancy between the FINUDA and KEK sets of data, it can be observed that in ref. [197] the proton energy was measured by a combination of time-of-flight and total energy deposit measurements. The energy loss inside the thick targets was corrected on an event-by-event basis. The energy resolution becomes poorer in the high energy-region, especially above 100 MeV, with the consequence that the KEK spectra could be strongly distorted. On the contrary, with FINUDA the proton momenta were measured by means of a magnetic analysis, with an excellent resolution and no distortion on the spectra is expected, in particular in the high-energy region. The FINUDA spectrum thus is less biased, even if it has a limited statistics.
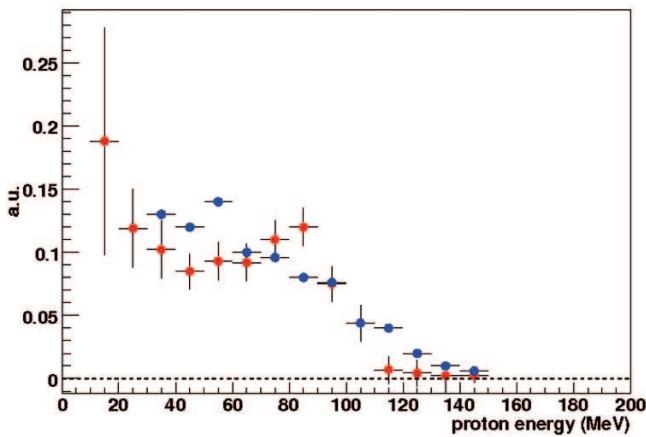
Fig. 33. FINUDA (red dots) and KEK (blue dots) [197] proton spectra from NMWD of $^{12}_{\Lambda}$C; the spectra are normalized to have the same area beyond 35 MeV. From ref. [261].
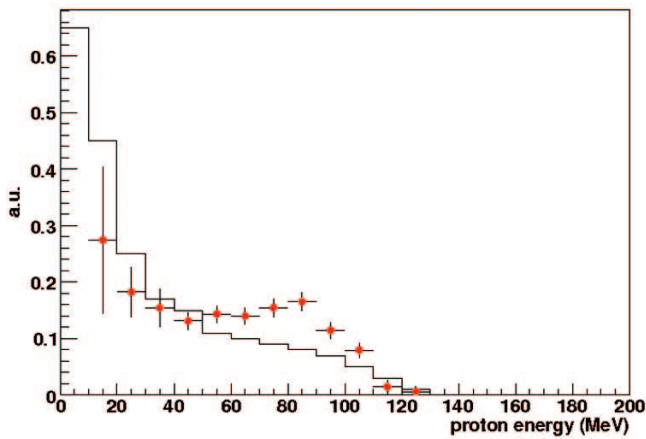

Fig. 34. FINUDA (red dots) and theoretical (continuous histogram) [265] proton spectra from NMWD of $^{12}_{\Lambda}$C; The two spectra are normalized to the same area beyond 15 MeV. From ref. [261].

The FINUDA experiment has then reported the NMWD proton spectra for $^{9}_{\Lambda}$Be, $^{11}_{\Lambda}$B, $^{12}_{\Lambda}$C, $^{13}_{\Lambda}$C, $^{15}_{\Lambda}$N and $^{16}_{\Lambda}$O [28]; they are given in fig. 35 together with the previous results for $^{5}_{\Lambda}$He and $^{7}_{\Lambda}$Li. Despite these distributions are affected by considerable errors, in particular in the low-energy region, they show a clear trend as a function of A (from 5 to 16): a peak around 80 MeV is broadened by the Fermi motion of nucleons and more and more blurred as A increases. The peak is smeared, on its low-energy side, by a rise that can be ascribed to FSI and two-nucleon induced weak decays.

The spectra of fig. 35 complete the FINUDA systematic study of the MWD and NMWD of p-shell Hypernuclei. In particular, as we shall discuss in sect. 4.7, these spectra make possible a determination of the two-nucleon induced decay contribution to NMWD in a model-independent way. It must be noted that FINUDA has not determined the value of Γ_p from the proton distributions, which are affected by unavoidable FSI and two-nucleon

induced reaction effects; the extraction of Γ_p would have been based mainly on the choice of the particular theoretical model adopted to describe the NMWD. The study of the A-dependence of the spectral shape, on the other hand, made possible to obtain information on the two-nucleon induced decay mechanism by relying only on simple theoretical assumptions, whose validity can be verified from the results of the measurements, and on previous experimental data on the one-nucleon induced decay rates.

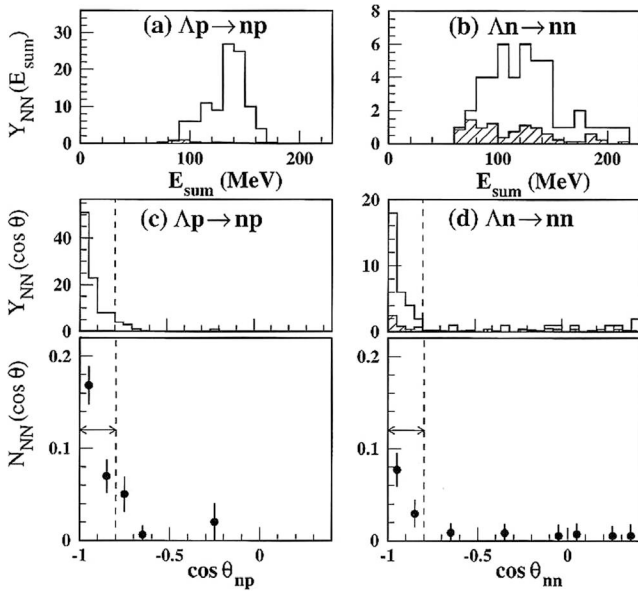### 4.6.2 Nucleon-nucleon coincidence spectra analyses

Simultaneous measurements of NMWD neutron and proton distributions turned out to be very important in clarifying the inconsistencies of the old experiments, in which only protons were measured and the determined Γ_n/Γ_p ratios were in clear disagreement with theory. To extract the value of Γ_n/Γ_p from a measured nucleon spectra it is always necessary to correct the distributions for nucleon FSI; by measuring the yield ratio N_n/N_p, the problem was only partially removed and a correction based on FSI calculations was still needed to determine a reliable value of Γ_n/Γ_p. In addition, the results of these single nucleon measurements could be possibly affected by a two-nucleon induced NMWD contribution.

Indeed, a real step forward in the solution of the Γ_n/Γ_p puzzle came from the measurement of the nucleon spectra in double coincidence and their theoretical analyses. Both the $\Lambda n \to nn$ and $\Lambda p \to np$ processes in nuclei are (quasi) two-body decay processes, so that the two NMWD nucleons have a clean back-to-back correlation if both of them do not suffer FSI and do not originate from two-nucleon induced effects; the one-nucleon induced processes could be thus clearly observed by measuring the yields of np and nn pairs in the back-to-back configuration and requiring that the sum of their kinetic energies correspond to the Q-value of the NMWD reaction. With these angular and energy restrictions, nucleon FSI and two-nucleon induced decay processes should provide small effects and a measurement of the N_{nn}/N_{np} ratio could directly provide the experimental value of Γ_n/Γ_p.

A nucleon-nucleon coincidence measurement for $^{5}_{\Lambda}$He NMWD [25] was performed at KEK-E462; the light target was chosen to reduce the influence of FSI. The upper panels of fig. 36 show the np and nn pair raw yields, Y_{np} and Y_{nn}, as a function of the kinetic energy sum of the nucleon pairs, before the application of the efficiency correction; only events in which each nucleon of the pair has a kinetic energy E_N above 30 MeV are considered, while the back-to-back topology requirement is not yet applied. The hatched histograms represent the contamination coming from the absorption of the π^- emitted in the MWD of $^{5}_{\Lambda}$He. In the energy sum spectrum of np pairs, a peak located around the Q-value of the NMWD process can be seen; its sharp shape indicates that the FSI effect is not severe and one-nucleon induced NMWD gives the main contribution. The nn pair energy distribution is instead broader, due to the limited resolution in the neutron energy measurement, and has a bigger background
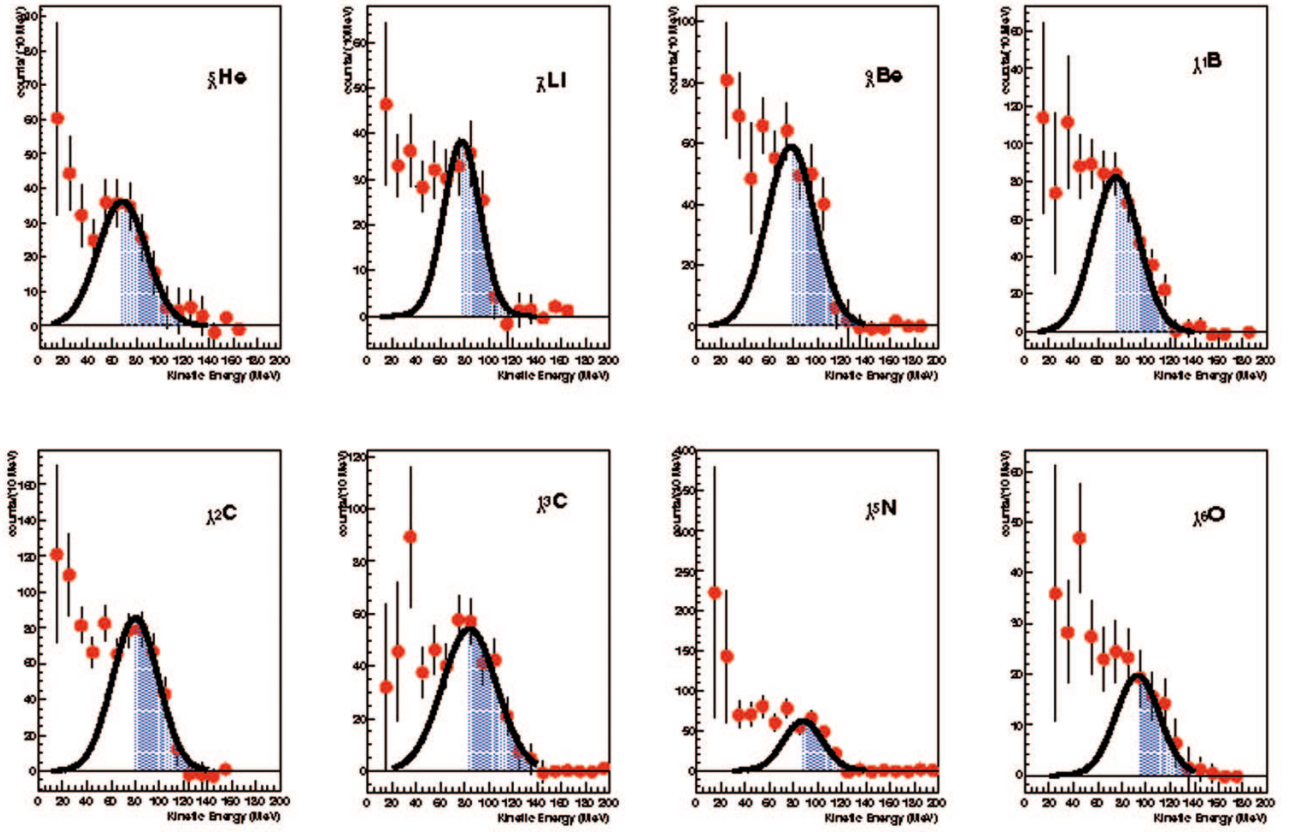
Fig. 35. Proton spectra from the NMWD of $^{5}_{\Lambda}$He, $^{7}_{\Lambda}$Li, $^{9}_{\Lambda}$Be, $^{11}_{\Lambda}$B, $^{12}_{\Lambda}$C, $^{13}_{\Lambda}$C, $^{15}_{\Lambda}$N and $^{16}_{\Lambda}$O measured by FINUDA. For more details, see sect. 4.7. From ref. [28].

Fig. 36. KEK-E462 nucleon-nucleon coincidence spectra for the NMWD of $^{5}_{\Lambda}$He. (a) and (b): np and nn pair raw yields as a function of the energy sum of the pair nucleons, before efficiency correction; a 30 MeV threshold was applied to both nucleons. (c) and (d): The upper panel shows the opening angle dependence of the np and nn raw yields; the lower panel shows the final angular spectra normalized for NMWD. From ref. [25].

contribution. In the lower panel, the raw yields, Y_{np} and Y_{nn}, are reported together with the efficiency corrected yields normalized per NMWD, N_{np} and N_{nn}, as a function of the opening angle between the two nucleons, θ_{np} and θ_{nn}. A strong angular correlation is evident and can be interpreted as a signature of the direct observation of the neutron- and proton-induced NMWD processes. Similar correlation measurements were then performed for $^{12}_{\Lambda}$C by KEK-E508 [26].

To determine Γ_n/Γ_p from the coincidence measurements, only events with $E_N > 30$ MeV and $\cos\theta_{NN} < -0.8$ were considered. In particular, taking into account that, in the N_{nn}/N_{np} ratio, factors as the NMWD branching ratio, the FSI effect and the solid angle acceptance cancel out in first approximation, it is possible to simply write: $\Gamma_n/\Gamma_p = N_{nn}/N_{np} = (Y_{nn}\epsilon_p)/(Y_{np}\epsilon_n)$, where ϵ_N is the detection efficiency of the nucleon N, if two-nucleon induced NMWD is neglected.

In this way, the results obtained by KEK-E462 and KEK-E508 are: $\Gamma_n/\Gamma_p(^{5}_{\Lambda}\text{He}) = 0.45 \pm 0.11 \pm 0.03$ [25] and $\Gamma_n/\Gamma_p(^{12}_{\Lambda}\text{C}) = 0.51 \pm 0.13 \pm 0.05$ [26]. These values were considered in refs. [25,26] to be free from ambiguities due to FSI and two-nucleon induced NMWD, due to the particular cuts imposed on the nucleon energy and nucleons angular correlation.

An evaluation of the effects of FSI and two-nucleon induced NMWD in coincidence nucleon spectra was per-

Table 10. Theoretical determinations of the Γ_n/Γ_p ratio obtained by fitting the KEK-E462 and KEK-E508 data on N_{nn}/N_{np}. The $1N$ results only include one-nucleon induced NMWD, while the $1N + 2N$ ones also include two-nucleon induced NMWD.

Ref.	$^{5}_{\Lambda}$He	$^{12}_{\Lambda}$C
[265]	0.40 ± 0.11 $(1N)$	0.38 ± 0.14 $(1N)$
	0.27 ± 0.11 $(1N + 2N)$	0.29 ± 0.14 $(1N + 2N)$
[30]		0.37 ± 0.14 $(1N)$
		0.34 ± 0.15 $(1N + 2N)$

formed in refs. [265, 266], with a OME model for the $\Lambda N \rightarrow nN$ transition in finite nuclei, a phenomenological approach of the two-nucleon stimulated channel and an INC code to take into account nucleon FSI. In particular, a weak-decay model-independent analysis of KEK-E462 and KEK-E508 coincidence measurements was performed. A fit of the N_{nn}/N_{np} data (taken with $E_N > 30$ MeV and $\cos \theta_{NN} < -0.8$) allowed the determination of the values of Γ_n/Γ_p reported in table 10. We see that the theoretical fits of data prefer smaller values for Γ_n/Γ_p than the purely experimental determinations of refs. [25, 26], given in the previous paragraph, which neglected nucleon FSI and two-nucleon induced decays. As one may expect, the differences are smaller with the fits neglecting the two-nucleon induced channels. This may signal a non-negligible effect of both FSI and two-nucleon induced processes in the N_{nn}/N_{np} data (however, we note that theoretical fits and pure data agree with each other within 1σ). This conclusion was corroborated by a recent analysis [30], analogous to the one of ref. [265] but performed entirely within a microscopic, nuclear matter formalism adapted to finite nuclei via the local density approximation. All the isospin channels for the two-nucleon induced mechanism were taken into account in ref. [30]: this also includes the channels $\Lambda nn \rightarrow nnn$ and $\Lambda pp \rightarrow npp$ besides the standard mode $\Lambda np \rightarrow nnp$ of the phenomenological approach of ref. [265]. The results of ref. [30] are also reported in table 10 and agree with the fits of ref. [265] despite the difference between the two frameworks.

In table 11 we summarize the theoretical and experimental determinations of Γ_n/Γ_p; the listed values correspond to the theoretical results and experiments of table 8 for Γ_{NM}. Some calculation can explain the recent KEK-E462 and KEK-E508 data for both Γ_n/Γ_p and Γ_{NM}. It is a widely shared opinion that this fact definitely provides a solution of the Γ_n/Γ_p puzzle. However, we note that, concerning Γ_n/Γ_p, the calculations tend to be more in agreement with the fits of refs. [30, 265], given in table 10, which do not neglect FSI and two-nucleon induced decays, than with the experimental determinations by refs. [25, 26], in which it was assumed that $\Gamma_n/\Gamma_p = N_{nn}/N_{np}$ when $E_p > 30$ MeV and $\cos \theta_{NN} < -0.8$. Together with the discussion of the previous paragraph, this comparison may signal a non-negligible effect of FSI and two-nucleon induced decays even in the favourable conditions of the performed correlation measurements.

4.7 Two-nucleon induced process and FSI effect in NMWD

In ref. [260], KEK-E508 single and coincidence spectra of nucleons from the NMWD of $^{12}_{\Lambda}$C were analyzed theoretically. One- and two-nucleon induced NMWD processes were described by phase-space arguments, without resorting to any weak decay model, while an INC code was used to incorporate nucleon FSI effects. Without the two-nucleon induced mechanism, a quenching of the observed nucleon spectra was found with respect to the calculated spectra. This quenching was interpreted as the effect of the two-nucleon induced NMWD, which cannot be separated kinematically from FSI-induced decays processes, since, in a first approximation, these decays share the same phase-space.

It was argued that the value of Γ_2 could be inferred from the measured spectra with the above theoretical description, by considering this rate as a free parameter. Figure 37 shows the experimental energy dependence of the sum of proton and neutron distributions, normalized per NMWD, from ref. [260]. The experimental spectra was simulated with different values of the $\Gamma_2/\Gamma_{\mathrm{NM}}$ ratio and an indication of a contribution as high as 40% to the total NMWD width was deduced.

In ref. [27], the same authors applied a different implementation of the INC calculations to estimate the FSI effect. The strengths of the used NN cross-sections were varied to fit the measured inelastic total cross-section data for ^{12}C(p, p') reactions, thus eliminating the uncertainties left in the previous INC implementation. The $^{12}_{\Lambda}$C experimental single- and double-coincidence nucleon spectra were reproduced by using the value $\Gamma_2/\Gamma_{\mathrm{NM}} = 0.29 \pm 0.13$, which is sizably lower than the previous indication. The following experimental values of the partial decay rates for $^{12}_{\Lambda}$C (in units of the free Λ decay rate Γ_Λ) were consequently determined by using previous KEK-E508 data on Γ_{NM} and Γ_n/Γ_p: $\Gamma_2 = 0.27 \pm 0.13$, $\Gamma_1 = 0.68 \pm 0.13$, $\Gamma_n = 0.23 \pm 0.08$ and $\Gamma_p = 0.45 \pm 0.10$. Figure 38 shows KEK-E508 $^{12}_{\Lambda}$C data together with the results of the theoretical fit for the momentum sum correlation ($p_{12} = |\boldsymbol{p}_1 + \boldsymbol{p}_2|$) of the sum of the nn and np distributions, the angular correlation of the sum of the nn and np distributions and the sum of the single n and p kinetic-energy distributions.

We also mention that an old BNL experiment, E788, which observed single-nucleon spectra from $^{4}_{\Lambda}$He NMWD, published only recently the final results [177]. An upper limit for the contribution of the two-nucleon induced mechanism to NMWD was established: $\Gamma_2/\Gamma_{\mathrm{NM}} \leq 0.24$ (95% CL). This result agrees with the discussed KEK-E508 determination of ref. [27], although it is for a lighter Hypernucleus.

The FINUDA experiment adopted a completely different approach to determine $\Gamma_2/\Gamma_{\mathrm{NM}}$. Starting from the measured inclusive single-proton spectra of $^{5}_{\Lambda}$He, $^{7}_{\Lambda}$Li, $^{9}_{\Lambda}$Be, $^{11}_{\Lambda}$B, $^{12}_{\Lambda}$C, $^{13}_{\Lambda}$C, $^{15}_{\Lambda}$N and $^{16}_{\Lambda}$O, a technique was introduced to disentangle the contribution coming from the two-nucleon induced decays from those of the one-nucleon induced decays and FSI [28]. The systematics over the mass number range $A = 5$–16, covered by the FINUDA measurements,

Table 11. Theoretical and experimental determinations of the Γ_n/Γ_p ratio.

Ref. and model	$^5_\Lambda$He	$^{12}_\Lambda$C
Sasaki *et al.* [244, 245]	0.70	
$\pi + K + $ DQ		
Jido *et al.* [239]		0.53
$\pi + K + 2\pi/\sigma + 2\pi + \omega$		
Parreño and Ramos [254]	0.46	0.34
$\pi + \rho + K + K^* + \omega + \eta$		
Itonaga *et al.* [253]	0.39	0.37
$\pi + 2\pi/\sigma + 2\pi/\rho + \omega$		
Barbero *et al.* [255]	0.24	0.21
$\pi + \rho + K + K^* + \omega + \eta$		
Bauer and Garbarino [165]		0.34
$\pi + \rho + K + K^* + \omega + \eta$		
BNL [178]	0.93 ± 0.55	$1.33^{+1.12}_{-0.81}$
KEK [200]		$1.87^{+0.67}_{-1.16}$
KEK [256]	1.97 ± 0.67	
KEK-E307 [201]		0.87 ± 0.23
KEK-E462 [25]	$0.45 \pm 0.11 \pm 0.03$	
KEK-E508 [26]		$0.51 \pm 0.13 \pm 0.05$
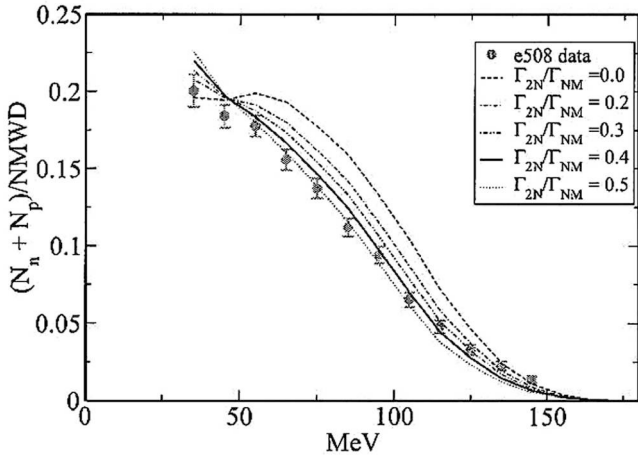
Fig. 37. Kinetic-energy dependence of the sum of single proton and neutron spectra per NMWD. Data are from KEK-E508 [259]. The curves represent calculations of the energy distribution with different contributions from the two-nucleon induced NMWD. From ref. [260].

was exploited and only simple assumptions were made in the calculations. Each spectrum was fitted, from 80 MeV proton kinetic energy on, with a Gaussian function to determine, by its mean value, the energy corresponding to the maximum of the one-proton induced contribution. The spectrum was then divided in two parts, one below

the mean value, with area A_{low}, and one above the mean value, with area A_{high}. It was assumed that the first part is populated by one-proton induced decays, two-nucleon induced decays and FSI processes, while the second part has contributions from one-proton induced decays and FSI, neglecting the two-nucleon induced decays contribution, which, above 70 MeV, accounts for only 5% of the total two-nucleon induced strength [265]. Then, the areas could be written as follows:

$$A_{\text{low}} = 0.5N(\Lambda p \rightarrow np) + N(\Lambda np \rightarrow nnp) + N_{\text{low}}^{\text{FSI}}, \quad (54)$$

$$A_{\text{high}} = 0.5N(\Lambda p \rightarrow np) + N_{\text{high}}^{\text{FSI}}, \quad (55)$$

where $N(\Lambda p \rightarrow np)$ is the number of protons coming from the one-proton induced decay and $N(\Lambda np \rightarrow nnp)$ is the number of protons coming from the two-nucleon induced decay $\Lambda np \rightarrow nnp$. Here the approximation $\Gamma_2 \sim \Gamma_{np}$ was made, which is suggested by ref. [247]. Moreover, $N_{\text{low}}^{\text{FSI}}$ is the difference between the number of detected protons and the number of primary protons, including one- and two-nucleon induced sources, for the low energy part of the spectrum and $N_{\text{high}}^{\text{FSI}}$ is the corresponding difference for the high-energy region.

For each Hypernucleus, of mass number A, the ratio

$$R(A) = \frac{A_{\text{low}}(A)}{A_{\text{low}}(A) + A_{\text{high}}(A)} \quad (56)$$

was evaluated. Figure 39 shows the A-dependence of data for $R(A)$ obtained for $^5_\Lambda$He and p-shell Hypernuclei. Taking
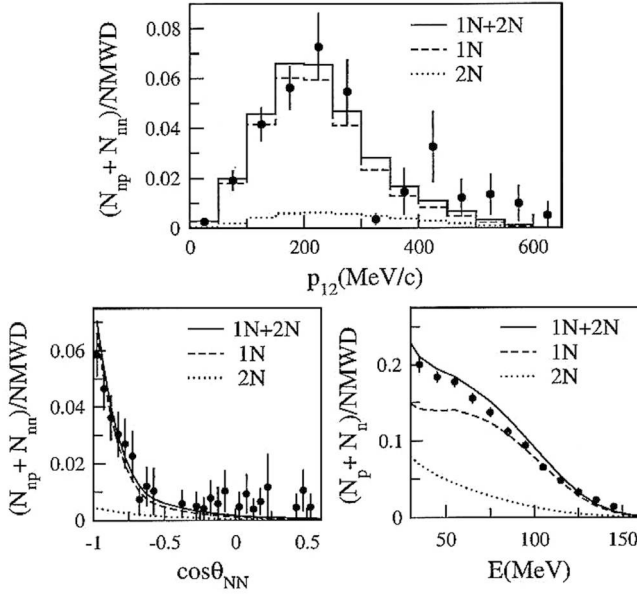
Fig. 38. Top: sum of the nn and np distributions as a function of the pair momentum sum correlation ($p_{12} = |\boldsymbol{p}_1 + \boldsymbol{p}_2|$). Bottom: sum of the nn and np distributions as a function of the pair opening-angle and kinetic-energy dependence of the sum of single n and p spectra. Data are from refs. [26, 259]. The curves represent the different contributions to the spectra obtained by the theoretical simulation of ref. [27]. Normalization is per NMWD.

into account that, following INC models, nucleon FSI effects can be assumed to be proportional to the number of nucleons of the residual nucleus and introducing the hypothesis that the Γ_2/Γ_p ratio is constant in the $A = 5$–16 Hypernuclear mass range [6, 163], one can then rewrite eq. (56) as

$$R(A) = \frac{0.5 + \dfrac{\Gamma_2}{\Gamma_p}}{1 + \dfrac{\Gamma_2}{\Gamma_p}} + bA, \tag{57}$$

where the b coefficient is the slope of the linear fit of fig. 39 and expresses the A-dependence of the FSI contribution. This equation can be solved for Γ_2/Γ_p, giving

$$\frac{\Gamma_2}{\Gamma_p} = 0.43 \pm 0.25. \tag{58}$$

To determine $\Gamma_2/\Gamma_{\mathrm{NM}}$, the data for Γ_n/Γ_p obtained in ref. [260] was used. The result is

$$\frac{\Gamma_2}{\Gamma_{\mathrm{NM}}} = 0.24 \pm 0.10. \tag{59}$$

This value supports both theoretical predictions [30, 165, 183, 184, 246, 247, 267] and the latest KEK experimental results of ref. [27], while it is lower than the KEK value suggested in ref. [260] by about 2σ.

A similar approach was afterwards used by the FI-NUDA experiment to extract the $\Gamma_2/\Gamma_{\mathrm{NM}}$ ratio for $A = 5$–16 Hypernuclei, but using np coincidence spectra [29].
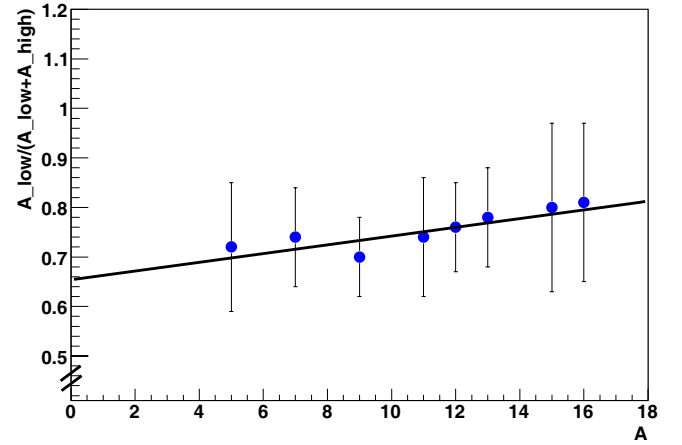
Fig. 39. The ratio $A_{\mathrm{low}}/(A_{\mathrm{low}} + A_{\mathrm{high}})$ as a function of the Hypernuclear mass number. The continuous line is a linear fit of the ratio. From ref. [28].

Neutrons were detected by the external scintillator barrel of the FINUDA apparatus and their kinetic energy was determined by means of time of flight measurements. (π^-, n, p) triple-coincidence events were selected, with a π^- momentum corresponding to the formation of bound Hypernuclear states.

To deduce the contribution of the two-nucleon induced process, np events with a proton of energy lower than an adequate threshold, $E_p^{\mathrm{thr}} = \mu - 20\,\mathrm{MeV}$, determined considering the mean value μ of the Gaussian functions used in the proton inclusive spectra analysis, and a restriction on the opening angle between the two nucleons, $\cos\theta_{np} \geq -0.8$, were considered for each Hypernucleus. In such a way, neutrons from two-nucleon induced processes were selected and could be counted for. With the applied selections, events due to the one-nucleon induced process would be excluded and only a small contribution of FSI is present.

For each nucleus the following ratio was then considered:

$$
\begin{aligned}
R_2(A) &= \frac{N_{np}(E_p \leq E_p^{\mathrm{thr}}, \cos\theta_{np} \geq -0.8)}{N_p(E_p > \mu)} \\
&= \frac{0.8 N(\Lambda np \to nnp) + FSI_{np}}{0.5 N(\Lambda p \to np) + FSI_p}, \tag{60}
\end{aligned}
$$

where $N_{np}(E_p \leq E_p^{\mathrm{thr}}, \cos\theta_{np} \geq -0.8)$ indicates the number of np events satisfying the condition which selects two-nucleon induced candidates and $N_p(E_p > \mu)$ is the number of protons in the part of the spectrum above the Gaussian mean value of ref. [28]; FSI_{np} and FSI_n indicate the residual effect of FSI processes on the corresponding samples. The factor 0.8 is due to the selections applied in the analysis. Figure 40 shows the dependence of R_2 on the Hypernuclear mass number.

Also in this case it is possible to apply the same considerations on the A-dependence of FSI and Γ_2 used for the study of the single proton spectra. In fig. 40 the trend of the ratio (60) is shown as a function of A: a roughly linear
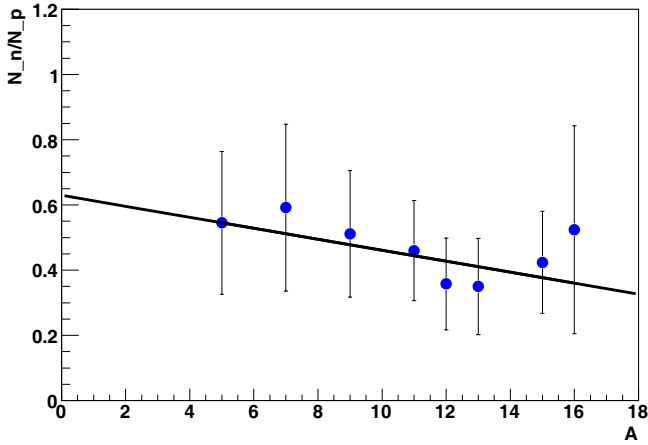
Fig. 40. The experimental and fitted R_2 ratio of eq. (60) as a function of the Hypernuclear mass number. From ref. [29].

behaviour of the above ratio, decreasing with A, is apparent. This is consistent with the simple hypothesis that the ratio R_2 is linearly correlated with the two-nucleon induced rate, which is in the first approximation independent of A [28], with a small contribution of FSI, which, in first approximation, increases linearly with A. By indicating with Γ_{np} the width of the np-induced decay of the Hypernucleus, it is possible to write

$$R(A) = \frac{0.8\Gamma_{np}}{0.5\Gamma_p} + bA, \qquad (61)$$

where the coefficient b is the slope of the linear fit of fig. 40 and expresses the A-dependence of the FSI contribution. This equation can be solved for Γ_{np}/Γ_p, getting

$$\frac{\Gamma_{np}}{\Gamma_p} = 0.39 \pm 0.16_{\text{stat}} {}^{+0.04}_{-0.03\,\text{sys}}. \qquad (62)$$

The obtained Γ_{np} width can be used to obtain Γ_2 by following the theoretical predictions of ref. [247]; moreover, by assuming again that Γ_n/Γ_p is independent of the Hypernuclear species and using for this ratio the data obtained by KEK [260], the FINUDA final result is

$$\frac{\Gamma_2}{\Gamma_{\text{NM}}} = 0.21 \pm 0.07_{\text{stat}} {}^{+0.03}_{-0.02\,\text{sys}}, \qquad (63)$$

where the error is reduced with respect to the one of ref. [28].

Finally, thanks to the large solid angle coverage of the FINUDA apparatus ($\sim 2\pi$ srad) and to its detection efficiency for neutrons and for protons with low kinetic energy, it has been possible to find one event [268] in which also the second neutron from pn-induced NMWD was detected, for which the angles between each neutron and the proton, and between the two neutrons are greater than $\pi/2$, which is the maximum angle expected for a simple nucleon-nucleon scattering. The projection of this event, occurring on a ^{7}Li target, onto the $\rho - \phi$ plane of the apparatus is shown in fig. 41. The analysis of the momentum
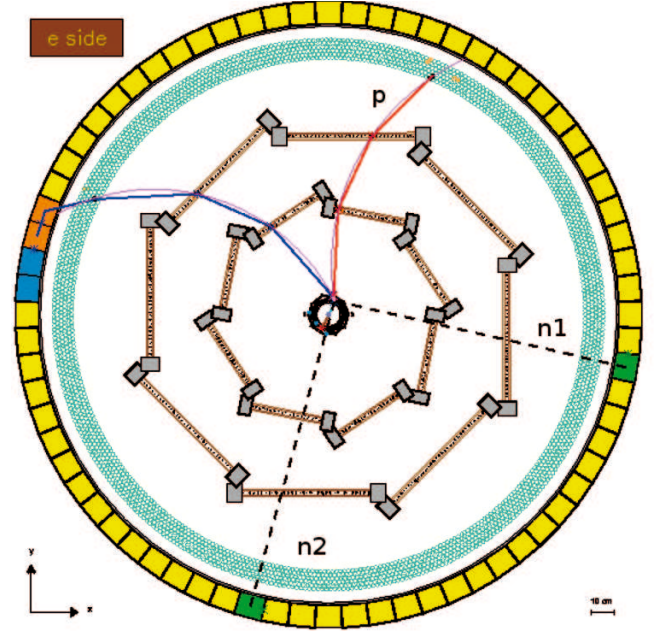
Fig. 41. Pictorial representation of the $\Lambda np \to nnp$ event seen by FINUDA on a ^{7}Li target. The blue track represents the trajectory of the π^- from the Hypernucleus formation reaction. From [268].

of the production π^- ((276.9 ± 1.2) MeV/c), indicated by the blue trajectory in fig. 41, of the total energy of the detected nucleons ($T_{nnp} = (172.7 \pm 16.3)$ MeV), together with the determination of the kinetic energy of the missing daughter nucleus ($T_{miss} = (6.3 \pm 4.3)$ MeV), leads to conclude that the event is a strong candidate for the decay reaction:

$$^7_\Lambda \text{Li} \to {}^4\text{He} + n + n + p, \qquad (64)$$
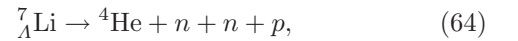
where the high binding energy of the ^{4}He (~ 28 MeV) allows to perform an exclusive identification of the final state, giving a value for the Q of the reaction as high as $Q = 167$ MeV. Moreover, the topology of the event and the particular values of the angles between the three detected nucleons ($\theta_{n_2 p} = (154.4 \pm 2.8)°$, $\theta_{n_1 p} = (102.3 \pm 2.2)°$, $\theta_{n_2 n_1} = (94.8 \pm 3.6)°$) allow to exclude the possibility of a proton-induced decay followed by a nucleon-nucleon scattering. A final remark is that both π^- and p are emitted in the same hemisphere (relative angle of $(33.4 \pm 3.7)°$), avoiding the possibility that they come from a physical event due to K^- capture on a correlated np pair, with a π^- of momentum comprised in the range for ground-state Hypernucleus formation, in coincidence with two random signals from the external TOF system (see fig. 41), taken as true neutron events. As a matter of fact, π^- and p from a K^- capture on a correlated np pair are emitted in opposite hemisphere [41]. All the reconstructed kinematical observables are detailed in table 12.

So, from the kinematic analysis, it is possible to conclude that the event can safely be attributed to the exclusive reaction (64) and represents the first direct ("smoking gun") experimental evidence of a two-nucleon induced NMWD.

Table 12. Kinematics of the $\Lambda(np) \to nnp$ event of fig. 41: p_{π^-} indicates the momentum of the Hypernucleus formation π^-, T_p the p kinetic energy, T_{n1} the kinetic energy of one of the neutrons, T_{n2} the kinetic energy of the second one, θ_{n1n2} the angle between the two neutrons, θ_{n1p} the angle between the first n and the p, θ_{n2p} the angle between the second n and the p, $\theta_{\pi^- p}$ the angle between the formation π^- and the p, p_{miss} the missing momentum of the final state, and MM the missing mass for the decay of the Hypernucleus from its ground state. The quoted error is statistical.

p_{π^-} (MeV/c)	276.9 ± 1.2
T_p (MeV)	51.11 ± 0.85
T_{n1} (MeV)	110 ± 23
T_{n2} (MeV)	16.9 ± 1.7
θ_{n1n2} (deg)	94.8 ± 3.8
θ_{n1p} (deg)	102.2 ± 3.4
θ_{n2p} (deg)	154 ± 19
$\theta_{\pi^- p}$ (deg)	33.4 ± 3.7
p_{miss} (MeV/c)	217 ± 44
MM (MeV/c^2)	3710 ± 23

Various theoretical approaches were applied to the calculation of Γ_2 [30,165,183,184,246,247,267]. We summarize the theoretical and experimental determinations of Γ_2 and $\Gamma_2/\Gamma_{\rm NM}$ in table 13 together with information on the Hypernucleus and the isospin channels considered in the calculations and on the Hypernucleus and the kind of spectra (single or in coincidence) analyzed in the experiments. All the calculations were performed with a nuclear matter approach and then extended to $^{12}_{\Lambda}$C via the local density approximation. In refs. [183,184], a phenomenological scheme based on data on pion absorption in nuclei was used to predict the np-induced decay rate Γ_{np}. ref. [184] updates the predictions of ref. [183] by using more realistic Λ wave functions in Hypernuclei and short-range correlations in the baryon-baryon strong interactions. All isospin channels of the two-nucleon stimulated decay, $\Lambda nn \to nnn$, $\Lambda np \to nnp$ and $\Lambda pp \to npp$, are included in the diagrammatic microscopic approach of refs. [165,246,247,267]. In particular, Pauli exchange and ground-state contributions were also studied in this kind of calculation [165,247]. Among the predictions of the microscopic approach, only the most updated, from ref. [165], are reported in table 13. The microscopic approach also lead to the following predictions for the two-nucleon induced partial rates: $\Gamma_{np} : \Gamma_{pp} : \Gamma_{nn} = 0.83 : 0.12 : 0.04$; as expected, the two-nucleon stimulated decay width is dominated by the np-induced process.

Considering instead the data reported in table 13, it must be noted that the two values obtained by FINUDA are not independent of each other, since the proton required in coincidence with a π^- in ref. [28] and with a (π^-, n) pair in ref. [29] belongs to the same experimental sample. To compare with the KEK-E508 determination [27], the FINUDA value of ref. [29], affected by a smaller error, can be used: the two results are com-

pletely compatible within errors and by evaluating their weighted mean it is possible to conclude that, for p-shell Λ-Hypernuclei, $\Gamma_2/\Gamma_{\rm NM} = 0.23 \pm 0.06$.

All the predictions of table 13 are consistent with the individual KEK and FINUDA experimental determinations of Γ_2 and $\Gamma_2/\Gamma_{\rm NM}$ (however, only the microscopic calculation of ref. [165] reproduces within 1σ the weighted mean datum of the previous paragraph). One may conclude that the two-nucleon induced NMWD of Hypernuclei is rather well understood at present.

A general conclusion concerning the study of NMWD of Hypernuclei is now in order. As discussed in sect. 4.3, thanks to the large momentum transfer of the NMWD channel, one expects to obtain information on the four-baryon, strangeness changing, $\Lambda N \to nN$ weak interaction from Hypernuclear decay measurements. However, the study of NMWD of p-shell Hypernuclei clearly indicates that the nuclear effects cannot be disregarded, since mechanisms such as FSI and two-nucleon induced decay are not at all inessential but partially mask the elementary four-baryon reaction.

Therefore, the best way to proceed for a detailed study of the $\Lambda N \to nN$ reaction seems to be to learn how to parametrize the nuclear effects from the systematic study of Hypernuclear NMWD over an appropriate mass number range, as done by FINUDA for p-shell Hypernuclei, and then to use this information to try to disentangle the four-baryon reaction properties from a very high-statistics decay measurement on a single nucleus, possibly with low mass number.

A determination of Γ_n, Γ_p and Γ_2 for $^{12}_{\Lambda}$C with a 10% error level is expected from J-PARC [269], from double- and triple-nucleon coincidence measurements. This will allow to lower the error on the determination of $\Gamma_2/\Gamma_{\rm NM}$.

4.8 Rare two-body NMWD of s-shell Hypernuclei

The decay of the light Hypernuclei $^{4}_{\Lambda}$He and $^{5}_{\Lambda}$He in two-body channels is a rare process because of the large momentum transfer and of the possible two-step mechanisms involved. It can occur through the following reactions:

$$^{4}_{\Lambda}\text{He} \to d + d, \tag{65}$$

$$^{4}_{\Lambda}\text{He} \to p + t, \tag{66}$$

$$^{4}_{\Lambda}\text{He} \to n + {}^{3}\text{He}, \tag{67}$$

$$^{5}_{\Lambda}\text{He} \to d + t. \tag{68}$$

The existing observations of two-body NMWD of Hypernuclei are very scarce and date back to bubble chamber and emulsion experiments [270–272]; in particular, reaction (67) has not yet been observed. The only existing calculation for the $^{4}_{\Lambda}$He two-body NMWD rates was performed long ago in ref. [273], and only one theoretical evaluation for the expected decay rates of $^{5}_{\Lambda}$He exists [274].

Recently, rare two-body NMWD have been studied by means of the FINUDA spectrometer [275]; the large solid angle coverage, the good p.id. properties and the good

Table 13. Summary of the theoretical and experimental values of Γ_2 and $\Gamma_2/\Gamma_{\mathrm{NM}}$.

Ref.	Γ_2	$\Gamma_2/\Gamma_{\mathrm{NM}}$	Notes
[183]	0.23	0.16	$^{12}_{\Lambda}\mathrm{C}$, $\Gamma_2 = \Gamma_{np}$
[184]	0.16	0.16	$^{12}_{\Lambda}\mathrm{C}$, $\Gamma_2 = \Gamma_{np}$
[165]	0.25	0.26	$^{12}_{\Lambda}\mathrm{C}$, $\Gamma_2 = \Gamma_{np} + \Gamma_{nn} + \Gamma_{pp}$
BNL-E788 [177]		≤ 0.24	$^{4}_{\Lambda}\mathrm{He}$, n and p spectra
KEK-E508 [27]	0.27 ± 0.13	0.29 ± 0.13	$^{12}_{\Lambda}\mathrm{C}$, nn and np spectra
FINUDA [28]		0.24 ± 0.10	$A = 5\text{–}16$, p spectra
FINUDA [29]		$0.21 \pm 0.07_{\mathrm{stat}}\,{}^{+0.03}_{-0.02\,\mathrm{sys}}$	$A = 5\text{–}16$, np spectra

momentum resolution of the experimental apparatus allowed the identification of reactions (65), (66) and (68), which are characterized by a back-to-back topology of the outgoing particles/clusters and by quite high momenta ($p_d = 570\,\mathrm{MeV}/c$ for (65), $p_p = 508\,\mathrm{MeV}/c$ for (66) and $p_d = 597\,\mathrm{MeV}/c$ for (68)).

Reactions (65), (66) and (68) have been studied as decays of $^{4}_{\Lambda}\mathrm{He}$ and $^{5}_{\Lambda}\mathrm{He}$ Hyperfragments produced by the interaction of stopped K^-'s on the various targets used in FINUDA and identified by means of the detection of the π^- emitted in the production reaction; in particular, (65) and (66) have been looked for on all the nuclear targets, while (68) has been searched for on $^6\mathrm{Li}$ and $^7\mathrm{Li}$ targets only.

Concerning the $^{4}_{\Lambda}\mathrm{He} \to d + d$ decay, an average yield value $Y(^{4}_{\Lambda}\mathrm{He} \to d + d) = (2.82 \pm 0.62) \times 10^{-5}/K^-_{\mathrm{stop}}$ is obtained. The $^{4}_{\Lambda}\mathrm{He} \to p + t$ decay at rest looks favoured: an average yield of $Y(^{4}_{\Lambda}\mathrm{He} \to p + t) = (5.42 \pm 3.43) \times 10^{-5}/K^-_{\mathrm{stop}}$ is obtained. As for the $^{5}_{\Lambda}\mathrm{He} \to d + t$ decay, the average yield value over $^6\mathrm{Li}$ and $^7\mathrm{Li}$ nuclei is $Y(^{5}_{\Lambda}\mathrm{He} \to d + t) = (1.23 \pm 0.70) \times 10^{-4}/K^-_{\mathrm{stop}}$, corresponding to a branching ratio of $(2.8 \pm 1.4) \times 10^{-3}$, in rough agreement with the theoretical expectation of a factor 100 less than the total NMWD branching ratio.

4.9 Asymmetry in NMWD of polarized Hypernuclei

Λ-Hypernuclei can also be produced in polarized states [276, 277]. Thanks to the large momentum transfer involved, the $n(\pi^+, K^+)\Lambda$ reaction was used, at $p_\pi = 1.05\,\mathrm{GeV}$ and small K^+ laboratory scattering angles ($2° \lesssim \theta_K \lesssim 15°$), to produce Hypernuclear states with a substantial amount of spin-polarization, preferentially aligned along the axis normal to the reaction plane [278, 279], the so-called polarization axis. The origin of Hypernuclear polarization is twofold [276, 277]. It is known that the distortions (absorptions) of the initial (π^+) and final (K^+) meson waves produce a small polarization of the Hypernuclear orbital angular momentum up to laboratory scattering angles $\theta_K \sim 15°$ (at larger scattering angles, the orbital polarization increases with a negative sign). At small but non-zero angles, the main source of polarization is due to an appreciable spin-flip interaction term in the elementary reaction $\pi^+ n \to \Lambda K^+$, which interferes with

the spin-nonflip amplitude. In a typical experimental situation with $p_\pi = 1.05\,\mathrm{GeV}$ and $\theta_K \sim 15°$, the polarization of the hyperon spin in the free $\pi^+ n \to \Lambda K^+$ process is about 0.75.

The distribution of protons produced in one-nucleon induced NMWD of polarized Hypernuclei shows an angular asymmetry: the difference between the number of protons emitted along the polarization axis and the number of protons outgoing in the opposite direction determines this asymmetry. It can be shown that the proton asymmetry is originated by the interference between the parity-violating and parity-conserving $\Lambda N \to nN$ transition amplitudes with different values of the isospin of the final NN pair [280]. Asymmetry studies are thus expected to provide new constraints on the strengths and (especially) the relative phases of the decay amplitudes, *i.e.*, on the dynamics of Hypernuclear decay.

Despite the important progress on the determination of the NMWD rates (especially the Γ_n/Γ_p and $\Gamma_2/\Gamma_{\mathrm{NM}}$ ratios) discussed above, another intriguing problem which was solved only recently concerns a strong disagreement between theory and experiment on the weak decay asymmetry.

The intensity of protons emitted in $\Lambda p \to np$ decays along a direction forming an angle θ with the polarization axis is given by [281]

$$I(\theta, J) = I_0(J)[1 + \mathcal{A}(\theta, J)], \qquad (69)$$

J being the total spin of the Hypernucleus and I_0 the (isotropic) intensity for an unpolarized Hypernucleus. In the shell-model weak-coupling scheme, one can write:

$$\mathcal{A}(\theta, J) = P_\Lambda(J)\, a_\Lambda \cos\theta, \qquad (70)$$

where P_Λ is the polarization of the Λ spin and a_Λ the *intrinsic* Λ asymmetry parameter, which is a characteristic of the elementary process $\Lambda p \to np$.

Nucleon FSI acting after the NMWD modify the weak decay intensity (69): this means that the intrinsic asymmetry a_Λ is not an observable. The *observable* asymmetry, $a_\Lambda^{\mathrm{M}}(J)$, which is expected to depend on the considered Hypernucleus, is therefore derived from the observable proton intensity, I^{M}. Assuming for I^{M} the same θ-dependence as in the weak decay intensity I, one obtains the observable

Table 14. Theoretical and experimental determinations of the asymmetry parameters.

Ref. and model	$^5_\Lambda$He	$^{12}_\Lambda$C
Sasaki *et al.* [244, 245]		
$\pi + K + DQ$	-0.68	
Parreño and Ramos [254]		
OME: $\pi + \rho + K + K^* + \omega + \eta$	-0.68	-0.73
Itonaga *et al.* [286]		
$\pi + K + \omega + 2\pi/\rho + 2\pi/\sigma$	-0.33	
Barbero *et al.* [287]		
OME: $\pi + \rho + K + K^* + \omega + \eta$	-0.54	-0.53
Alberico *et al.* [288]		
OME + FSI	-0.46	-0.37
Chumillas *et al.* [240]		
OME + $2\pi + 2\pi/\sigma$	$+0.041$	-0.207
OME + $2\pi + 2\pi/\sigma$ + FSI	$+0.028$	-0.126
Itonaga *et al.* [292]		
$\pi + K + \omega + 2\pi/\rho + 2\pi/\sigma + \rho\pi/a_1 + \sigma\pi/a_1$	$+0.083$	$+0.045$
KEK-E462 [283, 284]	$0.07 \pm 0.08^{+0.08}_{-0.00}$	
KEK-E508 [283, 284]		$-0.16 \pm 0.28^{+0.18}_{-0.00}$

asymmetry as

$$a_\Lambda^{\mathrm{M}}(J) = \frac{1}{P_\Lambda(J)} \frac{I^{\mathrm{M}}(0°, J) - I^{\mathrm{M}}(180°, J)}{I^{\mathrm{M}}(0°, J) + I^{\mathrm{M}}(180°, J)}. \quad (71)$$

One expects an attenuation of the asymmetry due to FSI, $|a_\Lambda^{\mathrm{M}}(J)| < |a_\Lambda|$.

Equation (71) is actually the relation used to determine experimentally $a_\Lambda^{\mathrm{M}}(J)$. These measurements generally suffer from large uncertainties, principally due to limited statistics and to the poor knowledge of the hyperon-spin polarization. For $^5_\Lambda$He, P_Λ was measured [282] by observing the asymmetric emission of negative pions in its mesonic decay and by assuming that the pion asymmetry in the mesonic decay of $^5_\Lambda$He coincides with the value measured in the free $\Lambda \to \pi^- p$ decay. Unfortunately, the small branching ratio and asymmetry for the mesonic decay of *p*-shell Hypernuclei makes a measurement of the Λ-spin polarization very difficult for these systems. Therefore, in the proton asymmetry measurements for $^{11}_\Lambda$B and $^{12}_\Lambda$C [279, 283, 284], P_Λ was evaluated theoretically by adopting the distorted wave impulse approximation of ref. [285]. Such kind of calculation requires a delicate analysis of 1) the polarization of the Hypernuclear states directly produced in the production reaction and 2) the depolarization effects due to strong and electromagnetic transitions of the populated excited states, which take place before the weak decay.

In table 14 we compare the theoretical and experimental determinations of the decay asymmetries for $^5_\Lambda$He and $^{12}_\Lambda$C. While inexplicable inconsistencies appeared between the first KEK asymmetry experiments of refs. [278, 279], the recent and more accurate KEK data [283,284] reported in table 14 favor small a_Λ^{M} values, compatible with a vanishing value, for both $^5_\Lambda$He and $^{12}_\Lambda$C.

On the contrary, theoretical models based on OME potentials and/or direct quark (DQ) mechanisms [244, 245, 254, 286, 287] predicted rather large and negative a_Λ values. It must be noted that, on the contrary, the mentioned models were able to account fairly well for the weak decay rates measured for *s*- and *p*-shell Hypernuclei. As can be seen from table 14, not even the inclusion of FSI in the theoretical analysis with OME potentials can explain the experimental data. To illustrate this point, we quote the result of ref. [288] for a proton kinetic energy threshold of 30 MeV (the data of table 14 were obtained for such an energy cut).

At this point we must note that an effective field theory approach to Hypernuclear decay [289], in which the weak two-body transition is based on tree-level pion- and kaon exchange and leading-order contact interactions, suggested a dominating spin- and isospin-independent contact term. Such central term turns out to be particularly important if one wants to fit the small and positive value of the intrinsic asymmetry for $^5_\Lambda$He indicated by KEK-E462. In a calculation scheme based on a OME model, this result can be interpreted dynamically as the need for the introduction of a meson-exchange contribution in the scalar-isoscalar channel. Prompted by the work of ref. [289], models based on OME and/or DQ mechanisms [290, 291] were supplemented with the exchange of the scalar-isoscalar σ-meson. Despite the phenomenological character of these works (the unknown σ weak couplings are fixed to fit NMWD data for $^5_\Lambda$He and $^{12}_\Lambda$C), they showed the importance of σ-exchange in the NMWD.

Then, an investigation was performed on the effects of a chirally motivated two-pion–exchange mechanism on the NMWD rates and asymmetries for *s*- and *p*-shell Hypernuclei [240]. The uncorrelated (2π) and correlated (in

the isoscalar channel, $2\pi/\sigma$) two-pion–exchange weak potentials were adopted from ref. [239] and added to the exchange of the pseudoscalar and vector mesons, π, ρ, K, K^*, ω and η, of the standard OME potentials. These scalar-isoscalar contributions are based on a chiral unitary model which describes $\pi\pi$ scattering data in the scalar sector up to around $1\,\mathrm{GeV}$, where all the coupling constants are determined from chiral meson-meson and meson-baryon Lagrangians by imposing $SU(3)$ symmetry. It was found that the two-pion–exchange mechanism modifies moderately the partial decay rates Γ_n and Γ_p but has a tremendous influence on the asymmetry parameter, due to the change of sign of the central, spin- and isospin-independent amplitudes [240]: the obtained asymmetry values agreed with data for the first time. It must to be noted that the main mechanism which permitted to achieve this result is the uncorrelated two-pion exchange. The resulting values of the asymmetry parameter are presented in table 14 for the case where no FSI are accounted for and also when a proton kinetic energy threshold of $30\,\mathrm{MeV}$ is imposed in the calculation with FSI.

From table 14 we see that a more recent and different approach [292], whose main characteristic is the use of correlated meson-pair exchange, proved that the exchange of the axial-vector a_1-meson is also relevant in asymmetry calculations. We note however that the one-meson–exchange plus two-pion–exchange model of ref. [240] turned out to be able to reproduce satisfactorily the total and partial NMWD rates as well as the asymmetries, for both $^5_\Lambda$He and $^{12}_\Lambda$C, within a minimal framework, *i.e.*, without invoking exotic decay mechanisms, nor a violation of the $\Delta I = 1/2$ isospin rule.

We can thus conclude that with the solution of the asymmetry puzzle a deeper theoretical understanding of the Hypernuclear decay mechanisms is now reached.

5 Mesonless multinucleon absorption of stopped K^-

5.1 Recent experimental data

Data on reactions of nuclear absorption of stopped K^- with emission of Λ, nucleons or light nuclei (deuterons, tritons) were very scarce up to a few years ago. The bulk of the data was coming from bubble chamber experiments, which mainly aimed at assessing the K^- capture rates of multipionic final states [293]. Thanks to the clever design of the FINUDA spectrometer, described in sect. 2.2, it was possible to identify in a clean way the Λ hyperons emitted following the interaction of stopped K^- in nuclei (^{6}Li, ^{7}Li, ^{12}C, ^{27}Al, ^{51}V) [294]. They can be identified by reconstructing the invariant mass of a proton and a negative pion, as shown in fig. 42(a). The peak position agrees with the known Λ mass, and the width of the peak is as narrow as $6\,\mathrm{MeV}/c^2$ FWHM.

When a K^- interacts with two protons, one expects that a hyperon-nucleon pair ($\Lambda + p$, $\Sigma^0 + p$ or $\Sigma^+ + n$) is emitted in opposite directions, ignoring a final-state interaction inside the nucleus. The angular correlation be-
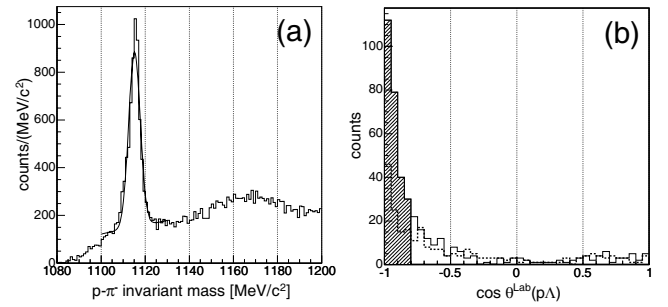

Fig. 42. (a) π^--p invariant-mass distribution; the continuous line is a fit with a Gaussian function plus a linear background. (b) Opening angle distribution between a Λ and a proton: solid line ^{6}Li, ^{7}Li and ^{12}C, dashed line ^{27}Al, ^{51}V. The shaded area is selected as back-to-back events ($\cos\theta^{\mathrm{lab}} < -0.8$). From ref. [294].

tween a Λ and a proton from the same point in the target (fig. 42(b)) clearly indicates the existence of this kind of reaction. Even for heavy nuclei such as ^{27}Al and ^{51}V similar correlations were observed, which might suggest that the absorption would take place at the surface of a nucleus. In the following steps of the analysis Λ-p pairs emitted in opposite directions ($\cos\theta^{\mathrm{lab}} < -0.8$) only from the light nuclear targets (^{6}Li, ^{7}Li and ^{12}C) were used. Since the back-to-back angular correlation between a Λ and a proton is so clear, it is naturally expected that the two particles are emitted from a K^-pp intermediate system. The angular correlation is smeared out due to the Fermi motions of the two protons at the surface of the nucleus by which the K^- is absorbed after cascading down the atomic orbits by emitting X-rays. If the reaction process were simply a two-nucleon absorption process, the mass of the system should be close to the sum of a kaon and two proton masses, namely $2.370\,\mathrm{MeV}/c^2$. The initial motion of the two protons does not affect the invariant-mass distribution. The invariant mass distribution of the Λ-p pairs is shown in fig. 43. A significant mass decrease of the K^-pp system with respect to its expected mass is observed. It can be interpreted as a bound state composed of a kaon and two protons, hereafter abbreviated as K^-pp. In the inset of fig. 43, the acceptance corrected invariant-mass distribution is shown. Since the trigger and detection acceptance are monotonically increasing functions of the invariant mass in this mass region, the peak further shifts to a lower mass side. By fitting the acceptance corrected peak with a Lorentzian function (folded with a Gaussian with $\sigma = 4\,\mathrm{MeV}/c^2$, corresponding to the detector resolution estimated with a Monte Carlo simulation) in the region of 2.22–$2.33\,\mathrm{GeV}/c^2$ values for the binding energy and width of such an hypothetical K^-pp bound state of $115^{+6}_{-5}(\mathrm{stat})^{+3}_{-4}(\mathrm{syst})\,\mathrm{MeV}$ and $67^{+14}_{-11}(\mathrm{stat})^{+2}_{-3}(\mathrm{syst})\,\mathrm{MeV}$ were obtained.

An alternative, conventional explanation for the above observed bump was put forward. In ref. [295] the bump in the Λ-p invariant-mass spectrum was explained as an artifact of the angular cuts applied to the flat spectrum of invariant mass of Λ-p events resulting from genuine
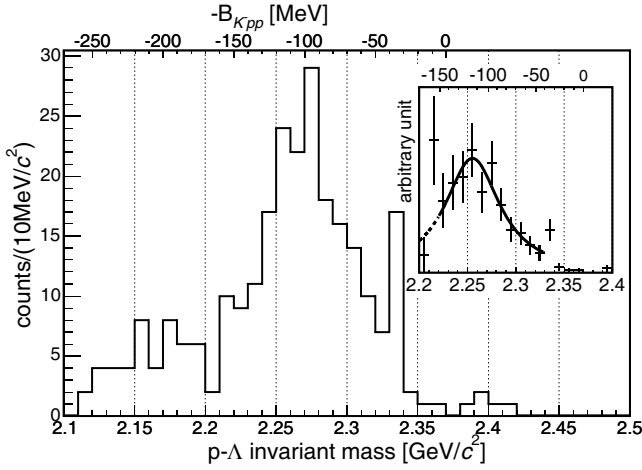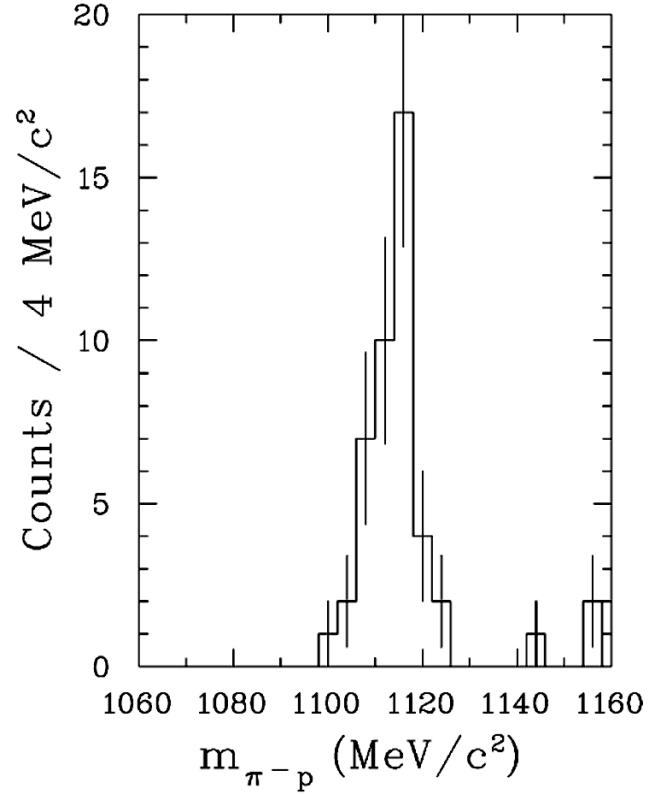
Fig. 43. Λ-p invariant-mass distribution for events with $\cos\theta^{\mathrm{lab}} < -0.8$ from light targets before the acceptance correction. The inset shows the result after the acceptance correction: the continuous line is a fit to the 2.22–2.33 GeV/c^2 region. From ref. [294].
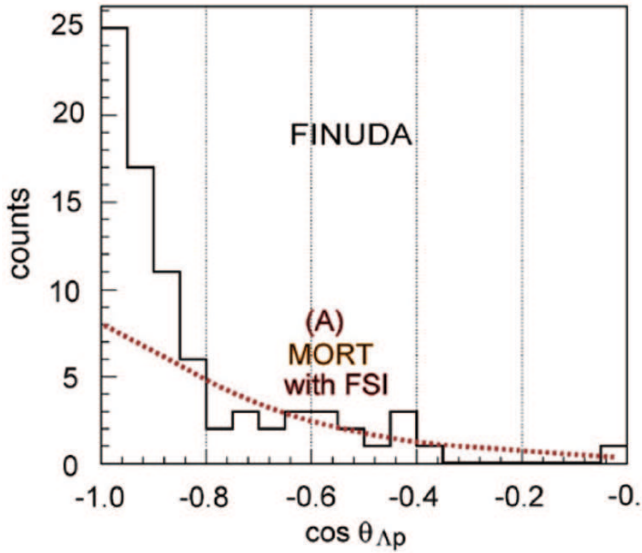
Fig. 44. Opening angle distribution between Λ and p. Histogram: from experiment; dotted line: from FSI mechanism [295]. From ref. [296].

Fig. 45. Invariant-mass distribution of $\pi^- p$ pairs, in coincidence with deuterons, for ^{6}Li. From ref. [297].

back-to-back pairs formed in simple K^--(np) interactions in the target nuclei that suffered a FSI. Even though such a mechanism cannot be completely excluded, other arguments are contradicting it. A first one is the shape of the angular correlation in the approach of ref. [295], showing a strong disagreement [296] with the steepness measured experimentally, as shown in fig. 44. A second one is a possible inadequacy of the FSI calculations leading to an overestimation of these interactions. As a matter of fact, as shown in fig. 34, calculations following a similar approach [265] failed to reproduce the spectrum of protons from NMWD of $^{12}_{\Lambda}$C, recently measured with a good precision [261]. A rough estimate on the yield of $K^-(pp) \to \Lambda + p$ provided

0.1% per stopped K^-, that is the same order of magnitude of the production of bound Λ-Hypernuclei.

Stimulated by these unexpected findings, the FINUDA Collaboration searched for correlated Λ-d pairs emitted following the absorption of stopped K^- in some selected targets (^{6}Li, ^{12}C) [297]. The measurement took advantage from both the excellent identification of Λ hyperons by the invariant-mass measurements and of deuterons by three independent measurements of dE/dx and time of flight. Figure 45 shows the invariant-mass distribution of π^--p pairs emitted in coincidence with deuterons from ^{6}Li targets. A well-defined and narrow peak, centered at the right mass of the Λ and nearly background free is evident. Figure 46 shows the invariant-mass distribution for the Λ-d events selected with the above criteria. A hint for a peak at a mass of 3251 ± 6 MeV appears. By selecting the events contained in this peak, they appear strongly back-to-back correlated, as shown by the inset of fig. 46. They could be interpreted as the decay of a $K^- ppn$ bound state with a binding energy of 58 ± 6 MeV and a width of 36.6 ± 14.1 MeV. This object could be formed thanks to the predominant $(\alpha + d)$ substructure of ^{6}Li, already observed in other K^- induced reactions [298]. As a matter of fact, the analogous distributions relative to events obtained with the ^{12}C target did not present similar features, as shown in fig. 47. There is no evidence for a peak in the invariant-mass distribution and the angular correlation of the events in the invariant mass range corresponding to
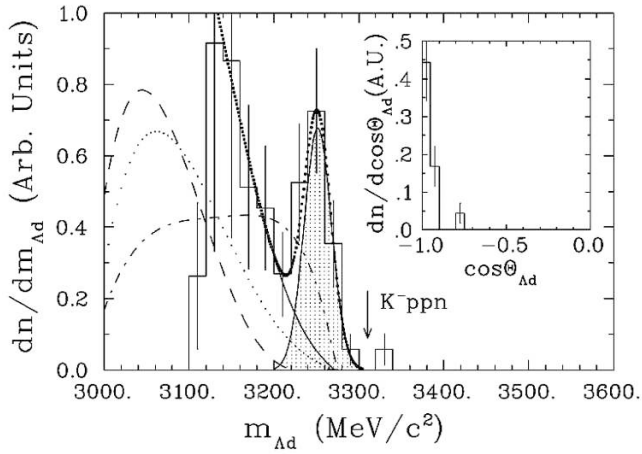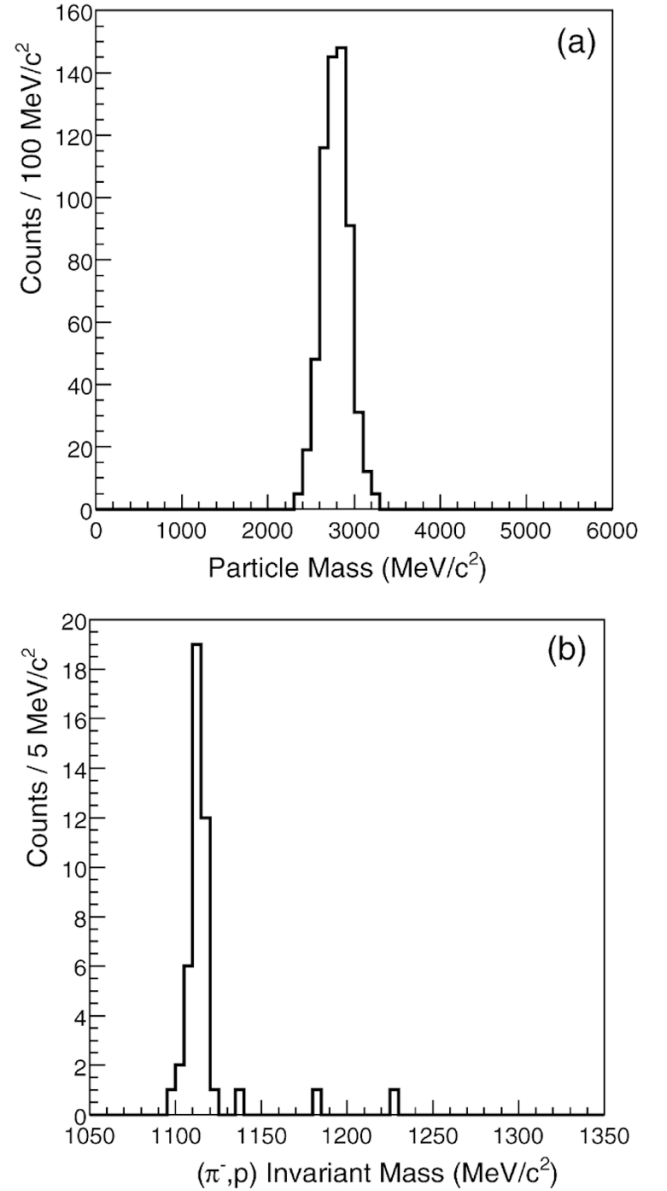
Fig. 46. Invariant-mass distribution of Λd pairs from the $^6\mathrm{Li}(K^-_{\mathrm{stop}}, \Lambda d)3N$ reaction. From ref. [297].
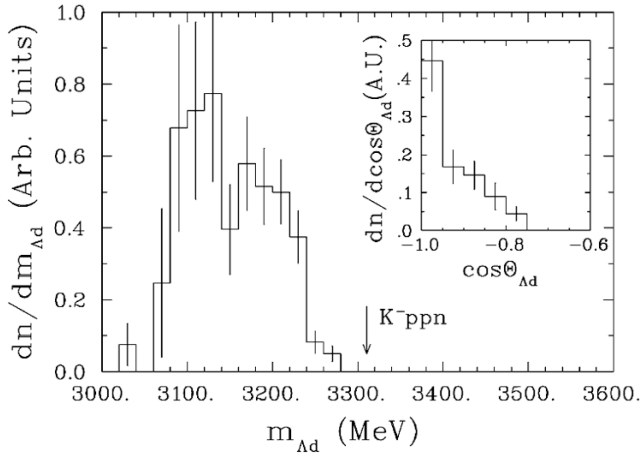
Fig. 47. Invariant-mass distribution of Λd pairs from the $^{12}\mathrm{C}(K^-_{\mathrm{stop}}, \Lambda d)A'$ reaction. From ref. [297].

Fig. 48. (a) Triton-mass identification. (b) Invariant-mass distribution of $\pi^- p$ pairs in coincidence with tritons. From ref. [301].

the peak observed in $^6\mathrm{Li}$ is quite broad. The peak observed for $^6\mathrm{Li}$ was interpreted in ref. [299] in terms of K^- absorption from three nucleons, leaving the remaining ones as spectators. The back-to-back correlation reported in the experiment of ref. [297] is reproduced too, not so well other observables. Such an explanation looks realistic, supporting also analogous measurements performed in ref. [300]. The yield for the production of the above peak was reported as $(4.4 \pm 1.4) \cdot 10^{-3}/\mathrm{stopped}\ K^-$, quite similar to that for the production of the $K^- pp$ system from light nuclei.

A further effort was then done by the FINUDA Collaboration for the search of correlated Λ-triton pairs emitted following the absorption of stopped K^- in $^6\mathrm{Li}$, $^7\mathrm{Li}$ and $^9\mathrm{Be}$. The identification of tritons was very hard, since tracks due to these particles were completely blurred in the huge amount of other charged particles (pions, protons, deuterons). However a very satisfactory separation was achieved, thanks to a clever use of the $\mathrm{d}E/\mathrm{d}x$ and time-of-flight information from the different layers of detectors [301]. The triton-mass identification by conditioned

$\mathrm{d}E/\mathrm{d}x$ is shown in fig. 48a. It was measured that it contains only 3% of other particles. As for the previous investigations the Λ hyperons were finally identified by the value of the π-p invariant mass. Figure 48b shows the invariant mass of π-p pairs detected in coincidence with tritons. The distribution of background events is flat outside the peak thus allowing for estimation of the number of events inside the peak itself. Such background events constitute 0.63 ± 0.67 out of 40 Λ events. The Λ-triton correlated events show a very nice back-to-back correlation, given in fig. 49. This distribution is inconsistent with that predicted by a four-body phase-space simulation of the reaction $K^-_{\mathrm{stop}}A \rightarrow \Lambda t N A'$, the simplest that could mimic the observed events. Detailed simulations of
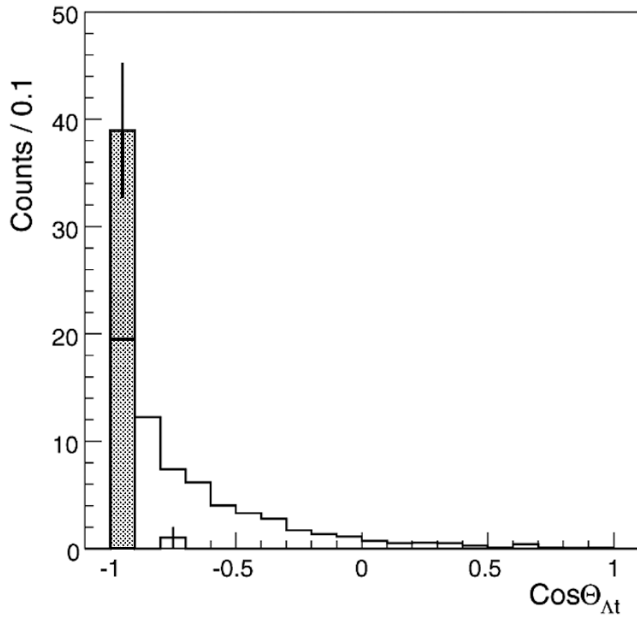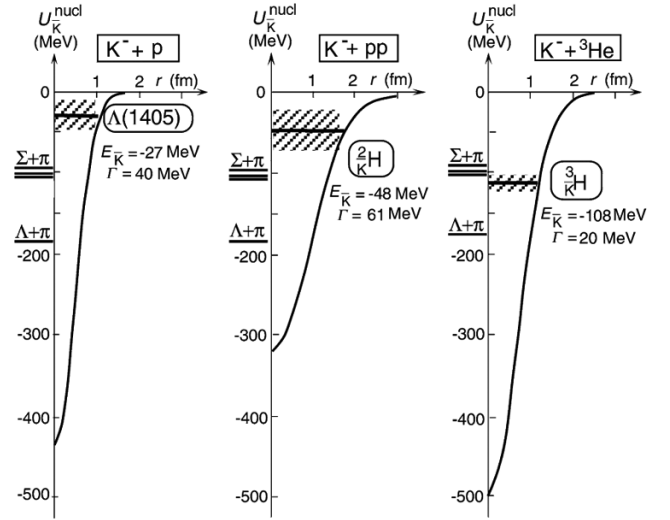
Fig. 49. Opening-angle distribution between Λ and t pairs ($\cos \Theta_{\Lambda t}$). Filled histogram: experimental data; open histogram: phase-space distribution for the $^6\mathrm{Li}(K^-_{\mathrm{stop}}, \Lambda t)A$ reaction. From ref. [301].

Fig. 50. Calculated $\bar{K}N$ and $\bar{K}$-nucleus potentials and bound levels: $\Lambda(1405)$, $^2_{\bar{K}}\mathrm{H}$ and $^3_{\bar{K}}\mathrm{H}$ for K^-p, K^-pp and K^-ppn systems, respectively. From ref. [303].

other possible reaction chains that could mask the events attributed to mesonless Λt emission showed that their importance was negligible. Due to the scarce number of events, it was not possible to obtain statistically reasonable distributions for the invariant mass of the Λ-t correlated events. The yield for the production of the Λ-t correlated events averaged over the 3 stopping targets is $(1.01 \pm 0.18_{\mathrm{stat}}{}^{+0.17}_{-0.10\,\mathrm{syst}}) \cdot 10^{-3}/K^-_{\mathrm{stop}}$. We note that it is the same, within the errors, of that measured for the production of Λ-p correlated events, and somehow lower than that for the production of Λ-d correlated events from $^6\mathrm{Li}$. The similarity of the production rates for mesonless Λ-few $(1,2,3)$ nucleons pairs induced by stopped K^- raises doubts on the interpretation, put forward in ref. [294] for Λ-p, that they are due to the decay, at rest, of a K^--$(1,2,3)$ nucleon(s) bound state. One should admit that these hypothetical states are produced with similar strengths, and this circumstance seems difficult to explain with simple models, given the inherent dynamical differences in the possible structure of these objects. To our knowledge, there are no models, at present, developed in order to explain the above production rates of mesonless absorption of stopped K^- by nuclear clusters in light nuclei.

5.2 The saga of the AntiKaonic Nuclear Clusters

The above-mentioned possible K^--(few nucleons) bound systems were named Anti Kaonic Nuclear Clusters (AKNC) or Deeply Bound anti(Kaon) States (DBKS). The first speculation about the possible existence of AKNC was put forward in ref. [302], based on the ob-
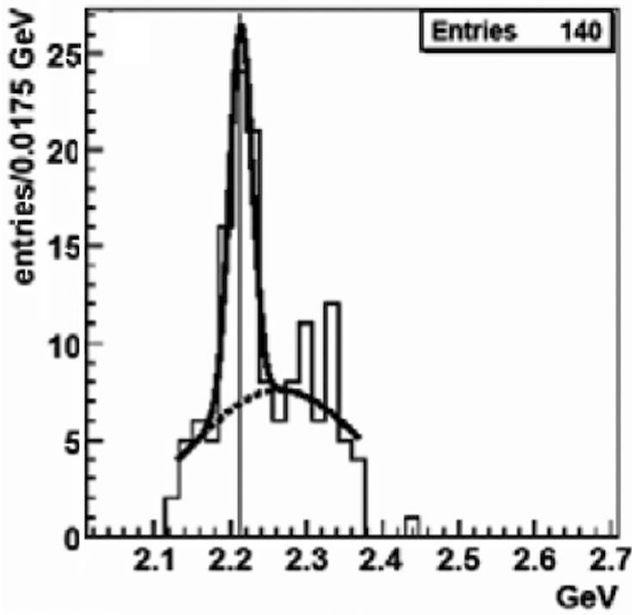
servation that the driving $\bar{K}N$ interaction in the isospin $I = 0$ channel is strongly attractive near threshold. A large binding energy B of about $100\,\mathrm{MeV}$ was found, but with a similarly large value of the width Γ. The theme received a strong boost by the prediction from ref. [303] of the possible existence of narrow discrete AKNC in few-body nuclear systems. The $\bar{K}$-nucleus potential was derived from a phenomenological $\bar{K}N$ potential accounting for several observables, with particular emphasis to the role of the $\Lambda(1405)$, assumed to be a bound (K^-p) system. The predicted binding energies B for $\bar{K}$-few nucleon systems were quite large (from 50 to more than $100\,\mathrm{MeV}$), but the distinctive feature was the narrowness (Γ of 20–30 MeV). It was due to the circumstance that, due to the high value of B, the main decay channel K^-p $(I = 0) \rightarrow \Sigma\pi$ is energetically forbidden, and the decay to $\Lambda\pi$ is suppressed by the isospin selection rules. Figure 50 shows the predicted binding energies and widths for the K^-p ($\Lambda(1405)$), K^-pp and K^-ppn AKNC.

A dynamical approach, allowing for the polarization of the nucleus by the strong $\bar{K}$-nucleus potential has been proposed in ref. [304]: according to this calculation, the depth of the potential is density dependent and AKNC are predicted with B of 100–$200\,\mathrm{MeV}$ and narrow enough widths of $50\,\mathrm{MeV}$, but only for relatively heavy nuclei. According to this approach, they could not be observed in the case of light targets, since in this case they should be too broad. The K^-pp bound system was studied in ref. [305] by a coupled-channel Faddeev calculation obtaining a B of 55–$70\,\mathrm{MeV}$ and a quite large width, of the order of 95–$100\,\mathrm{MeV}$.

Reference [306] examined the possible existence of AKNC by using energy-dependent $\bar{K}N$ interactions derived with the s-wave coupled-channels amplitudes involving the $\Lambda(1405)$ and resulting from chiral $SU(3)$ dynamics, plus p-wave amplitudes dominated by the $\Sigma(1385)$: it was

Fig. 51. Best fit to the Λp invariant-mass distribution for events observed following the annihilation of $\bar{p}$'s at rest on ^{4}He after suitable kinematical cuts. From ref. [309].

Table 15. Comparison between theory and experiment for the binding energies, B, and widths, Γ, of the $K^- pp$ system or $^2_{\bar{K}}$H.

		B (MeV)	Γ (MeV)	Ref.
$^2_{\bar{K}}$H	K^- at rest	-115 ± 9	67 ± 15	[294]
$^2_{\bar{K}}$H	$\bar{p}$ at rest	-151.0 ± 4.4	≤ 33.9	[308, 309]
$^2_{\bar{K}}$H	$pp \to pK^+\Lambda$	-105 ± 2	≤ 118	[310]
$^2_{\bar{K}}$H	theory	-48	61	[311]

were also analyzed to search for a $K^- pp$ bound system [310]. The observed spectra of the K^+ missing mass ($p\Lambda$ invariant mass) with high transverse momenta of p and K^+ revealed a broad distinct peak with a mass of $2265 \pm 2_{\text{stat}} \pm 5_{\text{syst}}$ MeV/c^2 and a width of $118 \pm 8_{\text{stat}} \pm 10_{\text{syst}}$ MeV. Following this experiment, the binding energy of the Λp system should be 105 MeV. Table 15 reports the binding energies and widths reported, as well as the theoretical prediction, showing in a compact way the present contradictions. We hope that new data from the dedicated experiments E15 and E27 at J-PARC and FOPI at GSI could soon clarify the situation.

6 Conclusions and perspectives

Strangeness nuclear physics has demonstrated to be able to provide a definite and precise answer to at least two problems for strangeness -1 systems; they are related to the fundamental issues of the ΛN strong interaction and the four-baryon, strangeness changing, weak interaction. Various experiments have shown that the above tasks are fully achievable.

Regarding the structure of Λ-Hypernuclei, in addition to the determination of the hyperon single-particle energy level schemes for heavy systems, quite limited up to recent times, by missing-mass (magnetic spectrometers) measurements, and the study of the small spin-doublet and Λ spin-orbit energy splittings performed by γ-ray measurements in coincidence, a program for the determination of other relevant observables (spin, parity and lifetime of Hypernuclear levels, Hypernuclear deformation and electric and magnetic moments of hyperons in Hypernuclei) should be started. To achieve this purpose, coincidence γ-rays spectroscopy or the recently assessed spectroscopy of charged pions from mesonic weak decay were shown to be suitable tools. A relevant improvement should come from the fine spectroscopy of π^0 from mesonic decay with a resolution of the order of the MeV. The experiment is hard, but in the capabilities of the present state-of-the-art technology. γ-ray spectroscopy experiments, interpreted within a shell model, has already allowed to extract important information on the spin-dependence of the ΛN effective interaction.

Improved approaches to the structure of single- and double-strangeness Hypernuclei, possibly establishing solid links with analogous calculations in dense stars, will be important. They should incorporate important effects

concluded that AKNC can possibly exist, with B from 60 to 100 MeV, but with decay widths of similar magnitude.

The theoretical speculation from ref. [303] received a strong boost from the claimed discovery of an AKNC with narrow width by KEK-PS E471 in a missing-mass experiment on the reaction ^{4}He $(K^-_{\text{stop}}, p/n)X$, afterwards withdrawn by the same Group (exp. KEK-PS E549) as due to an experimental artifact [307].

The experiments on correlated Λ-p and Λ-d events described in the previous paragraph were interpreted following the hypothesis of the existence of the AKNCs. For the $A = 2$ AKNC $(K^- pp)$ the width is close to that predicted, but B is twice. More difficult is the interpretation of the invariant mass of Λ-d correlated events in terms of formation of an $A = 3$ AKNC $(K^- ppn)$. The width is again compatible with that predicted, but the B is a half. The mass of this state would then be larger than the $\Sigma^+ \pi$ threshold, with a consequently large width.

Due to the large interest and theoretical effort, several experiments that took data with a Λ and a proton in the final states reanalysed their data looking for a confirmation of $K^- pp$ bound state. Events containing a Λ and a p following the annihilation of $\bar{p}$'s on ^{4}He nuclei measured by the OBELIX spectrometer at LEAR-CERN were analyzed selecting annihilations of $\bar{p}$'s on 3 or 4 nucleons, and using some *ad hoc* kinematics cuts [308,309]; the result is shown in fig. 51. A quite nice peak appears at a mass of $2223.2 \pm 3.2_{\text{stat}} \pm 1.2_{\text{syst}}$ MeV/c^2, and a width of less than 33.9 ± 6.2 MeV/c^2. The binding energy should then be of $151.0 \pm 3.2_{\text{stat}} \pm 1.2_{\text{syst}}$ MeV. The statistical significance of the peak over the experimental background is 4.71σ.

More recently, the data collected by the DISTO experiment on the exclusive $pp \to p\Lambda K^+$ reaction at 2.85 GeV

such as the ΛN-ΣN strong coupling and, for $S = -2$ Hypernuclei, the coupling among the ΞN, $\Lambda\Lambda$ and $\Sigma\Sigma$ states. Of paramount importance will be the experimental verification of the possible existence of Ξ-Hypernuclei, with the related possibility of extracting information on the Ξ-nucleus potential and then on the ΞN interaction. Studies on $\Lambda\Lambda$-Hypernuclei will allow to determine the $\Lambda\Lambda$ interaction, which is poorly known at present.

Particular attention should be devoted to the search for neutron-rich Λ-Hypernuclei, which are especially important in nuclear astrophysics. They provide information on the glue-like role of the hyperon, on the Σ hyperon admixture in Λ-Hypernuclei and on the neutron drip properties, thus they may play a role (like normal nuclei) in neutron capture nucleosynthesis. Other impurity nuclear physics issues such as the deformation properties and the collective motion in Hypernuclei should be clarified by experiments and new calculations.

Concerning the in-medium properties of the hyperon, the Λ magnetic moment is an important observable which is sensitive to the spin- and angular-momentum structure of the many-body system, to the spin-dependent part of the ΛN effective interaction and to the ΛN-ΣN coupling. This magnetic moment can be indirectly measured from the transition probability for Λ spin-flip transitions. In heavy-ion Hypernuclear production experiments such as HypHI, direct measurements of the Λ magnetic moment should be possible by observing the spin precession in a strong magnetic field.

Concerning the weak decay of Hypernuclei, convincing evidences have been achieved for a solution of the long-standing puzzles on the Γ_n/Γ_p ratio between the $\Lambda n \to nn$ and $\Lambda p \to np$ decay rates and on the asymmetry parameter in the non-mesonic weak decay of polarized Hypernuclei. On the one hand, this has been possible thanks to experimental and theoretical analyses of nucleon-coincidence emission spectra. On the other hand, theoretical approaches considering a one-meson–exchange weak potential supplemented by a two-pion–exchange mechanism could reproduce all the decay data for $^5_\Lambda$He and $^{12}_\Lambda$C. The questions which will be relevant for future developments concern the $\Delta I = 1/2$ isospin rule and the possible importance of mechanisms introduced by the $\Delta(1232)$ resonance in the non-mesonic weak decay of Λ-Hypernuclei.

Possible violations of the $\Delta I = 1/2$ rule should be studied for the non-mesonic weak decay of s-shell Λ-Hypernuclei. A theoretical approach could establish the link with the elementary $\Lambda N \to nN$ decay amplitudes and rates of the approach by Bloch and Dalitz, at the same time demonstrating the degree of reliability of this phenomenological model which is normally adopted to interpret the experimental data. A study on four- and five-body Hypernuclei will play an important role for establishing the detailed spin-isospin dependence of the $\Lambda N \to nN$ process.

A microscopic calculation of the non-mesonic weak decay emission spectra for Λ-Hypernuclei is very important, since it provides a fully quantum-mechanical approach in which a unified treatment of complex many-body effects

such as final-state interactions, ground-state correlations and ground-state normalization is considered. The nucleon spectra from the non-mesonic Hypernuclear decay are the real observables from which one extracts, via some theoretical scheme, the experimental values of the partial decay rates. In particular, the contributions of many-body terms introduced by the $\Delta(1232)$ resonance are expected to play a role in a detailed calculation of the non-mesonic decay rates and (especially) the nucleon emission spectra, thus possibly explaining the present incompatibilities between experiment and theory on the nucleon emission spectra. These contributions should be included in new calculations.

It will be also important to start a systematic investigation of rare weak decays of $\Lambda\Lambda$-Hypernuclei such as $\Lambda\Lambda \to \Lambda n$, $\Lambda\Lambda \to \Sigma^- p$, $\Lambda\Lambda \to \Sigma^0 n$ ($\Delta S = 1$) and $\Lambda\Lambda \to nn$ ($\Delta S = 2$). A reliable calculation of the rates for these Λ-induced Λ decay reactions is missing and no experimental evidence of such processes is available at present.

Like the majority of items related to experiments with nuclei, the firm and reliable determination of the physical quantities describing the ΛN interaction in the strong and weak sectors requires a systematic series of measurements that may be performed at dedicated laboratories, with a dedicated program and a strict collaboration with the theoreticians active in the field.

The situation is rather good worldwide in order to achieve this goal. The J-PARC complex of accelerators at Tokai (Japan) will be the main pillar for strangeness nuclear physics in the next decade. More than ten experiments on strangeness nuclear physics were approved with high priority but the unfortunate event of the terrifying earthquake in the area delayed the activity by at least one year. Experiments will be performed on the γ-ray spectroscopy of light to heavy Λ-Hypernuclei, the production of neutron-rich Λ-Hypernuclei, the Λ magnetic moment in nuclei and, concerning strangeness -2 systems, on the γ-ray spectroscopy of $\Lambda\Lambda$-Hypernuclei and the reaction spectroscopy of Ξ-Hypernuclei. In addition, new coincidence measurements of the non-mesonic weak decay of $A = 4$ and $^{12}_\Lambda$C Hypernuclei are planned. The first J-PARC results are hopefully expected for the forthcoming year.

Another laboratory which is expected to provide a good wealth of experimental information on high-resolution spectroscopy of Λ-Hypernuclei is TJNAF, after the on-going program of upgrade in energy of the electron accelerator complex.

New laboratories that will soon enter into the game of strangeness nuclear physics are MAMI-C in Mainz and GSI in Darmstadt. At MAMI-C, the complex of high-resolution spectrometers needed to perform Hypernuclear spectroscopy with the $(e, e'K^+)$ reaction was recently commissioned. The results will complement those from TJNAF. At GSI, a pilot experiment on the production of Hypernuclei by heavy ions (HyPHI), with special emphasis on the identification of neutron-rich Hypernuclei and their mesonic decay, has very recently completed the first data taking run.

The experimental teams engaged at the different laboratories are in very close contact and it is natural to

expect that the above mentioned program of coordinated measurements will be agreed among them. The degree of integration of the experimental teams with the theoreticians has a long tradition, initiated by R.H. Dalitz, and is very good.

In the long-term perspective, the FAIR-GSI complex and the powerful PANDA detector will play a major role in strangeness nuclear physics. The $\bar{p}$ source, unique in the world, will allow to produce abundantly $\Lambda\Lambda$-Hypernuclei by $\bar{p}$ annihilation into $\Xi\bar{\Xi}$ on nuclei, with subsequent interaction of the $\bar{\Xi}$ with a proton in the same nucleus, providing two low-momentum Λ's that may stick to other nucleons. These $\Lambda\Lambda$-Hypernuclei should be produced in excited states and the measurement of their energies by γ-ray coincidence would allow the determination of the $\Lambda\Lambda$ strong interaction parameters, an important result in hadronic physics. If successful, this method should be extended to the production of $\Lambda\Lambda\Lambda$-Hypernuclei, by using the $\Omega^-\Omega^+$ production from $\bar{p}$ annihilation in nuclei.

Finally, the middle-term strategy for the Anti Kaonic Nuclear Clusters is the unambiguous assessment of their existence and of their main features by some dedicated experiments already approved and ready to run. In the positive case, the long-term strategies are far reaching and could involve several laboratories worldwide and the construction of new dedicated detectors.

References

1. H. Yukawa, Proc. Phys. Math. Soc. Jpn. **17**, 48 (1935).
2. For a recent collection of reviews on nuclear physics with strangeness see the Special Issue on *Recent advances in Strangeness Nuclear Physics*, Nucl. Phys. A Vol. **804** (2008) pp. 1–348.
3. See also the *Proceedings of the 10th International Conference on Hypernuclear and Strange Particle Physics (Hyp–X)*, in Nucl. Phys. A Vol. **835** (2010) pp. 1–470.
4. O. Hashimoto, H. Tamura, Prog. Part. Nucl. Phys. **57**, 564 (2006).
5. T. Bressani, in *Strangeness and Spin in Fundamental Physics, Proceedings of the International School of Physics "E. Fermi", Course CLXVII*, edited by M. Anselmino, T. Bressani, A. Feliciello, P. Ratcliffe (SIF, Bologna and IOS Press, Amsterdam, 2008) p. 3.
6. W.M. Alberico, G. Garbarino, Phys. Rep. **369**, 1 (2002).
7. J. Schaffner-Bielich, Nucl. Phys. A **835**, 279 (2010).
8. D.J. Millener, Lect. Notes Phys. **724**, 31 (2007).
9. M. Kohno, Y. Fujiwara, Y. Watanabe, K. Ogata, M. Kawai, Prog. Theor. Phys. **112**, 895 (2004).
10. M. Kohno, Y. Fujiwara, Y. Watanabe, K. Ogata, M. Kawai, Phys. Rev. C **74**, 064613 (2006).
11. J. Dabrowski, J. Rozynek, Phys. Rev. C **78**, 037601 (2008).
12. S. Bart *et al.*, Phys. Rev. Lett. **83**, 5238 (1999).
13. H. Noumi *et al.*, Phys. Rev. Lett. **89**, 072301 (2002) **90**, 049902(E) (2003).
14. P.K. Saha *et al.*, Phys. Rev. C **70**, 044613 (2004).
15. Y. Yamamoto, Th.A. Rijken, Prog. Theor. Phys. Suppl. **185**, 72 (2010).
16. Th.A. Rijken, M.M. Nagels, Y. Yamamoto, Prog. Theor. Phys. Suppl. A **185**, 14 (2010).
17. Y. Fujiwara, Y. Suzuki, C. Nakamoto, Prog. Part. Nucl. Phys. **58**, 439 (2007).
18. T. Fukuda *et al.*, Phys. Rev. C **58**, 1306 (1998).
19. P. Khaustov *et al.*, Phys. Rev. C **61**, 054603 (2000).
20. K. Aoki *et al.*, *Spectroscopic study of Ξ-Hypernucleus, $^{12}_{\Xi}$Be, via the $^{12}C(K^-,K^+)$ reaction*, Proposal for J-PARK 50 GeV Proton Synchrotron, 1 (available at http://j-parc.jp/NuclPartProposal_e.html).
21. K. Nakazawa, H. Takahashi, Prog. Theor. Phys. Suppl. **185**, 335 (2010).
22. H. Takahashi *et al.*, Phys. Rev. Lett. **87**, 212502 (2001).
23. H.J. Schulze, Nucl. Phys. A **835**, 19 (2010).
24. K. Sumiyoski, K. Nakamoto, C. Ishizuka, A. Ohnishi, S. Yamada, H. Suzuki, Nucl. Phys. A **835**, 295 (2010).
25. B.H. Kang *et al.*, Phys. Rev. Lett. **96**, 062301 (2006).
26. M.J. Kim *et al.*, Phys. Lett. B **641**, 28 (2006).
27. M. Kim *et al.*, Phys. Rev. Lett. **103**, 182502 (2009).
28. FINUDA Collaboration (M. Agnello *et al.*), Phys. Lett. B **685**, 247 (2010).
29. FINUDA Collaboration (M. Agnello *et al.*), Phys. Lett. B **701**, 556 (2011).
30. E. Bauer, G. Garbarino, A. Parreño, A. Ramos, Nucl. Phys. A **836**, 199 (2010).
31. E. Bauer, G. Garbarino, Phys. Lett. B **698**, 306 (2011).
32. T. Watanabe *et al.*, Eur. Phys. J. A **33**, 265 (2007).
33. K. Itonaga, T. Ueda, T. Motoba, Nucl. Phys. A **691**, 197c (2001).
34. A. Parreño, A. Ramos, C. Bennhold, Phys. Rev. C **65**, 015205 (2002).
35. T. Takatsuka, S. Nishizaki, Y. Yamamoto, R. Tamagaki, Prog. Theor. Phys. **115**, 355 (2006).
36. M. Danysz, J. Pniewsky, Philos. Mag. **44**, 348 (1953).
37. H. Feshbach, K. Kerman, *Preludes in Theoretical Physics*, edited by A. De-Shalit, H. Feshbach, L. Van Hove (North Holland, Amsterdam, 1966) pp. 260-278.
38. G.C. Bonazzola *et al.*, Phys. Lett. B **53**, 297 (1974).
39. T. Motoba, K. Itonaga, Y. Yamamoto, Progr. Theor. Phys. Suppl. **185**, 197 (2010).
40. T. Motoba, P. Bydzovsky, M. Sotona, K. Itonaga, Y. Yamamoto, Progr. Theor. Phys. Suppl. **185**, 224 (2010).
41. T. Tamura *et al.*, Progr. Theor. Phys. Suppl. **117**, 1 (1989).
42. R.S. Hayano, T. Yamazaki, *Perspectives of Meson Science*, edited by T. Yamazaki, K. Nakai, K. Nagamine (North Holland, Amsterdam, 1992) pp. 493-517.
43. G. Charpak *et al.*, Nucl. Instrum. Methods **62**, 262 (1968).
44. M. Faessler *et al.*, Phys. Lett. B **46**, 468 (1973).
45. G.C. Bonazzola *et al.*, Nucl. Instrum. Methods **123**, 269 (1975).
46. A. Bamberger *et al.*, Phys. Lett. B **36**, 412 (1971).
47. W. Bruckner *et al.*, Phys. Lett. B **55**, 107 (1975).
48. W. Bruckner *et al.*, Phys. Lett. B **79**, 157 (1978).
49. D.J. Millener, *LAMPF Workshop on (π, K) Physics*, edited by B.F. Gibson, W.R. Gibbs, M.B. Johnson (AIP, New York, 1991) pp. 128-140.
50. R.E. Chrien, Nucl. Phys. A **691**, 501c (2001).
51. H. Hotchi *et al.*, Phys. Rev. C **64**, 044302 (2001).
52. T. Bressani, *Proceedings of Workshop for Physics and detectors for DAΦNE, Frascati April 9-12 1991*, edited by G. Pancheri (Laboratori Nazionali di Frascati, 1991) pp. 475-485.

53. The FINUDA Collaboration (M. Agnello *et al.*), FINUDA Technical Report, LNF Internal Report LNF - 95/024 (IR) 1995.
54. M. Agnello *et al.*, Phys. Lett. B **622**, 35 (2005).
55. M. Iodice *et al.*, Phys. Rev. Lett. **99**, 052501 (2007).
56. J.P. Bocquet *et al.*, Phys. Lett. B **192**, 312 (1987).
57. T.A. Armstrong *et al.*, Phys. Rev. C **47**, 1957 (1993).
58. W. Cassing *et al.*, Eur. Phys. J. A **16**, 549 (2003).
59. K.J. Nield *et al.*, Phys. Rev. C **13**, 1263 (1976).
60. S. Avramenko *et al.*, Nucl. Phys. A **547**, 95c (1992).
61. B.I. Abelev *et al.*, Phys. Rev. C **79**, 034909 (2009).
62. J. Adams *et al.*, Nucl. Phys. A **757**, 102 (2005).
63. B.I. Abelev *et al.*, Science **328**, 58 (2010).
64. J.H. Chen, Nucl. Phys. A **830**, 761 (2009).
65. J.H. Chen, Nucl. Phys. A **835**, 117 (2010).
66. V. Koch, A. Majumder, J. Randrup, Phys. Rev. Lett. **95**, 182301 (2005).
67. S. Zhang, J.H. Chen, H. Crawford, D. Keane, Y.G. Ma, Z.B. Xu, Phys. Lett. B **684**, 224 (2010).
68. P.M.M. Maessen, T.A. Rijken, J.J. de Swart, Phys. Rev. C **40**, 2226 (1989).
69. T.A. Rijken, V.G.J. Stoks, Y. Yamamoto, Phys. Rev. C **59**, 21 (1999).
70. T.A. Rijken, Phys. Rev. C **73**, 044007 (2006).
71. T.A. Rijken, Y. Yamamoto, Phys. Rev. C **73**, 044008 (2006).
72. Th.A. Rijken, M.M. Nagels, Y. Yamamoto, Nucl. Phys. A **835**, 160 (2010).
73. B. Holzenkamp, K. Holinde, J. Speth, Nucl. Phys. A **500**, 485 (1989).
74. A. Reuber, K. Holinde, J. Speth, Nucl. Phys. A **570**, 543 (1994).
75. J. Haidenbauer, U.-G. Meißner, Phys. Rev. C **72**, 044005 (2005).
76. H. Polinder, J. Haidenbauer, U.-G. Meißner, Nucl. Phys. A **779**, 244 (2006).
77. H. Polinder, J. Haidenbauer, U.-G. Meißner, Phys. Lett. B **653**, 29 (2007).
78. J. Haidenbauer, U.-G. Meißner, Phys. Lett. B **684**, 275 (2010).
79. K. Sasaki, E. Oset, M.J. Vicente Vacas, Phys. Rev. C **74**, 064002 (2006).
80. Y. Fujiwara, C. Nakamoto, Y. Suzuki, Phys. Rev. C **54**, 2180 (1996).
81. Y. Fujiwara, C. Nakamoto, Y. Suzuki, Phys. Rev. Lett. **76**, 2242 (1996).
82. S.R. Beane *et al.*, Nucl. Phys. A **794**, 62 (2007).
83. H. Nemura, N. Ishii, S. Aoki, T. Hatsuda, Phys. Lett. B **673**, 136 (2009).
84. T. Inoue *et al.*, Prog. Theor. Phys. **124**, 591 (2010).
85. O. Hashimoto *et al.*, Nucl. Phys. A **835**, 121 (2010).
86. K. Itonaga, T. Motoba, O. Richter, M. Sotona, Phys. Rev. C **49**, 1045 (1994).
87. D.J. Millener, Nucl. Phys. A **691**, 93 (2001).
88. E. Hiyama, M. Kamimura, T. Motoba, T. Yamada, Y. Yamamoto, Phys. Rev. Lett. **85**, 270 (2000).
89. D.J. Millener, C.B. Dover, A. Gal, Phys. Rev. C **38**, 2700 (1988).
90. M. Agnello *et al.*, Phys. Lett. B **698**, 219 (2011).
91. F. Cusanno *et al.*, Phys. Rev. Lett. **103**, 202501 (2009).
92. A. Cieplý, E. Friedman, A. Gal, V. Krejčiřík, Phys. Lett. B **698**, 226 (2011).
93. E. Hiyama, M. Kamimura, Y. Yamamoto, T. Motoba, T.A. Rijken, Prog. Theor. Phys. Suppl. **185**, 106 (2010).
94. M. Kohno, Y. Fujiwara, T. Fujita, C. Nakamoto, Y. Suzuki, Nucl. Phys. A **674**, 229 (2000).
95. B.J. Schaefer, M. Wagner, J. Wambach, T.T.S. Kuo, G.E. Brown, Phys. Rev. C **73**, 011001 (2006).
96. H. Dapo, B.J. Schaefer, J. Wambach, Eur. Phys. J. A **36**, 101 (2008).
97. Y. Akaishi, T. Harada, S. Shinmura, K.S. Myint, Phys. Rev. Lett. **84**, 3539 (2000).
98. E. Hiyama, M. Kamimura, T. Motoba, T. Yamada, Phys. Rev. C **65**, 011301 (2002).
99. H. Tamura *et al.*, Phys. Rev. Lett. **84**, 5963 (2000).
100. S. Ajimura *et al.*, Phys. Rev. Lett. **86**, 4255 (2001).
101. H. Akikawa *et al.*, Phys. Rev. Lett. **88**, 082501 (2002).
102. M. Ukai *et al.*, Phys. Rev. Lett. **93**, 232501 (2004).
103. H. Tamura *et al.*, Nucl Phys. A **835**, 3 (2010).
104. D.J. Millener, Nucl. Phys. A **835**, 11 (2010).
105. M. Ukai *et al.*, Phys. Rev. C **77**, 054315 (2008).
106. A. Gal, J.M. Soper, R.H. Dalitz, Ann. Phys. (N.Y.) **63**, 53 (1971).
107. A. Gal, J.M. Soper, R.H. Dalitz, Ann. Phys. (N.Y.) **72**, 445 (1972).
108. A. Gal, J.M. Soper, R.H. Dalitz, Ann. Phys. (N.Y.) **113**, 79 (1978).
109. R.H. Dalitz, A. Gal, Ann. Phys. (N.Y.) **116**, 167 (1978).
110. D.J. Millener, A. Gal, C.B. Dover, R.H. Dalitz, Phys. Rev. C **31**, 499 (1985).
111. E.H. Auerbach, A.J. Baltz, C.B. Dover, A. Gal, S.H. Kahana, L. Ludeking, D.J. Millener, Ann. Phys. (N.Y.) **148**, 381 (1983).
112. H. Kohri *et al.*, Phys. Rev. C **65**, 034607 (2002).
113. H. Tamura *et al.*, Nucl. Phys. A **835**, 3 (2010).
114. D.J. Millener, A. Gal, Phys. Lett. B **701**, 342 (2011).
115. D. Halderson, Phys. Rev. C **77**, 034304 (2008).
116. D.J. Millener, J. Phys. Conf. Ser. **312**, 022005 (2011).
117. T. Motoba, H. Bandō, K. Ikeda, T. Yamada, Prog. Theor. Phys. Suppl. **81**, 42 (1985).
118. Y. Yamamoto, H. Bandō, Prog. Theor. Phys. **83**, 254 (1990).
119. Y. Yamamoto, T. Motoba, H. Himeno, K. Ikeda, S. Nagata, Prog. Theor. Phys. Suppl. **117**, 361 (1994).
120. H. Hiyama, T. Motoba, T.A. Rijken, Y. Yamamoto, Progr. Theor. Phys. Suppl. **185**, 1 (2010).
121. H. Nemura, Y. Akaishi, Y. Suzuki, Phys. Rev. Lett. **89**, 142504 (2002).
122. E. Hiyama, M. Kamimura, K. Miyazaki, T. Motoba, Phys. Rev. C **59**, 2351 (1999).
123. E. Hiyama, Y. Yamamoto, T.A. Rijken, T. Motoba, Phys. Rev. C **74**, 054312 (2006).
124. K. Tsushima, K. Saito, J. Haidenbauer, A.W. Thomas, Nucl. Phys. A **630**, 691 (1998).
125. P.A.M. Guichon, A.W. Thomas, K. Tsushima, Nucl. Phys. A **814**, 66 (2008).
126. H. Shen, H. Toki, Nucl. Phys. A **707**, 469 (2002).
127. Y. Fujiwara, M. Kohno, K. Miyagawa, Y. Suzuki, Phys. Rev. C **70**, 047002 (2004).
128. P. Finelli, N. Kaiser, D. Vretenar, W. Weise, Nucl. Phys. A **831**, 163 (2009).
129. T. Motoba, H. Bandō, K. Ikeda, Prog. Theor. Phys. **70**, 189 (1983).
130. K. Tanida *et al.*, Phys. Rev. Lett. **86**, 1982 (2001).
131. H. Tamura, Eur. J. Phys. A **13**, 181 (2002).

132. J.M. Yao, Z.P. Li, K. Hagino, M. Thi Win, Y. Zhang, J. Meng, arXiv:1104.3200 [nucl-th].
133. E. Hiyama, M. Kamimura, T. Motoba, T. Yamada, Y. Yamamoto, Prog. Theor. Phys. **97**, 881 (1997).
134. E. Hiyama, M. Kamimura, T. Motoba, T. Yamada, Y. Yamamoto, Phys. Rev. Lett. **85**, 270 (2000).
135. M. Thi Win, K. Hagino, Phys. Rev. C **78**, 054311 (2008).
136. X.R. Zhou, H.J. Schulze, H. Sagawa, C. Xu Wu, En-Guang Zhao, Phys. Rev. C **76**, 034312 (2007).
137. H.J. Schulze, M. Thi Win, K. Hagino, H. Sagawa, Prog. Theor. Phys. **123**, 569 (2010).
138. M. Thi Win, K. Hagino, T. Koibe, Phys. Rev. C **83**, 014301 (2011).
139. L. Majling, Nucl. Phys. A **585**, 211c (1995).
140. D. Vretenar, W. Poschl, G.A. Lalazissis, P. Ring, Phys. Rev. C **57**, 1060 (1998).
141. X.R. Zhou, A. Polls, H.J. Schulze, I. Vidana, Phys. Rev. C **78**, 054306 (2008).
142. R.H. Dalitz, R. Levi Setti, Nuovo Cimento **30**, 489 (1963).
143. A. Umeya, T. Harada, Phys. Rev. C **79**, 024315 (2009).
144. A. Umeya, T. Harada, Phys. Rev. C **83**, 034310 (2011).
145. Y. Akaishi, K.S. Myint, Few Body Sys. Suppl. **12**, 277 (2008).
146. E. Hiyama, M. Kamimura, T. Motoba, T. Yamada, Y. Yamamoto, Phys. Rev. C **53**, 2075 (1996).
147. E. Hiyama, Y. Yamamoto, T. Motoba, M. Kamimura, Phys. Rev. C **80**, 054321 (2009).
148. T.Yu. Tretyakova, D.E. Lanskoy, Phys. At. Nucl. **66**, 1651 (2003).
149. T. Harada, A. Umeya, Y. Hirabayashi, Phys. Rev. C **79**, 014603 (2009).
150. K. Kubota et al., Nucl. Phys. A **602**, 327 (1996).
151. T.Yu. Tretyakova, D.E. Lanskoy, Nucl. Phys. A **691**, 51c (2001).
152. P.K. Saha et al., Phys. Rev. Lett. **94**, 052502 (2005).
153. M. Agnello et al., Phys. Lett. B **640**, 145 (2006).
154. M. Agnello et al., Phys. Rev. Lett. **108**, 042501 (2012).
155. A. Sakaguchi et al., Production of Neutron-Rich Λ-Hypernuclei with the double exchange, Proposal for J-PARK 50 GeV Proton Synchrotron, 1 (2006) (available at http://j-parc.jp/NuclPartProposal_e.html).
156. T.R. Saito et al., Int. J. Mod. Phys. E **19**, 2656 (2010).
157. Particle Data Group (K. Nakamura et al.), J. Phys. G **37**, 075021 (2010).
158. A.O. Gattone, M. Chiapparini, E.D. Izquierdo, Phys. Rev. C **44**, 548 (1991).
159. J. Cohen, J.V. Noble, Phys. Rev. C **46**, 801 (1992).
160. C.B. Dover, H. Feshbach, A. Gal, Phys. Rev. C **51**, 541 (1995).
161. K. Saito, M. Oka, T. Suzuki, Nucl. Phys. A **625**, 95 (1997).
162. W.M. Alberico, A. De Pace, M. Ericson, A. Molinari, Phys. Lett. B **256**, 134 (1991).
163. W.M. Alberico, G. Garbarino, in Hadron Physics, Proceedings of the International School of Physics "E. Fermi" Course CLVIII, edited by T. Bressani, A. Filippi, U. Wiedner, (SIF, Bologna and IOS Press, Amsterdam, 2005) p. 125.
164. H. Outa, in Hadron Physics, Proceedings of the International School of Physics "E. Fermi" Course CLVIII, edited by T. Bressani, A. Filippi, U. Wiedner, (SIF, Bologna and IOS Press, Amsterdam, 2005) p. 219.
165. A. Bauer, G. Garbarino, Phys. Rev. C **81**, 064315 (2010).
166. J. Cohen, Progr. Part. Nucl. Phys. **25**, 139 (1990).
167. A. Parreño, Lect. Notes Phys. **724**, 141 (2007).
168. R.J. Prem et al., Phys. Rev. **136**, B1803 (1964).
169. R.E. Phillips et al., Phys. Rev. **180**, 1307 (1969).
170. G. Bohm et al., Nucl. Phys. B **16**, 46 (1970).
171. G. Keyes et al., Phys. Rev. D **1**, 66 (1970).
172. G. Keyes et al., Nucl. Phys. B **67**, 269 (1973).
173. Y.W. Kang et al., Phys. Rev. **139**, B401 (1965).
174. H. Outa et al., Nucl. Phys. A **585**, 109c (1995).
175. H. Outa et al., Nucl. Phys. A **639**, 251c (1998).
176. V.J. Zeps, Nucl. Phys. A **639**, 261c (1998).
177. J.D. Parker et al., Phys. Rev. C **76**, 035501 (2007).
178. J.J. Szymanski et al., Phys. Rev. C **43**, 849 (1991).
179. S. Kameoka et al., Nucl. Phys. A **754**, 173c (2005).
180. R. Grace et al., Phys. Rev. Lett. **55**, 1055 (1985).
181. H. Park et al., Phys. Rev. C **61**, 054004 (2000).
182. K. Itonaga et al., Nucl. Phys. A **639**, 329c (1998).
183. A. Ramos, E. Oset, L.L. Salcedo, Phys. Rev. C **50**, 2314 (1994).
184. W.M. Alberico, A. De Pace, G. Garbarino, A. Ramos, Phys. Rev. C **61**, 044314 (2000).
185. V.I. Noga et al., Sov. J. Nucl. Phys. **43**, 856 (1986).
186. V. Metag et al., Nucl. Instrum. Methods **114**, 445 (1974).
187. R.H. Dalitz, Phys. Rev. **112**, 605 (1958).
188. R.H. Dalitz, L. Liu, Phys. Rev. **116**, 1312 (1959).
189. R.H. Dalitz, Nucl. Phys. **41**, 78 (1963).
190. D. Ziemińska, Nucl. Phys. A **242**, 461 (1975).
191. D. Ziemińska, R.H. Dalitz, Nucl. Phys. A **238**, 453 (1975).
192. D. Kiełczewska, D. Ziemińska, R.H. Dalitz, Nucl. Phys. A **333**, 367 (1980).
193. D. Bertrand et al., Nucl. Phys. B **16**, 77 (1970).
194. M.M. Bloch et al., Proceedings of the International Conference on Hyperfragments, St. Cergue, CERN64-1 (1964), 63.
195. D.H. Davis et al., Nucl. Phys. **41**, 73 (1963).
196. D.H. Davis, Nucl. Phys. A **754**, 3c (2005).
197. S. Okada et al., Nucl. Phys. A **754**, 178c (2005).
198. M. Agnello et al., Phys. Lett. B **681**, 139 (2009).
199. A. Sakaguchi et al., Phys. Rev. C **43**, 73 (1991).
200. H. Noumi et al., Phys. Rev. C **52**, 2936 (1995).
201. Y. Sato et al., Phys. Rev. C **71**, 025203 (2005).
202. T. Motoba, H. Bandō, T. Fukuda, J. Žofka, Nucl. Phys. A **534**, 597 (1991).
203. H. Bandō, T. Motoba, J. Žofka, in Perspectives of Meson Science, edited by T. Yamazaki, K. Nakai, K. Nagamine (North Holland, Amsterdam, 1992) pp. 571-660.
204. T. Motoba, K. Itonaga, H. Bandō, Nucl. Phys. A **489**, 683 (1988).
205. T. Motoba, K. Itonaga, Progr. Theor. Phys. Suppl. **117**, 477 (1994).
206. H. Bandō, H. Takaki, Progr. Theor. Phys. Suppl. **72**, 109 (1984).
207. H. Bandō, H. Takaki, Phys. Lett. B **150**, 409 (1985).
208. E. Oset, L.L. Salcedo, Nucl. Phys. A **443**, 704 (1985).
209. E. Oset, P. Fernández de Córdoba, L.L. Salcedo, R. Brockmann, Phys. Rep. **188**, 79 (1990).
210. E. Friedman et al., Phys. Rev. C **72**, 034609 (2005) and references to earlier works therein.
211. E. Friedman, A. Gal, Phys. Rep. **452**, 89 (2007).
212. R.S. Hayano et al., Phys. Lett. B **231**, 355 (1989).
213. H. Outa et al., Progr. Theor. Phys. Suppl. **117**, 177 (1994).
214. T. Nagae et al., Phys. Rev. Lett. **80**, 1605 (1998).

215. T. Harada *et al.*, Nucl. Phys. A **507**, 715 (1990).
216. Y. Kuriraha *et al.*, Progr. Theor. Phys. **71**, 561 (1984).
217. Y. Kuriraha *et al.*, Phys. Rev. C **31**, 971 (1985).
218. I. Kumagai-Fuse *et al.*, Phys. Lett. B **345**, 386 (1995).
219. I. Kumagai-Fuse, private communication.
220. E. Oset, P. Fernandez de Cordoba, J. Nieves, A. Ramos, L.L. Salcedo, Progr. Theor. Phys. Suppl. **117**, 461 (1994).
221. A. Montwill *et al.*, Nucl. Phys. A **234**, 413 (1974).
222. J. Sasao *et al.*, Phys. Lett. B **579**, 258 (2004).
223. A. Gal, Nucl. Phys. A **828**, 72 (2009).
224. S. Cohen, D. Kurath, Nucl. Phys. **73**, 1 (1965).
225. S. Cohen, D. Kurath, Nucl. Phys. A **101**, 1 (1967).
226. O. Hashimoto *et al.*, Nucl. Phys. A **639**, 93c (1998).
227. D. Ziemińska, Nucl. Phys. A **242**, 461 (1975).
228. D.J. Millener, Nucl. Phys. A **804**, 84 (2008).
229. L. Tang, Int. J. Mod. Phys. E **19**, 2638 (2010).
230. W. Cheston, H. Primakoff, Phys. Rev. **92**, 1537 (1953).
231. M.M. Block, R.H. Dalitz, Phys. Rev. Lett. **11**, 96 (1963).
232. W.M. Alberico, G. Garbarino, Phys. Lett. B **486**, 362 (2000).
233. J.B. Adams, Phys. Rev. **156**, 1611 (1967).
234. B.J.H. McKellar, B.F. Gibson, Phys. Rev. C **30**, 322 (1984).
235. G. Nardulli, Phys. Rev. C **38**, 832 (1988).
236. J.F. Dubach *et al.*, Nucl. Phys. A **450**, 71c (1986).
237. A. Parreño, A. Ramos, C. Bennhold, Phys. Rev. C **56**, 339 (1997).
238. A. Parreño, A. Ramos, Phys. Rev. C **65**, 015204 (2002).
239. D. Jido, E. Oset, J.E. Palomar, Nucl. Phys. A **694**, 525 (2001).
240. C. Chumillas, G. Garbarino, A. Parreño, A. Ramos, Phys. Lett. B **657**, 180 (2007).
241. C.Y. Cheung, D.P. Heddle, L.S. Kisslinger, Phys. Rev. C **27**, 335 (1983).
242. D.P. Heddle, L.S. Kisslinger, Phys. Rev. C **33**, 608 (1986).
243. T. Inoue *et al.*, Nucl. Phys. A **633**, 312 (1998).
244. K. Sasaki *et al.*, Nucl. Phys. A **669**, 331 (2000).
245. K. Sasaki *et al.*, Nucl. Phys. A **678**, 455 (2000).
246. E. Bauer, F. Krmpotic, Nucl. Phys. A **739**, 109 (2004).
247. E. Bauer, G. Garbarino, Nucl. Phys. A **828**, 29 (2009).
248. A. Parreño, A. Ramos, C. Bennhold, K. Maltman, Phys. Lett. B **435**, 1 (1998).
249. R.A. Schumacher, Nucl. Phys. A **547**, 143c (1992).
250. S. Ajimura *et al.*, *Exclusive study on the ΛN weak interaction in A = 4 Λ–Hypernuclei*, Letter of intent for an experiment (E22) at J–PARC (2007).
251. H. Ohm *et al.*, Phys. Rev. C **55**, 3062 (1997).
252. P. Kulessa *et al.*, Nucl. Phys A **639**, 283c (1998).
253. K. Itonaga *et al.*, Phys. Rev. C **65**, 034617 (2002).
254. A. Parreno, A. Ramos, Phys. Rev. C **65**, 015204 (2001).
255. C. Barbero, C. De Conti, A.P. Galeão, F. Krmpotić, Nucl. Phys. A **726**, 267 (2003).
256. H. Noumi *et al.*, *Proceedings of the IV International Symposium on Weak and Electromagnetic Interactions in Nuclei*, edited by H. Ejiri, T. Kishimoto, T. Sato (World Scientific, 1995) p. 550.
257. O. Hashimoto *et al.*, Phys. Rev. Lett. **88**, 042503 (2002).
258. H.J. Kim *et al.*, Phys. Rev. C **68**, 065201 (2003).
259. S. Okada *et al.*, Phys. Lett. B **597**, 249 (2004).
260. H. Bhang *et al.*, Eur. Phys. J. A **33**, 259 (2007).
261. M. Agnello *et al.*, Nucl. Phys. A **804**, 151 (2008).
262. A. Ramos *et al.*, Phys. Rev. C **55**, 735 (1997).
263. A. Ramos *et al.*, Phys. Rev. C **66**, 039903 (2002).
264. CERN Program Library Entry W 5013, *GEANT*.
265. G. Garbarino, A. Parreno, A. Ramos, Phys. Rev. C **69**, 054603 (2004).
266. G. Garbarino, A. Parreno, A. Ramos, Phys. Rev. Lett. **91**, 112501 (2003).
267. E. Bauer, Nucl. Phys. A **818**, 174 (2009).
268. M. Agnello *et al.*, *Hypernuclear weak decay studies with FINUDA*, to be published in Nucl. Phys. A, DOI:10.1016/j.nuclphysa.2012.01.024.
269. H. Bhang *et al.*, *Coincidence measurement of the weak decay of $^{12}_{\Lambda}C$ and the three-body weak interaction process*, Letter of intent for an experiment (E18) at J–PARC (2006).
270. G. Coremans *et al.*, Nucl. Phys. B **16**, 209 (1970).
271. M.M. Bloch *et al.*, *Proceedings of the 1960 Annual International Conference on High Energy Physics at Rochester* (New York, 1964) p. 419.
272. G. Keyes *et al.*, Nuovo Cimento A **31**, 401 (1976).
273. M. Rayet, Nuovo Cimento B **52**, 238 (1966).
274. P.G. Thurnauer, Nuovo Cimento **26**, 869 (1962).
275. M. Agnello *et al.*, Nucl. Phys. A **835**, 439 (2010).
276. H. Bandō, T. Motoba M. Sotona, J. Žofka, Phys. Rev. C **39**, 587 (1989).
277. T. Kishimoto, H. Ejiri, H. Bandō, Phys. Lett. B **232**, 24 (1989).
278. S. Ajimura *et al.*, Phys. Lett. B **282**, 293 (1992).
279. S. Ajimura *et al.*, Phys. Rev. Lett. **84**, 4052 (2000).
280. H. Bandō, T. Motoba, J. Žofka, Int. J. Mod. Phys. A **5**, 4021 (1990).
281. A.A. Ramos, E. van Meijgaard, C. Bennhold, B.K. Jennings, Nucl. Phys. A **544**, 703 (1992).
282. S. Ajimura *et al.*, Phys. Rev. Lett. **80**, 3471 (1998).
283. T. Maruta *et al.*, Nucl. Phys. A **754**, 168c (2005).
284. T. Maruta *et al.*, Eur. Phys. J. A **33**, 255 (2007).
285. T. Motoba, K. Itonaga, Nucl. Phys. A **577**, 293c (1994).
286. K. Itonaga, T. Motoba, T. Ueda, *Electrophotoproduction of Strangeness on Nucleons and Nuclei*, Sendai 03, edited by K. Maeda, H. Tamura, S.N. Nakamura, O. Hashimoto (World Scientific, 2004) p. 397.
287. C. Barbero, A.P. Galeão, F. Krmpotić, Phys. Rev. C **72**, 035210 (2005).
288. W.M. Alberico, G. Garbarino, A. Parreño, A. Ramos, Phys. Rev. Lett. **94**, 082501 (2005).
289. A. Parreño, C. Bennhold, B.R. Holstein, Phys. Rev. C **70**, 051601(R) (2004).
290. K. Sasaki, M. Izaki, M. Oka, Phys. Rev. C **71**, 035502 (2005).
291. C. Barbero, A. Mariano, Phys. Rev. C **73**, 024309 (2006).
292. K. Itonaga, T. Motoba, T. Ueda, Th.A. Rijken, Phys. Rev. C **77**, 044605 (2008).
293. P.A. Katz *et al.*, Phys. Rev. D **1**, 1267 (1970).
294. M. Agnello *et al.*, Phys. Rev. Lett. **94**, 212303 (2005).
295. V.K. Magas *et al.*, Phys. Rev. C **74**, 025206 (2006).
296. Y. Yamazaki, Y. Akaishi, Nucl. Phys. A **792**, 229 (2007).
297. M. Agnello *et al.*, Phys. Lett. B **654**, 80 (2007).
298. M. Agnello *et al.*, Nucl. Phys. A **775**, 35 (2006).
299. V.K. Magas, E. Oset, A. Ramos, Phys. Rev. C **7**, 065210 (2008).
300. T. Suzuki *et al.*, Phys. Rev. C **76**, 068202 (2007).
301. M. Agnello *et al.*, Phys. Lett. B **669**, 229 (2008).
302. S. Wycech, Nucl. Phys. A **450**, 399c (1986).
303. T. Yamazaki, Y. Akaishi, Phys. Lett. B **535**, 70 (2002).

304. J. Mares, E. Friedman, A. Gal, Nucl. Phys. A **770**, 84 (2006).
305. N.V. Shevchenko, A. Gal, J. Mares, Phys. Rev. Lett. **98**, 082301 (2007).
306. W. Weise, R. Hartle, Nucl. Phys. A **804**, 173 (2008).
307. M. Iwasaki *et al.*, Nucl Phys. A **804**, 186 (2008).
308. G. Bendiscioli *et al.*, Nucl. Phys. A **789**, 222 (2007).
309. G. Bendiscioli *et al.*, Eur. Phys. J. A **40**, 11 (2009).
310. T. Yamazaki *et al.*, Phys. Rev. Lett. **104**, 132501 (2010).
311. Y. Akaishi, T. Yamazaki, Phys. Rev. C **65**, 0444005 (2002).